UNIVERSITÄTSKLINIKUM HAMBURG-EPPENDORF

Zentrum für Geburtshilfe, Kinder- und Jugendmedizin
Klinik für Geburtshilfe und Pränatalmedizin
&
Zentrum für Diagnostik
Institut für Immunologie

The interrelation of maternal microchimerism, immunity and tissue homeostasis.

Dissertation

zur Erlangung des Doktorgrades Dr. rer. biol. hum.
an der Medizinischen Fakultät der Universität Hamburg

vorgelegt von:

Dennis Irfan Yüzen
aus München

Hamburg 2023

Für Mama

Angenommen von der
Medizinischen Fakultät der Universität Hamburg am: 16.02.2024

Veröffentlicht mit Genehmigung der
Medizinischen Fakultät der Universität Hamburg.

Prüfungsausschuss, der/die Vorsitzende: Prof. Dr. Petra C. Arck

Prüfungsausschuss, zweite/r Gutachter/in: Prof. Dr. Hans-Willi Mittrücker

Prüfungsausschuss, dritte/r Gutachter/in: Prof. Dr. Nicola Gagliani

Table of contents

List of figures

List of tables

1 Introduction

1.1 Pregnancy – between tolerance and protection

Pregnancy forms an immunological paradox as first famously stated by the Oxford's immunologist Peter Medawar.[1] During his studies of graft rejection, Medawar pointed out that although the immune system constantly patrols the body for non-self-antigens and rapidly clears them upon immune activation, pregnancy creates a state in which the mother tolerates the genetically foreign fetus.[2] Even though his attempts in explaining this contradicting observation by postulating immunological immaturity of the fetus or a general immunosuppression of the mother were not accurate, his idea of the placenta as barrier at the feto-maternal interface should prove to be true.

Today, it is broadly accepted that in order to maintain a functioning immune system, pregnancy is not accompanied by a general immunosuppression. Pregnancy rather forms a unique immunological status characterized by a delicate immunological adaption to the growing fetus. This adaptation is not static but highly dynamic depending on the state of pregnancy. Whereas the onset of pregnancy is characterized by a state of inflammation in order to enable the successful implantation of the blastocyst into the uterine endometrium, pregnancy maintenance is achieved by generating an anti-inflammatory state at the feto-maternal interface.[3,4] This includes the remodelling of the local immunological niche. The cytotoxicity of uterine natural killer cells, the most abundant immune cell population in the endometrium, is down-regulated. Concurrently, regulatory T cells, a subgroup of $CD4^+$ T cells, are locally enriched, which modulate the immune response towards tolerance of the foreign fetus.[5] These local adaptations are accompanied by extensive systemic changes. The complement system is activated and hormone levels are modified, e.g., levels of estradiol increase drastically, affecting the ratio of pro-inflammatory and anti-inflammatory T helper cells.[6-8] These changes are accompanied by a uniquely reorganized presentation of foreign fetal antigens to the maternal immune system, which results in limited T cell priming favouring fetal tolerance.[9] Towards the end of pregnancy, again a pro-inflammatory environment is created in order to induce labour.

Despite the constant immunological adaptations, the mother still needs to be protected against foreign pathogens. Especially at the mucosal surfaces, an inflammatory status needs to be maintained in order to prevent invasion of harmful microbes.[10] This is of particular relevance since pregnant women are at increased risk to develop more severe infections by common pathogens including influenza virus and herpes simplex virus.[11-13] Several maternal infections are associated with risks for the developing fetus since specific pathogens are able to colonize the placenta or even infect the fetus in-utero.[13-15] Hence, an infection with the food-born pathogen *Listeria monocytogenes* can lead to vertical transmission to the fetus resulting in congenital diseases, miscarriage, stillbirths or fetal death.[16-18] However, even during the

absence of placental or fetal colonization and no increased initial susceptibility of pregnant individuals, maternal infection poses a significant threat to the successful course of pregnancy as observed during the recent SARS-CoV-2 pandemic.[19] It became evident that maternal SARS-CoV-2 infection has been associated with increased risk for adverse pregnancy outcome, e.g., preeclampsia, preterm birth and stillbirth.[20-22]

1.2 The formation of immunological memory

Considering the permanent confrontation of the immune system with foreign and potentially harmful microbes, the immune system of pregnant women and non-pregnant individuals alike performs a tremendous task in preventing infections. This is possible due to coordinated engagement of various immunological defence mechanisms which are classically separated in the innate and adaptive immunity. Whereas the innate immunity mediates a rapid response upon pathogen encounter, the adaptive immunity has the potential to orchestrate a tailored immune response specific to the pathogenic threat.[23] One key factor is the vast repertoire of the T cell receptor, which is a result of somatic recombination in the thymus.[24] Although the actual diversity of T cells within the human body is finite due to the size of immunological niches and limited resources for T cell development, there is the potential of forming 10^{12} to 10^{15} different T cell receptors.[24-26] Equally compelling, each naïve T cell population specific for a unique antigen constitutes of just 100–10.000 cells.[24,27,28] Most pre-existing T cells never encounter their respective antigen. However, after contact of the naïve T cell population with their matching foreign antigen within the secondary lymphoid organs, they selectively proliferate forming clones of their original parent cell – a process referred to as clonal selection.[25] Thus, high specificity and rapid proliferation of T cells equips the immune system with the ability to precisely react to different pathogenic threats.

Another essential hallmark of the adaptive immune system is the potential to establish immunological memory. Immunological memory is defined by the ability of the immune system to rapidly respond to pathogenic threats that have been encountered before.[29] A premise for a secondary memory response is the existence of a clonally expanded population of antigen-specific memory lymphocytes formed after initial pathogen encounter.[30] Classically, one distinguishes between humoral and cellular immunological memory formation. If circulating antibodies do not suffice in neutralization of the pathogen, memory B cells, arisen from naïve B cells after initial antigen contact, are activated in the peripheral lymphoid organs.[31,32] They give rise to plasma cells that produce immunoglobulin G (IgG) antibodies with high affinity for the antigen forming the humoral immune response.[33] The cellular secondary immune response is mediated by memory T cell subsets that belong to both the $CD4^+$ and $CD8^+$ T cell lineage. They can be differentiated in distinct subpopulation by their surface markers and their cytokine profile that ultimately dictate their function. After initial priming by foreign antigens, $CD8^+$ T cells either form central memory T cells (T_{CM}) that home to the secondary lymphoid organs forming

a reservoir that proliferates upon recurrent antigen contact or effector memory T cells (T_{EM}). T_{EM} patrol the body trough lymphoid organs and non-lymphoid tissues.[34-36] Although their initial formation is well described, T_{EM} cells constitute a heterogeneous subset with various effector functions. Pioneered by the studies of Lefrancois and Masopust, it became evident that antigen-experienced $CD8^+$ T_{EM} cells have the capacity to home to peripheral tissue, where they occupy stable immunological niches and form local populations of immune memory.[36,37] The number and characteristics of these by now resident memory T cells (T_{RM}) vary between tissues but they share the ability to locally react to pathogenic threats.[38,39] Although opposing the idea of terminal residency, recent studies provide evidence for the capability of T_{RM} to re-join the circulation.[40,41] Still, the exact mechanism that dictates their fate as resident cell and even allows their release from the tissue are a matter of ongoing discussion.

1.3 The placenta and the transfer of memory

The placenta forms the central barrier tissue at the feto-maternal interface. Although the human hemochorial placenta assures the direct contact of fetal chorionic villi with maternal blood, the placental border is lined by a unique cell layer named syncytiotrophoblast, which, as Medawar correctly stated, protects the fetus from maternal infections. Still, the placenta is highly selective in regulating the adequate transfer of nutrients and hormones as well as the exchange of gases to guarantee fetal growth. In addition to passive diffusion, the placenta possesses active transport mechanism that regulate the transplacental transfer of antibodies to the fetus.

1.3.1 Antibodies

After birth and during the first months of life newborns are not yet equipped with a functioning immune system, leaving them highly susceptible to infections. Early-life infections, e.g., respiratory infections, therefore pose a significant risk to the health of the newborn. This immunological vulnerability is evolutionarily met by the active transport of antibodies from the mother to the fetus across the placenta.[42] Transplacental transfer of antibodies is limited to IgG antibodies, which are taken up by syncytiotrophoblasts cells and then bind to the neonatal Fc receptor within the endosomal compartment. The antibodies are then released to the fetal circulation after fusion of the endosome with the basolateral side of the cell.[43] The in-utero transfer of antibodies is amended by the transfer of IgA antibodies via the breast milk. Here, the IgA antibody binds to the Ig-receptor at the surface of the mammary gland epithelium, which is then internalized by the cells. The endosome, containing the IgA-receptor complex, fusions with the apical membrane of the mammary gland epithelium and releases the IgA antibody into the lumen of the mammary gland.[44] The number of transferred antibodies strongly depends on the concentration of maternal antibodies, which is influenced by the maternal infection history and by the current vaccination status of the mother.[43]

1.3.2 Maternal microchimerism

Beside antibodies, small numbers of cells cross the placenta. This bidirectional exchange of cells, from mother to the fetus and *vice versa*, is referred to as pregnancy-induced microchimerism.[45,46] Accordingly, maternal cells found in the fetus are termed maternal microchimeric cells (MMc).[45] Although being genetically foreign, MMc seem to be tolerated by the offspring's immune system and thus can be detected years after birth up until adulthood.[46,47] This observation even sparked the concept of a "microchiome", meaning the transfer of MMc across multiple generations.[48,49] This idea was recently supported by the detection of grandmaternal cells in the cord blood of neonates.[50] The transfer of MMc is tightly linked with the maturation of the placenta. In humans, MMc can be detected in the offspring with the beginning of the second trimester after placentation is established.[51,52] Similarly, MMc in rodents are transferred around mid-gestation, in which their number increases towards birth.[53,54] There is further evidence that the number of MMc decreases with recurrent pregnancies, indicating a possible effect of fetal antigens from former pregnancies on transplacental cell transfer.[55] In addition to a transmission in-utero, MMc can be transferred during lactation.[56]

Interestingly, once transferred MMc seed into lymphatic and non-lymphatic tissues and are comprised of different cell types mirroring the cellular heterogeneity of the maternal organism.[54,57-59] Since MMc transfer requires a connection of blood circulation between mother and fetus, the origin of MMc has been assumed to be hematopoietic.[59,60] However, the identification of non-hematopoietic maternal cells found in the murine liver, pancreas, lung, kidney, and skin challenge this hypothesis.[61-63] The diversity of cell types among the MMc subset indicates their multifactorial function in health and disease. Several studies link MMc with adverse consequences for offspring's health, such as the increased frequency of microchimeric cytotoxic $CD8^+$ T cells in graft-versus-host disease in mice. MMs are further associated with inflammatory bowel disease, juvenile dermatomyositis, neonatal lupus syndrome and lead to an increased risk for autoimmune diseases such as diabetes type 1 in humans or as demonstrated in transgenic mouse models of the disease.[62,64-68] However, the risk of diabetes type 1 seems not to be associated with the number of MMc found in the cord blood of patients.[69]

On the contrary, a high MMc count protects from the development of asthma as shown in children. Moreover, MMc contribute to establishing immune tolerance by transferring non-inherited maternal antigens to the offspring.[70,71] The immunological properties in educating the offspring's immune response go in line with a recent study conducted in our group. Stelzer *et al.* demonstrated that MMc seed to the fetal bone marrow, where they skew the haematopoiesis towards the formation of myeloid immune cells, which results in decreased susceptibility to early-life infections of neonatal mice. Similar observations were made in

human male neonates, who show improved protection against respiratory infections in association with a higher number of MMc.[72]

The multifactorial function of MMc depend on their tissue microenvironment. In the murine brain, MMc have been shown to cluster in the prefrontal cortex of fetal mice, which is responsible in shaping attention and cognitive performance. MMc were demonstrated to execute regulatory functions in the developing brain of neonates.[73] More specifically, as recently shown by Schepanski *et al.*, MMc in the murine brain guarantee microglia homeostasis by impeding excessive microglia activation and phagocytosis. Accordingly, as demonstrated in *in vitro* experiments, an absence of MMc leads to reduced neuronal branching and growth. By using animal models in which the number of MMc is greatly diminished, the overshooting presynaptic elimination by microglia cells in the fetal brain results in dysfunction of the prefrontal neuronal network leading to reduced cognitive abilities and emotional dysregulation of neonates.[73] To further evaluate whether the presence of MMc in the fetal brain has further consequences for the tissue homeostasis, *ex vivo* approaches could be used to obtain insights on the molecular properties of the tissue, e. g. by relying on spectroscopic techniques.

Despite the effort in characterizing local MMc populations, we still lack a general understanding on fundamental aspects of MMc transfer and function. One highly relevant aspect is the question of cellular memory transfer from the mother to the child. Since the mother was exposed to various infections during her life and received several vaccinations prior to pregnancy, it can be hypothesized that microchimeric T cells also include antigen-experienced immune cells. This idea is supported by the fact that MMc encompass high frequencies of T cells, e.g., in the fetal bone marrow, and that MMc are more prevalent among memory T cells compared to naïve T cells of cord blood mononuclear cells.[72,74,75] Two case report underpin this notion, as maternal $CD8^+$ T cells specific for human cytomegalovirus (CMV) or Epstein-Barr virus (EBV) could be identified in two 3-months old patients both suffering from severe combined immunodeficiency. *In vitro* analysis revealed that these cells exerted antiviral function by producing inflammatory cytokines in response to viral antigens.[76,77] The transfer of antigen-specific immune cells could provide antigen-specific protection of the neonate, which – given the longevity of T cells – could exceed the protection conveyed by maternal IgG antibodies.[50,78] This is especially relevant during the first months of life, before the recommended vaccination schemes are initiated.

Another poorly studied aspect of MMc biology is the regulation of MMc transfer. Quantitative analysis of MMc in human cord blood revealed a high variation in the number of transferred MMc, with some newborns having high MMc counts and some having few to none.[72,79] Similar variability has been observed measuring cord blood antibody titers.[43] Although cell and antibody transfer are differentially mediated, for both the transplacental transfer is highly dependent on the status of the placental tissue. Recent findings indicate that a maternal

immune activation leads to a dysregulation of placental tissue which correlates with altered transplacental transfer.[80,81] Despite the central role of the placenta in regulating cellular transfer, little is known regarding the properties of the placental tissue which favour or impair transplacental transfer. This is mainly due to the limited tools available to investigate placental function during an ongoing pregnancy.

1.4 Extracellular vesicles – mirrors of the host tissue

Extracellular vesicles (EV) serve as an umbrella term that summarizes a variety of lipid-bilayered particles, which are naturally released by essentially every cell type into the blood stream. EV can be classified based on whether they originate from the endosomal compartment and are released by the host cell after fusion of multivesicular bodies with the plasma membrane (exosomes) or are formed via outward blebbing of the plasma membrane (ectosomes).[82] Ectosomes comprise microparticles, oncosomes and microvesicles.[82] However, to date no general markers are established to reliably categorize EV based on their site of origin. Thus, EV are mainly classified based on their size as small EV (sEV, < 200 nm) or large EV (lEV > 200 nm).[83] sEV are further characterized by the presence or absence of tetraspanins, namely CD63, CD81 and CD9, which are transmembrane proteins involved in the synthesis of EV.[84,85] Despite their classification, all EV carry a multitude of different proteins and lipids on their surface, which reflect the expression profile of the host cell membrane.[85] Additionally, EV contain cargo molecules such as DNA, RNA and proteins, which allows to deduce information on their target tissue and their functional properties exerted both locally or after transfer to distant target tissues.[86-88] EV can be isolated from virtually all biofluids, e.g., serum, amniotic fluid, or bronchoalveolar lavage fluid.[89-91] For now, analysis of EV is still in its infancy but has high potential for a better understanding of cellular communication, for diagnostics and even for therapeutics.

1.4.1 Placenta-derived extracellular vesicles in the maternal organism

Placental growth and blood flow are routinely measured in the clinics via ultrasound assessment forming the gold standard of placental evaluation. Still, ultrasound assessment does not suffice to provide information on transplacental transfer of antibodies and cells. A novel tool to fill this blind spot in pregnancy care might be the analyses of placenta-derived EV present in the in the peripheral blood of the pregnant women (Fig. 1). The placenta is a highly perfused organ and releases high amounts of EV during the course of pregnancy. EV are shed from different placental cell types, e.g., extravillous trophoblasts, syncytiotrophoblasts and cytotrophoblast, and flushed into the maternal circulation via the uterine veins.[92] EV released by different trophoblast cell types will be further summarized as placenta-derived EV. Formation of placenta-derived EV starts in the sixth week of pregnancy and increases with gestational age reaching the highest concentration directly before birth.[93,94] Placenta-derived

EV are commonly identified by staining for the placental surface protein placental alkaline phosphatase (PLAP).[95] PLAP belongs to a gene family encoding for four alkaline phosphatase isoenzymes, in which PLAP is the only family member specific for the placenta.[96] Despite PLAP, placenta-derived EV carry other placenta-specific molecules such as placental growth factor and human leukocyte antigen G.[97,98] Increased number of placenta-derived EV have been associated with pregnancy complications such as preeclampsia and gestational diabetes mellitus.[93,99-101]

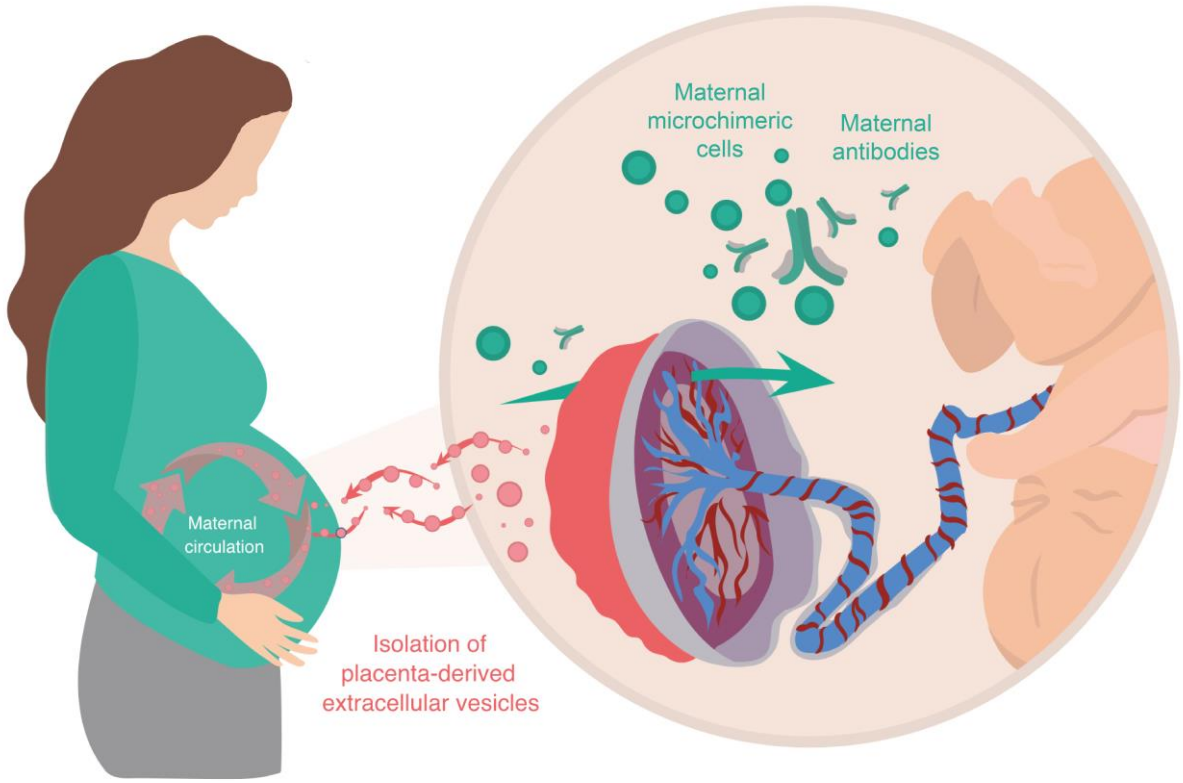

Figure 1. Placenta-derived EV as indicator for placental transfer.
Placental-derived EV released into the maternal circulation can be isolated for placental tissue evaluation to gain insights on the transplacental transfer of maternal cells and antibodies to the fetus.

In healthy pregnancies, placenta-derived EV mediate feto-maternal communication both locally and systemically by transporting various cargo materials such as proteins, including growth factors and cytokines, DNA and RNA molecules.[102-105] Locally at the feto-maternal interface, placenta-derived EV interact with maternal leukocytes and decidual cells to create an inflammatory environment that supports embryo implantation, induces angiogenesis and mediates invasion of the trophoblast.[106-108] Further, they are speculated to assist with the transfer of maternal IgG to the fetus at the placenta surface.[109] Once circulating in the maternal organism, placenta-derived EV are not cleared from the maternal blood. Instead, they have to be shown to target regional or distant tissues, where placenta-derived EV execute a broad variety of functions by interacting with fibroblasts and endothelial cells.[110,111] In contrast to their

pro-inflammatory effect at the beginning of pregnancy, placenta-derived EV also execute immune suppressive functions. sEV released by the placenta contain Fas-Ligand and further apoptosis-inducing ligands that promote death of peripheral blood mononuclear cells, T cells and other leukocytes *in vitro*; a mechanism that could contribute to the reduced severity of autoimmune diseases during pregnancy.[112-114] However, despite their systemic and local effects, placenta-derived EV are ultimately a mirror of their origin tissue with both their surface markers and cargo material. Thus, characterization of placenta-derived EV provides an opportunity to gain novel insights into placental tissue modulation and to placental transfer function.

1.5 Objectives

The aim of this thesis is to investigate the function of MMc in the fetus and to gain insight into the maternofetal transfer of cells.

I sought to investigate the hypothesis that among the leukocyte subset of MMc, antigen-specific T cells are transferred from mother to the fetus where they protect the neonate from infection. Further, I conducted a follow-up experiment to elucidate the modulation of the murine brain tissue by MMc. Also, I aimed to investigate the potential of EV as indicator for placental MMc transfer in healthy and SARS-CoV-2-infected pregnant women.

This thesis is separated in three sections, which address the aforementioned aspects based on the following objectives:

- Maternofetal transfer of antigen-specific T cells
    i. Identify antigen-specific MMc in the murine fetus after preconceptual infection of the mother.
    ii. Evaluate the protective capacities of antigen-specific MMc upon neonatal infection.
- Modulation of brain tissue by MMc
    Investigate the effects of MMc on the neonatal murine prefrontal cortex using Fourier-transform infrared spectroscopy.
- Placenta-derived EV as indicator for placental MMc transfer
    i. Analyse placenta-derived EV from serum samples of healthy and SARS-CoV-2 infected pregnant women.
    ii. Assess placenta-derived EV as indicators for transplacental transfer of MMc in pregnant women.

2 Material and Methods

2.1 Material

Table 1. Antibodies

Murine antibodies			
Antigen	**Clone**	**Conjugated fluorochrome**	**Company**
B220	RA3-6B2	APC	Becton Dickinson, Franklin Lakes, NJ, USA
B220	RA3-6B2	BV650	BioLegend, San Diego, CA, USA
CD11b	M1/70	PE-Cy7	Becton Dickinson, Franklin Lakes, NJ, USA
CD11c	N418	BV785	BioLegend, San Diego, CA, USA
CD3	145-2C11	PerCP-Cy5-5	eBioscience/Thermo Fisher Scientific, Waltham, MA, USA
CD4	RM4-5	FITC	Becton Dickinson, Franklin Lakes, NJ, USA
CD44	IM7	PE	Becton Dickinson, Franklin Lakes, NJ, USA
CD45	30-F11	APC-Cy-7	Becton Dickinson, Franklin Lakes, NJ, USA
CD45.1	A20	FITC	BioLegend, San Diego, CA, USA
CD45.2	104	APC-Cy7	BioLegend, San Diego, CA, USA
CD62L	MEL-14	BV711	BioLegend, San Diego, CA, USA
CD8	53-6.7	BV650	BioLegend, San Diego, CA, USA
Class I MHC OVA Tetramer	N/A	Pacific Blue	provided by the National Institutes of Health Tetramer Core Facility, Atlanta, GA, USA
Fixable viability dye eFluor™	N/A	V500	Invitrogen, Waltham, MA, USA
H2-D^{b}	KH95	PE	BioLegend, San Diego, CA, USA
H2-D^{d}	34-1-2S	APC	BioLegend, San Diego, CA, USA
MACS® MicroBeads against APC	N/A	N/A	Miltenyi Biotec, Bergisch Gladbach, Germany
TruStain fcX (anti-mouse CD16/32)	N/A	N/A	BioLegend, San Diego, CA, USA
Human antibodies			
Antigen	**Clone**	**Conjugated fluorochrome**	**Company**
CD63	H5C6	Pacific Blue	BioLegend, San Diego, CA, USA
CD81	5A6	Pacific Blue	BioLegend, San Diego, CA, USA

CD81	5A6	FITC	BioLegend, San Diego, CA, USA
CD9	MM2/57	Pacific Blue	BioRad, Hercules, CA, USA
CD9	HI9a	PE	BioLegend, San Diego, CA, USA
MACS® MicroBeads against FITC	N/A	N/A	Miltenyi Biotec, Bergisch Gladbach, Germany
PLAP	N/A	FITC	LifeSpan BioScience, Shirley, MA, USA

Table 2. Bacterial stocks

Ovalbumin recombinant *Listeria monocytogenes* (LmOVA)	Provided by Dr. Dietmar Zehn, Technical University of Munich
Attenuated ovalbumin recombinant *Listeria monocytogenes* strain deleted for *act*A (LmOVA Δ*act*A)	

Table 3. Buffers and solutions

Cell lysis buffer	0.1% TEAB, 1% SDC in ddH_20
ImageStream Buffer	2% exofree FCS in particle-free PBS
MACS Buffer (500ml)	2,5 mg BSA, 2mM EDTA in PBS
Percoll-HBSS-Solution	100 U/ml Heparin, 40% Percoll-Working-Solution, 60% HBSS
Percoll-Working-Solution (100 ml)	92,5 ml Percoll, 7,2 ml 10xPBS, 1.2 ml 7,5% $NaHCo_3$-Solution in ddH_20

For EV experiments all reagents were either purchased exosome-depleted or manually 0.2 µm filtrated and can be therefore considered particle free.

Table 4. Chemicals

Dulbecco's Phosphate Buffered Saline (PBS) Buffer	Invitrogen, Carlsbad, CA, USA Gibco/Thermo Fisher Scientific, Waltham, MA, USA
Accutase®	Stemcell Technologies, Vancouver, Canada
Ampicillin	Ratiopharm, Ulm, Germany
Bovine serum albumin (BSA)	Sigma-Aldrich Chemie GmbH, Munich, Germany
Collagenase IV	Roche Holding AG, Basel, Switzerland
EDTA	Sigma-Aldrich Chemie GmbH, Munich, Germany
Exosome-depleted Fetal calf serum (FCS)	Gibco/Thermo Fisher Scientific, Waltham, MA, USA
FCS	Gibco/Thermo Fisher Scientific, Waltham, MA, USA
Formaldehyde solution	Sigma-Aldrich Chemie GmbH, Munich, Germany

Hanks´ Balanced Salt Solution (HBSS)	Sigma-Aldrich Chemie GmbH, Munich, Germany
HEPES Buffer Solution (1M)	Sigma-Aldrich Chemie GmbH, Munich, Germany
Hyaluronidase	Sigma-Aldrich Chemie GmbH, Munich, Germany
Normal rat serum (NRS)	Jackson Immuno Research, Cambridgeshire UK
OptiPrep™ Density Gradient Medium	Sigma-Aldrich Chemie GmbH, Munich, Germany
Paraformaldehyde (PFA)	Biochemica, Billingham, UK
Percoll®	GE Healthcare, Chicago, IL, USA
Red blood cell lysis buffer	Invitrogen, Carlsbad, CA, USA
RPMI Medium 1640	Gibco/Thermo Fisher Scientific, Waltham, MA, USA
Triton-X-100	Merck Millipore, Darmstadt, Germany
Trypan Blue Stain (0.4%)	Gibco/Thermo Fisher Scientific, Waltham, MA, USA

Table 5. Instruments

CellDrop™ Automated Cell Counter	DeNovix, Wilmington, DE, USA
Dionex Ultimate 3000 UPLC system	Thermo Fisher Scientific, Waltham, MA, USA
DynaMeg™-2	Thermo Fisher Scientific, Waltham, MA, USA
FACS LSR/Fortessa	Becton Dickinson, Franklin Lakes, NJ, USA
FACS Symphony™ A3	Becton Dickinson, Franklin Lakes, NJ, USA
ImageStream® Mk II	Luminex Corporation, Austin, TX, USA
NanoSight LM10	NanoSight, Malvern, United Kingdom
Orbitrap Fusion	Thermo Fisher Scientific, Waltham, MA, USA

Table 6. Plastic materials

The routine laboratory plastic materials were purchased from

B. Braun, Melsungen, Germany
BD Bioscience, Heidelberg, Germany
Beckman Coulter, Brea, CA, USA
Corning Incorporated, Corning, NY, USA
Eppendorf AG, Hamburg, Germany
Greiner Bio-One International GmbH, Kremsmünster, Austria
Sarstedt AG & Co., Nürmbrecht, Germany
Th. Geyer GmbH & Co. KG, Renningen, Germany
Thermo Fisher Scientific, Waltham, MA, USA

Table 7. Software

Adobe Illustrator 2023	Adobe, San José, CA, USA
FACSDiva™ Software	Becton Dickinson, Franklin Lakes, NJ, USA

FlowJO Version 10.8.1	Becton Dickinson, Franklin Lakes, NJ, USA
GraphPad Prism Version 9	Insight Partners, New York City, NY, USA
NanoSight NTA 3.0	NanoSight, Malvern, United Kingdom
Orange (Quasar) 1.7.0	University of Ljubljana, Slovenia
Proteome Discoverer software 3.0	Thermo Fisher Scientific, Waltham, MA, USA
ZEN 3.3	Carl Zeiss AG, Jena, Germany

Table 8. Webservices

DAVID Bioinformational Database	Frederick National Laboratory for Cancer Research, Frederick, MD, USA
Reactome	Ontario Institute for Cancer Research, Toronto, Canada NYU Langone Health, New York City, NY, USA EMBL's European Bioinformatics Institute, Hinxton, United Kingdom Oregon Health & Science University, Portland, OR, USA
UniProt/Swiss-Prot	SIB Swiss Institute of Bioinformatics, Lausanne, Switzerland EMBL's European Bioinformatics Institute, Hinxton, United Kingdom Protein Information Resource, Newark, DE, USA

2.2 Methods

2.2.1 Mice

Animal care and experimental procedures were conducted based on the mandatory requirements in accordance with the German Animal Welfare Act and institutional guidelines of the University Medical Centre Hamburg-Eppendorf. The ethical approvals (Germany, approval numbers N125/19, G010/17) were issued by the State Authority of Hamburg. C57BL/6J (CD45.2, H-2D^{b}) and Balb/c CD45.1 (CD45.1, H-2D^{d}, CByJ.SJL(B6)-Ptprc^{a}/J) were purchased from The Jackson Laboratory (Bar Harbour, ME) and C57BL/6J Rag2$^{-/-}$IL-2rγc$^{-/-}$ (B6.129-Rag2^{tm1Cgn}Il2rg^{tm1Cgn}) were obtained from the animal breeding facility of University Medical Centre Hamburg-Eppendorf. Female mice were housed in groups, whereas male mice were situated separately in the animal facility of the University Medical Centre Hamburg-Eppendorf. Adequate housing was ensured at a room temperature of 21°C and humidity at 43% in a 12-hour light/12-hour dark cycle. Mice were provided with chow and water ad libitum. For experiments female mice were used at 8-10 weeks of age and male mice were used starting from fertile age up until 1 year of age.

2.2.2 *Listeria monocytogenes* infection

Female mice aged 8-10 weeks were infected with 1×10^4 colony forming units (CFU) of ovalbumin recombinant *L. monocytogenes* (LmOVA) in 100 µl sterile PBS via the lateral tail vein. Control mice were injected accordingly with 100 µl sterile PBS. One week after injection, both groups were treated with ampicillin in the drinking water (1 g/l) for seven days and mice were given an additional week of regeneration. For the evaluation of non-specific fetal immune activation, preconceptually infected female mice were re-infected during pregnancy at gestation day (gd) 17.5 with 1×10^4 CFU of LmOVA. For neonatal infection at day seven after being born, 1×10^4 CFU of the attenuated ovalbumin recombinant *L. monocytogenes* strain deleted for *act*A (LmOVA Δ*act*A) in 100 µl sterile PBS were injected intraperitoneally. Control neonates were injected with 100 µl sterile PBS. Concentration of inocula used for infection experiments were verified by plating serial dilutions on TSB agar plates.

2.2.3 Pregnancy mouse experiment design

To exclude environmental factors on housing and pregnancy maintenance, non-litter mates of female mice of all groups were kept and mated in the same animal facility. All experiments were independently repeated at least three times and data from individual fetuses derived from at least three separate litters were used. Mating of 12-13 weeks old females with one male were started at 3 to 5 p.m. for a maximum of 5 consecutive days. Overnight insemination was verified by the presence of a vaginal plug at 8 to 10 a.m. at the subsequent day and defined as gd 0.5. Body weight measurement at gd 10.5 was used to confirm successful pregnancy (10–15% body weight increase relative to gd 0.5). Fetal loss rate was calculated as the percentage of abortions among implantation sites. For experiments with MMc^{low} neonates, male offspring was excluded due to hemizygosity of the γc gene.

2.2.4 Tissue-collection and processing

For infection experiments, fetal tissue was collected by decapitating fetuses on gd 18.5. To sustain homogeneity in fetal size, offspring were exclusively used from mothers giving birth to at least 8 up to 11 neonates. Pregnancies and tissue harvesting were stringently timed to minimize differences in fetal age. Collected fetal tissues (bone marrow from femur and tibia, spleen, liver) and maternal tissues (uterus, liver, spleen and uterus-draining lymph nodes) were mechanically minced and washed through a filter to obtain single-cell suspensions. Fetal bone marrow samples were pooled to guarantee adequate cell numbers for subsequent analysis. A similar approach was chosen for fetal spleen samples. For maternal spleen samples, erythrocyte lysis was required. Maternal uterus samples were digested with Accutase®. Maternal blood was collected by retroorbital puncture in an EDTA-coated microvette. Liver and spleen of neonates were selected for further analysis due to being the primary infection site of *L. monocytogenes* infection. Neonatal tissues (liver and spleen) were

collected at day 14 after birth by decapitating neonatal mice and processed as described. Neonatal spleen samples were pooled to guarantee adequate cell numbers. Neonatal liver cells were additionally purified using Percoll gradient.

2.2.5 Enrichment of MMc by magnetic-activated cell sorting

To allow reliable characterization of MMc, MMc within the bone-marrow, spleen and liver samples were enriched based on their lack of H-2D^d expression by magnetic-activated cell sorting (MACS) following published protocols for low frequency cell subsets [115]. In detail, two fetal spleens of litter mates were pooled to ensure a sufficient amount of fetal cells. Similarly, cells from fetal hind and front leg bones originated from two litter mates were pooled. Fetal livers were individually processed. Harvested cells were incubated for 30 minutes at 4°C with normal rat serum and anti-mouse CD16/32 in order to block unspecific FcγRII/III binding. To separate fetal from maternal cells, fetal cells were stained with APC-conjugated anti-H-2D^d antibody for 30 minutes at 4°C in the dark. Subsequent incubation with magnetically labelled anti-APC MicroBeads for 15 minutes at 4°C, enabled separation through MACS columns. While unlabelled MMc (H2-D^d negative and H2-D^b positive) were passing the column and were collected in the flow-through fraction, fetal cells (H2-D^d positive and H2-D^b negative) were retained within the column and later eluted (Fig. 2).

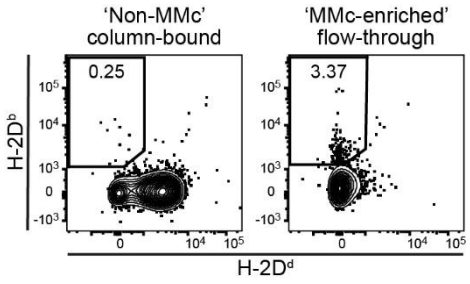

Figure 2. MACS Enrichment of MMc
Representative dot plots of column bound 'non-MMc' fraction (left) and 'MMc-enriched' flow-through fraction (right) after negative selection of MMc via antibody labelling of paternal H-2D^d and magnetic-activated cell sorting (MACS) gated on CD45.2$^+$ CD45.1$^-$ cells.

2.2.6 Flow cytometry

Cells were incubated with normal rat serum and anti-mouse CD16/32 in order to block unspecific FcγRII/III binding. Fluorochrome-conjugated antibodies, staining for cell viability and H-2K^b chicken ovalbumin amino acid 257-264 (SIINFEKL) tetramers conjugated to Brilliant Violet 421 were added to the cell suspension and incubated for 30 min at 4°C in the dark. Effector memory CD8$^+$ T cells were identified based on their expression of CD44 and CD62L (Fig. 3).

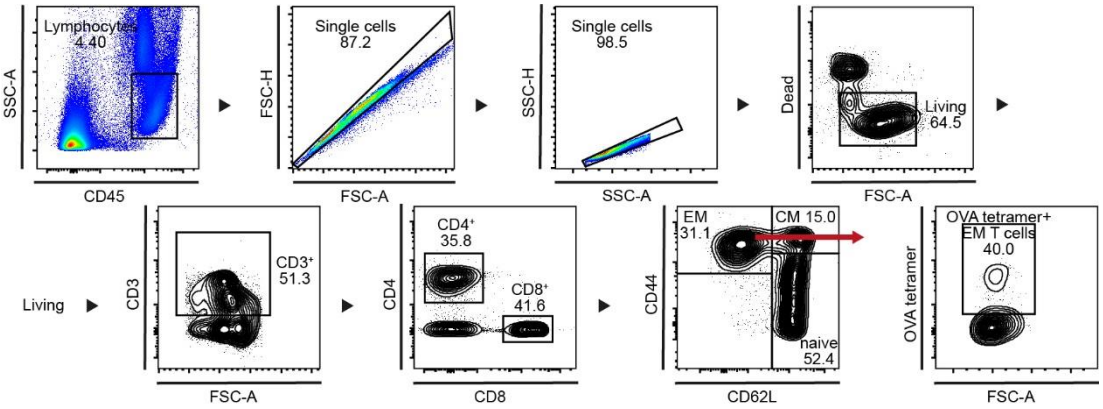

Figure 3. Gating strategy of CD8⁺ T effector/effector memory cells.
Blood of pregnant mice at gd 18.5 after preconceptual infection.

To identify MMc among fetal cells, CD45 and MHC class I (H-2D) expression was evaluated. Maternal origin of cells was verified by CD45.2 expression by concurrent absence of CD45.1. Subsequent determination of H-2D^{b} expression and H-2D^{d} absence was used to refine the gating strategy. After identification, MMc were further characterized based on specific lineage marker (Fig. 4). Samples were acquired using a Fortessa and A3 flow cytometer using 1×10^{6} cells per fetal bone marrow, fetal liver and neonatal samples and 0.2×10^{6} cells for fetal spleen if possible. Absolute MMc number was calculated depending on their relative abundance among fetal cells. Doublets and dead cells were excluded in the gating process. To control for adequate gating of cell populations, fluorescence minus one controls (FMO) containing all antibodies of a staining panel except one were used.

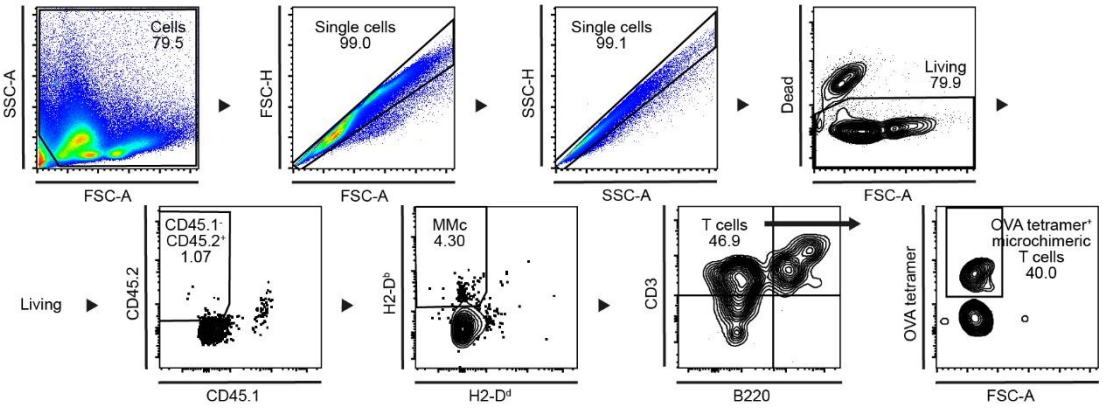

Figure 4. Gating strategy of 'MMc-enriched' flow-through.
Bone marrow of fetal mice at gd 18.5 born to a preconceptually infected mother.

2.2.7 Placenta histology

For each litter, two placentas from male and female offspring were collected at gd 18.5, fixed in 4% formaldehyde solution and embedded in paraffin. Placentas were then cut in 4 µm sections at the mid sagittal plate. To perform histomorphological evaluation of placental areas, placental tissue was processed using Masson-Goldner trichrome staining. Placental labyrinth

(L) and junctional zone (JZ) were quantified and placental ratio (L/JZ) was calculated. Quantification was conducted by two independent individuals.

2.2.8 Perfusion and brain sectioning

Male murine neonates were intraperitoneally anesthetized at day 8 after being born using 10% ketamine / 2% xylazine in 0.9 NaCl solution. Neonates were then transcardially perfused for 10 minutes with 4% paraformaldehyde in 0.1 M phosphate buffer. After decapitation, fixated brains were isolated and immediately post-fixed in 4% paraformaldehyde in 0.1 M phosphate buffer for 4 hours at 4°C. Brains were cryoprotected with 30% sucrose solution in 0.1 M phosphate buffer for 48 hours at 4°C, subsequently frozen in 2-methylbutane and stored at -80°C as published by Sanchez-Molina *et al.*[116] Frozen brain samples were coronally sectioned with a thickness of 8 µm and applied to barium fluoride (BaF_2) optical windows. Samples were air-dried at room-temperature and stored protected from light until use.

2.2.9 Fourier Transform Infrared Microspectroscopy

Fourier Transform Infrared Microspectroscopy (µFTIR) based on synchrotron radiation was carried out at the MIRAS beamline of ALBA synchrotron light source (Catalonia, Spain). For measurements a Hyperion 3000 microscope equipped with a 36x magnification objective and coupled to a Vertex 70 spectrometer was used. Collection of spectra was performed in transmission mode. In order to detect regional differences with high spatial resolution of the tissue, samples of the prelimbic cortex were mapped with 650 spectra using an aperture size of 10 µm x 10 µm and a step size of 4 µm x 4 µm. Whole brain mapping was performed overnight with an aperture size of 20 µm x 20 µm and a step size of 4 µm x 4 µm resulting in 11.500 spectra for each sample. During measurements, background spectra were regularly collected from a clean are of the BaF^2 window every 10 minutes. A mercury cadmium telluride detector was used, and both the microscope and spectrometer were continuously purged with a flow of dried air. Spectral processing was performed after the second derivatives were calculated and unit vector normalization was performed. Results were generated by integrating the area underneath the curve (IAUC) of the functional groups of interest (Table 9). Obtained values were normalized to the IAUC of the Amid I band (1649-1664 cm^{-1}).

Table 9. µFTIR spectroscopy functional groups of interest

Band assignment	Analysed spectral range (cm^{-1})	Description[a,b]
Lipid I	2954-2968	$\nu_{as}(CH_3)$
Lipid II	2915-2935	$\nu_{as}(CH_2)$
Lipid III	2869-2880	$\nu_{s}(CH_3)$
Lipid IV	2845-2859	$\nu_{s}(CH_2)$
Ester formation	1733-1750	$\nu_{s}(C=O)$

Protein conformation I	1650-1662	α-helix structure
Amid I	1649-1664	v(C=O)
Protein conformation II	1629-1641	β-sheet structure
Amid II	1535-1556	δ(N-H)
Tyrosin	1509-1522	δ(C-H) of phenyl rings
Carbohydrates I	1128-1148	v(C-OH)
Carbohydrates II	1101-1113	v(C-O), v(C-C) ring in polysaccharides
Nucleic acid I	1083-1101	$v_s(PO_2^-)$ in RNA and DNA
Carbohydrates III	1039-1061	v_s(CO-O-C) in RNA and DNA
Nucleic acid II	1015-1032	v(CH_2OH)
Carbohydrates IV	982-1006	v(C-C) and v(C-O) of deoxyribose
Nucleic acid III	929-946	Z-type helix DNA
Nucleic acid IV	880-895	A/B-type helix DNA

[a]v=stretching vibrations, δ=bending vibrations, s=symmetric vibrations, as=asymmetric vibrations
[b]Detailed review for reference from FTIR spectroscopy imaging studies of biological tissues[117]

2.2.10 Patient samples

Patient samples were kindly provided by the PRINCE (Prenatal Identification of Children's Health) and PRINCE-COVID study. The PRINCE study and the PRINCE-COVID study were initiated in 2011 and respectively in 2020 at the Department of Obstetrics and Prenatal Medicine of the University Medical Centre Hamburg-Eppendorf. Both are prospective longitudinal pregnancy studies that included women at an age ≥18 with a viable pregnancy at 12–14 weeks of gestation. Women with chronic infections, known drug or alcohol abuse, multiple pregnancies or pregnancies induced by assisted reproductive technology were excluded. Further details of the PRINCE study have been described elsewhere.[118] The PRINCE-COVID study solely included women that suffered from SARS-CoV-2 infection during pregnancy.[119]

2.2.11 EV-Isolation

Human serum samples were diluted with particle-free PBS and layered on top of 40% iodixanol-PBS stained with phenolred. After ultracentrifugation, the EV were enriched at the top of the of the iodixanol-PBS layer forming a visible interface, whereas other serum components were concentrated at the bottom of the tube. By puncturing the tube with a syringe, the interface containing the EV was extracted and transferred to a new tube, which underwent a second ultracentrifugation step leading to accumulation of the EV at the bottom of the tube. The EV were resuspended and a small aliquot was stored for Nanoparticle-Tracking-Analysis, whereas the rest was stored at -80°C for Imaging Flow Cytometry and proteome analysis.

2.2.12 Nanoparticle Tracking Analysis

Aliquots containing EV were diluted and analysed via real-time microscopic visualization. According to the Brownian motion of the particles, their size and concentration were calculated based on five separate videos recordings.

2.2.13 Imaging Flow Cytometry

Isolated EV were treated with exosome-depleted FCS in order to block unspecific FcγRII/III binding. After-blocking, EV were stained with fluorochrome-conjugated antibodies against tetraspanins (CD63, CD81, CD9), which are considered to be EV-specific surface markers, and antibodies against PLAP, a specific marker for placental trophoblast cells. For each measured sample, 30.000 particle were recorded using the ImageStream. Imaging Flow Cytometry enables individual visual evaluation of EV and provides information on concentration, purity and size distribution.

2.2.14 Enrichment of EV by magnetic-activated sorting

Placenta-derived EV were stained with FITC-conjugated antibodies against PLAP. In a next step magnetically labelled anti-FITC MicroBeads were added and incubated for 15 minutes at 4°C. Magnetically labelled placenta-derived EV were enriched at the side of the reaction tube, whereas the supernatant containing the non-enriched particles was discarded. The magnet was removed and the enriched $PLAP^+$ EV were resuspended in particle-free PBS. Enrichment was verified by Imagestream Flow Cytometry analysis of the 'non-enriched' supernatant and the tube bound '$PLAP^+$ enriched' fraction.

2.2.15 Proteomic analysis

Proteomic analysis of EV was performed by the staff personnel of the in-house Core Facility Mass Spectrometric Proteomics of the University Medical Centre Hamburg-Eppendorf under the direction of Prof. Hartmut Schlüter.

Placenta-derived EV, as well as a reference cell line, were resuspended in cell lysis buffer and heated for protein extraction. Samples were sonicated using a sonication probe to remove interfering DNA. Extracted proteins were tryptically digested, as described by Hughes at al.[120] Tryptic peptides were dried and stored at -20°C until further usage. Liquid chromatography–tandem mass spectrometer (LC–MS/MS) measurements were performed on a quadrupole-ion-trap-orbitrap MS coupled to a nano-UPLC. Tryptic peptides were injected to the LC system via an autosampler, purified and desalted by using a reverse phase trapping column and thereafter separated with a reverse phase column. Eluting peptides were ionized by using a nano-electrospray ionization source with a spray voltage of 1800 V, transferred into the MS and analysed in data dependent acquisition mode. Data acquisition was performed as described in Kement *et al*.[121]

LC-MS/MS raw spectra were searched with a combined workflow, including the CHIMERYS and SEQUEST algorithm integrated in the Proteome Discoverer software against a reviewed human Swissprot database, obtained in December 2022, containing 20.300 entries. A strict cut-off (false discovery rate <0.01) was set for peptide and protein identification. Protein quantification was carried out using the Minora algorithm implemented in Proteome Discoverer. At the peptide level, no normalization was performed. Scaling was disabled. Protein abundances were log2 transformed and median normalized across columns for protein level normalization. Prior to statistical analyses and normalization, the cell line reference was removed. DAVID Bioinformational Database was used for gene ontology analysis and the Reactome software was applied for pathway analysis.

2.2.16 Statistical analysis

Statistical parameters including biological replicates *n* (if not specified otherwise), precision measures (mean ± SEM), and statistical significance are reported in the figures and figure legends. Data was tested for normal distribution and the hypothesis judged to be non-zero with statistical significance when $p<0.05$ by unpaired Student's T-Test, Mann-Whitney-U test, Ordinary one-way ANOVA or Kruskal–Wallis test. In figures, asterisks denote statistical significance (*$p<0.05$; **$p<0.01$; ***$p<0.001$; ****$p<0.0001$). Outliers were removed by using outlier removal function in GraphPad PRISM 9 with a false discovery rate of 1%. Statistical analysis was performed in GraphPad PRISM 9.

To identify similarities and differences between individual proteomes of EV samples, principal component analysis (PCA) was applied in the Orange Software. To identify differentially expressed proteins (DEPs) Student´s t-test with $p<0.05$ was applied. For the validation of significantly changed proteins, an additional cut-off value for the log2-fold change was applied (the protein must be at least 1.5 times higher abundant in one group).

3 Results

3.1 Transfer of antigen-specific MMc

3.1.1 Preconceptual infection with LmOVA leads to the enrichment of CD4⁺ and CD8⁺ cells in the uterus.

By analysing maternal tissues after preconceptual infection with LmOVA I aimed to demonstrate the formation and persistence of OVA-specific T cells and assign them to a subpopulation of $CD8^+$ T cells.

Mice infected with LmOVA generate a $CD8^+$ T cell response to *L. monocytogenes* characterized by the formation of specific memory T cell subset against the immunodominant peptide ovalbumin$_{257-264}$ (SIINFEKL). C57BL/6 female adult mice were preconceptually infected with LmOVA, following a treatment with ampicillin 7 days after infection to ensure complete clearance of the pathogen. Females were then allogenically mated to Balb/c males (Fig. 5A). On gd 18.5 and 5 weeks post infection with LmOVA overall $CD45^+$ leukocyte numbers in the uteri did not differ between infected and control mice (Fig. 5B). However, a significant increase of $CD4^+$ and $CD8^+$ T cells in the pregnant uterus of mice could be detected when compared to non-infected females (Fig. 5C, D).

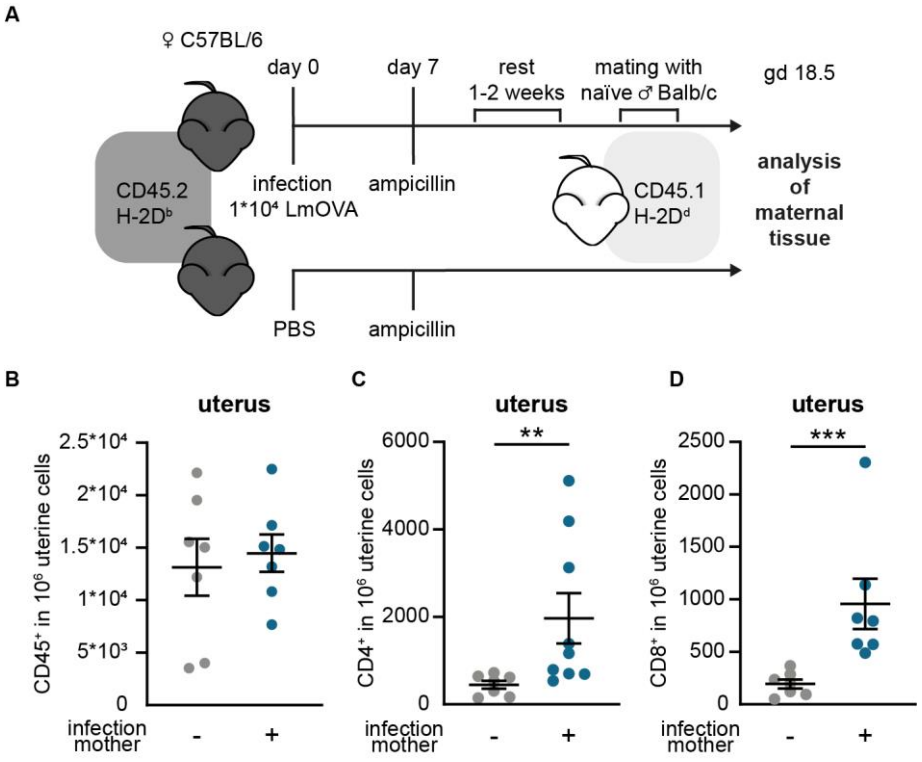

Figure 5. Preconceptual infection with LmOVA leads to the enrichment of CD4⁺ and CD8⁺ cells in the uterus.

(A) Infection and mating strategy. **(B)** Number of $CD45^+$ cells in10^6 uterine cells on gd 18.5 after preconceptual infection of mothers in comparison with naïve mothers (*n*=7 each). **(C, D)** Numbers of $CD4^+$ **(C)** and $CD8^+$ **(D)** in 10^6 uterine cells on gd 18.5 after preconceptual infection of the mother in comparison with non-infected mothers (*n*=7, *n*=9). T cells were identified as $CD45^+$ $CD3^+$ and either $CD4^+$ or $CD8^+$ cells. **(B-D)** Scatter-plots represent mean ±SEM. Asterisks indicate significance level of unpaired Student's t-test or Mann-Whitney-U test after testing for normal distribution.

Next, the phenotype of $CD8^+$ T cells was further characterized in in the blood, uterus-draining lymph nodes, spleen and uterus. Hereby, $CD8^+$ T cells were sub-classified based on their expression of CD44 and CD62L, in which naïve T cells were defined as $CD62L^+CD44^-$, central memory (CM) T cells as $CD62L^+CD44^+$ and effector/effector memory (EM) T cells as $CD44^+CD62L^-$ (Fig. 6A). Higher frequencies of EM T cells within the $CD8^+$ T cell compartment were detected in the peripheral blood and spleen of preconceptually infected females, whereas no differences could be shown in the uterus-draining lymph nodes compared to control mice (Fig. 6B-E). In the blood, lymph node, and spleen naïve T cells form the major subset of $CD8^+$ T cells in both preconceptually infected and control mice (Fig. 6F-H). In the uterus, EM T cells comprised the major $CD8^+$ T cell compartment, which was further expanded after infection with LmOVA (Fig. 6I).

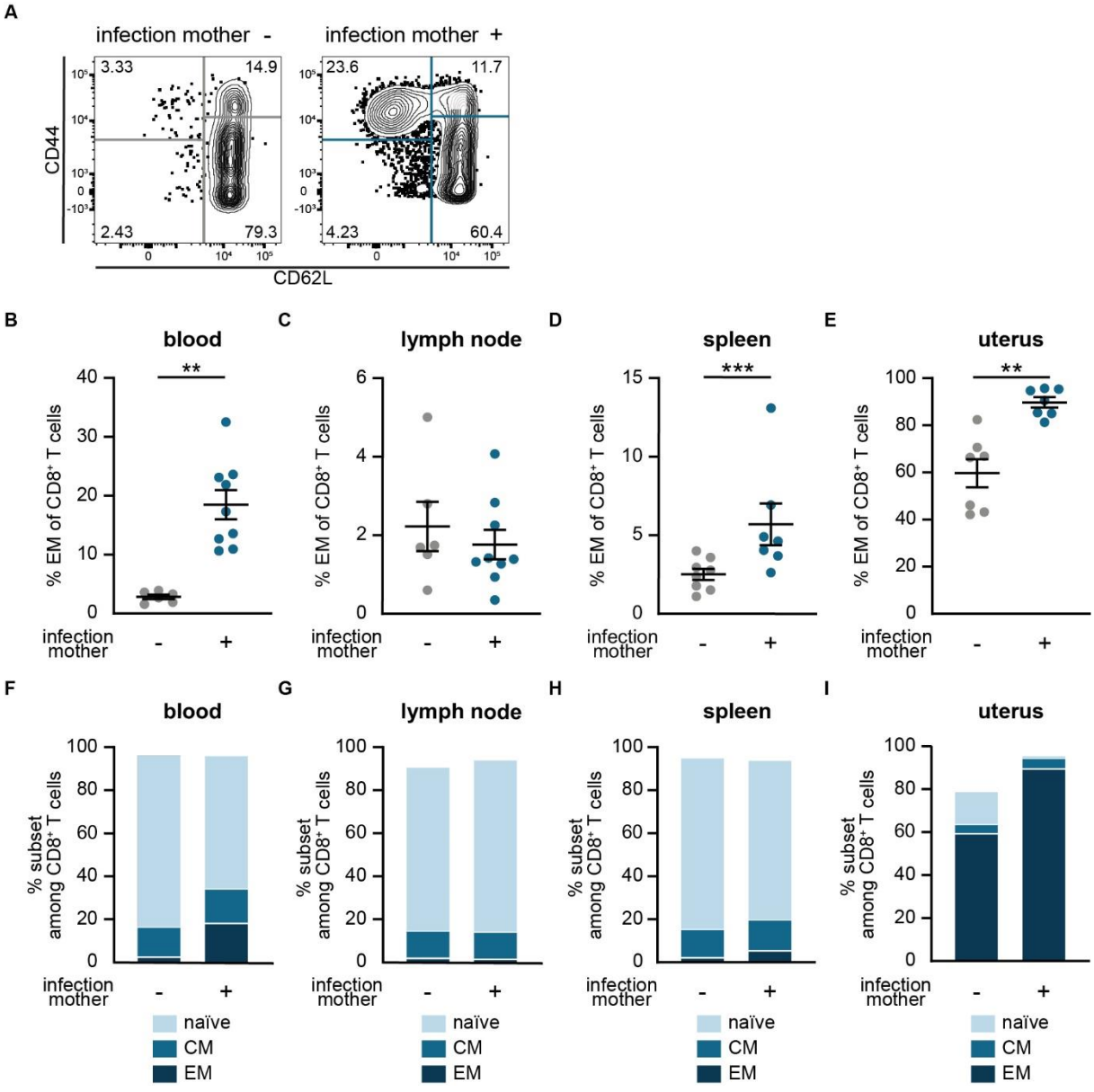

Figure 6. Preconceptual infection with LmOVA increases the percentage of CD8⁺ effector memory T cells.

(A) Representative dot plots of CD8⁺ T cells from peripheral blood divided in CD44⁺ CD62L⁻ effector/effector memory (EM), CD44⁺ CD62L⁺ central memory (CM), and CD44⁻ CD62L⁺ naïve subpopulations. Left: non-infected pregnant control mouse, right: previously infected pregnant mouse. **(B-E)** percentage of EM T cells (CD44⁺, CD62L⁻) among CD8⁺ T cells; **(F)** peripheral blood (*n*=6, *n*=9), **(G)** uterus-draining lymph nodes (*n*=6, *n*=9), **(H)** spleen (*n*=7, *n*=8), **(I)** uterus (*n*=7 each). **(B-E)** Scatter-plots represent mean ±SEM. **(F-I)** Stacked bar plots represent mean. Asterisks indicate significance level of unpaired Student's t-test or Mann-Whitney-U test after testing for normal distribution.

When assessing the percentage of ovalbumin-specific T cells within the CD8⁺ EM T cells by using H-2K^b ovalbumin$_{257-264}$ tetramers (OVA tetramers) (Fig. 7A), it could be demonstrated that preconceptual infection with LmOVA results in up to 10% of CD8⁺ EM T cells in blood, uterus-draining lymph nodes, spleen and uterus specific for ovalbumin (Fig. 7B-E).

Preconceptual infection of female mice with LmOVA resulted in the enrichment of CD4⁺ and CD8⁺ T cells in the uterus of which EM CD8⁺ T cells formed the major fraction. OVA-specific CD8⁺ EM were identified in the blood, secondary lymphoid organs and the uterus.

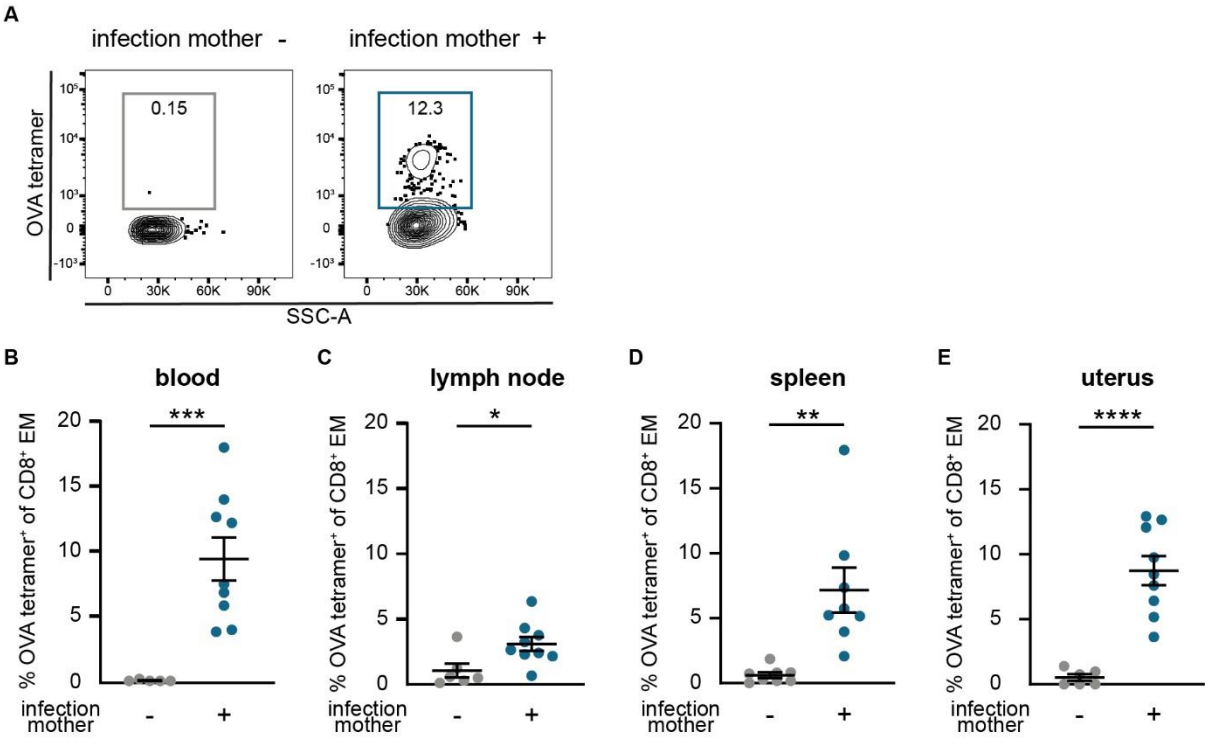

Figure 7. Accumulation of OVA-specific CD8⁺ EM T cells in different organs after preconceptual infection.

(A) Representative dot plots of ovalbumin-specific CD8⁺ EM T cells stained with H-2K^b ovalbumin$_{257-264}$ tetramers (OVA tetramers) from peripheral blood. Left: non-infected pregnant control mouse, right: previously infected pregnant mouse. **(B-E)** Percentage of ovalbumin-specific CD8⁺ EM T cells; **(B)** peripheral blood (*n*=7, *n*=9), **(C)** uterus-draining lymph nodes (*n*=7, *n*=9), **(D)** spleen (*n*=8 each), **(E)** uterus (*n*=6, *n*=9). **(B-E)** Scatter-plots represent mean ±SEM. Asterisks indicate significance level of unpaired Student's t-test or Mann-Whitney-U test after testing for normal distribution.

3.1.2 Transfer of OVA-specific MMc from mother to fetus

In order to investigate the intrauterine transfer of antigen-specific MMc from the mother to the fetus, OVA tetramers were used to specifically stain OVA-specific cells among microchimeric T cells.

In order to exclude possible confounders that might have an impact on the offspring's immune response, e.g., microbial colonization at birth, or the number of MMc due to breastfeeding, fetal mice were analysed one day before birth at gd. 18.5. First, pregnancy outcome parameters were evaluated, which showed no differences in fetal loss rate, number of implantations and male/female fetal sex ratio between preconceptually infected mothers and non-infected controls (Fig. 8A-C). However, fetuses born to previously infected mothers had a significantly lower body weight at gd. 18.5 (Fig. 8D). Infection of the mother did not affect placental morphology as evaluated by placental histology. No differences between placental tissue were detected regarding the size of placental compartments and calculated placental ratio (Fig. 8E-H).

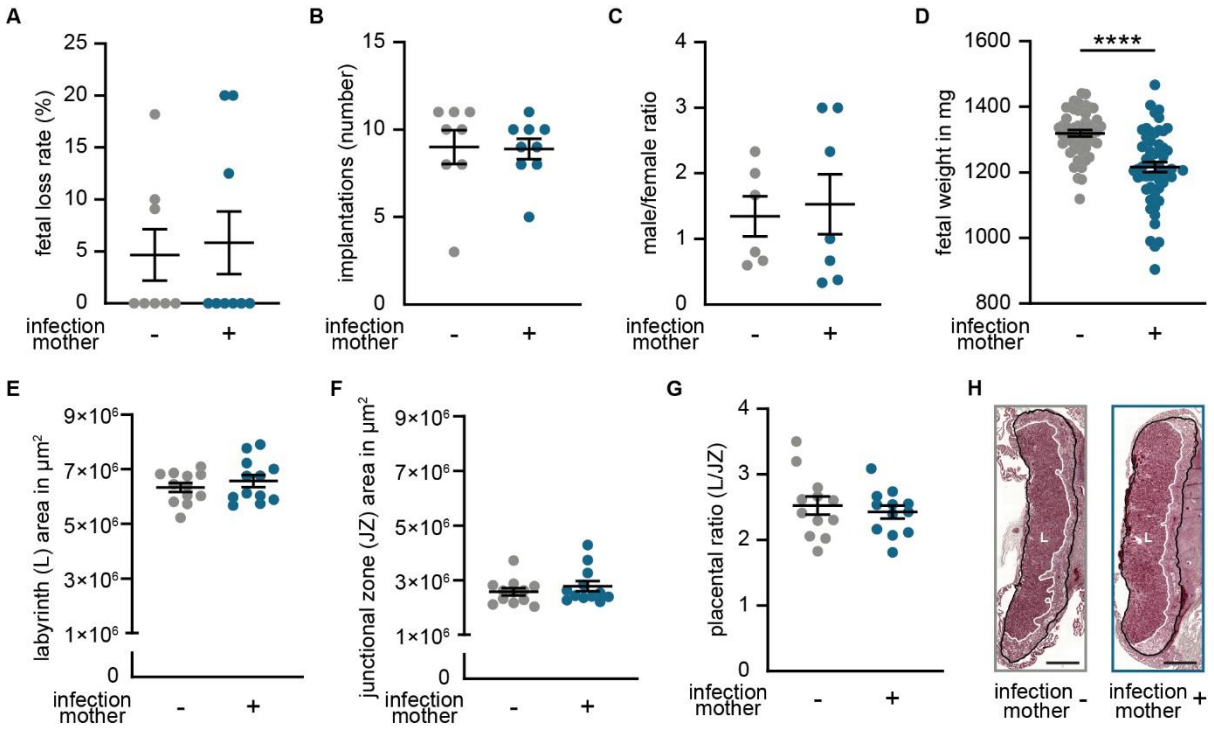

Figure 8. No differences in pregnancy outcome following preconceptual infection.
(A) Percentage of fetal loss rate (*n*=8, *n*=9). **(B)** Number of implantations on gd 18.5 (*n*=7, *n*=9). **(C)** Male/female ratio of offspring (*n*=6, *n*=7). **(D)** Fetal weight on gd 18.5 (*n*=54, *n*=55). **(E)** Area of placental labyrinth (L) (*n*=12 each). **(F)** Area of placental junctional zone (JZ) (*n*=12-13). **(G)** Ratio of placental labyrinth to the junctional zone (L/JZ ratio) as an indicator for placental function on gd 18.5 (*n*=12 each). **(H)** Representative depiction of murine placenta assessment, highlighted for labyrinth (L, white) and labyrinth + junctional zone (black). Bar=1000 µm. **(A-G)** Scatter-plots represent mean ±SEM. Asterisks indicate significance level of unpaired Student's t-test or Mann-Whitney-U test after testing for normal distribution.

To identify MMc in the fetal tissue, MMc were detected based on the expression of CD45 variants and the H-2D haplotype.[72] For this, an established allogenic mating model was used, in which leukocytes from female mice were homozygous for CD45.2 and H-2D^{b}, whereas those of males were homozygous for CD45.1 and H-2D^{d}. Consequently, MMc can be detected by selecting for CD45.2^{+}CD45.1^{-} and H-2D^{b+}H-2D^{d-} cells among CD45.1^{+}CD45.2^{+} and H-2D^{b+} H-2D^{b+} fetal cells (Fig. 9A). Since MMc number are sparse among fetal cells, enrichment of MMc via magnetic-activated sorting subsequently to tissue-processing was performed.[72] Fetal cells expressing the paternal markers CD45.1 and H-2D^{d} were labelled with magnetic beads and retained in the column by applying a magnetic field, whereas CD45.1^{-} and H-2D^{d-} MMc were enriched in the flow-through. No differences in MMc number in bone marrow, spleen and liver were observed between fetuses of preconceptually infected mothers and controls (Fig. 9B-D). Similarly, the percentage of microchimeric CD3^{+} T cells in bone marrow, spleen and liver were comparable between groups (Fig 9E-G). In the fetal bone marrow and the spleen, the frequencies of CD3^{+} B220^{+} MMc were higher in fetuses of preconceptually infected mothers, whereas frequencies of myeloid MMc were decreased compared to controls. Further microchimeric dendritic cells were lower in the bone marrow and liver of fetuses born to infected mice (Fig. 9E-G). Staining of MMc with OVA tetramers revealed OVA-specific CD3^{+} T cells in the fetal bone marrow, spleen and liver of fetuses of preconceptually infected mothers, providing evidence for an intergenerational transfer of OVA-specific T cells from the mother to the fetus during pregnancy (Fig. 9H). Comparable percentages of OVA-specific T cells were found in all three investigated fetal organs, suggesting non-organ specific distribution of cells in the fetus (Fig. 9I-K).

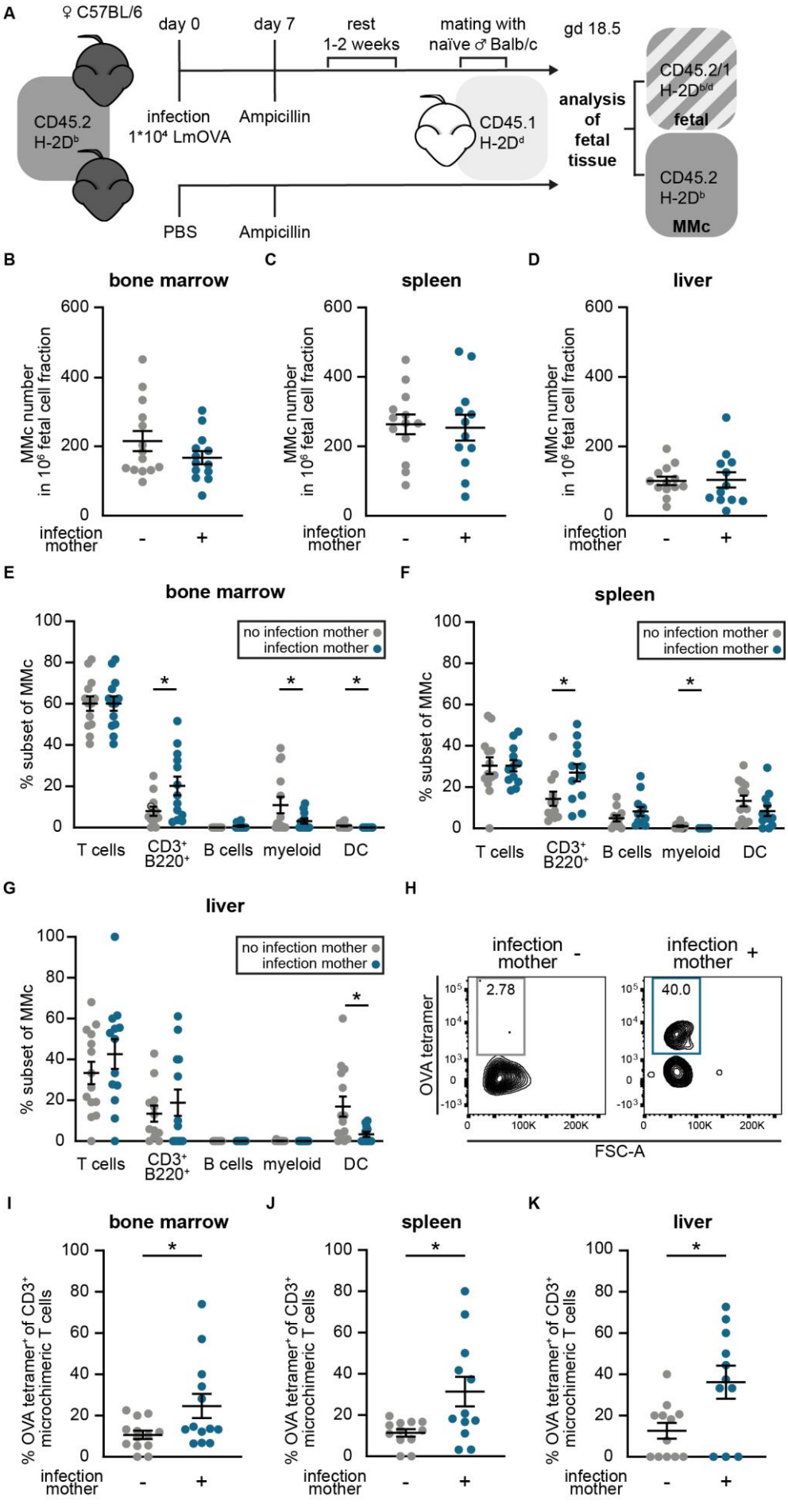
A
♀ C57BL/6
day 0
day 7
rest
1-2 weeks
mating with
naïve ♂ Balb/c
gd 18.5
CD45.2
H-2D^b
infection
1*10^4 LmOVA
Ampicillin
CD45.1
H-2D^d
analysis
of
fetal
tissue
CD45.2/1
H-2D^b/d
fetal
CD45.2
H-2D^b
MMc
PBS
Ampicillin
B
bone marrow
C
spleen
D
liver
MMc number
in 10^6 fetal cell fraction
infection
mother
E
bone marrow
F
spleen
no infection mother
infection mother
% subset of MMc
T cells
CD3+
B220+
B cells
myeloid
DC
G
liver
H
infection
mother -
infection
mother +
2.78
40.0
OVA tetramer
FSC-A
I
bone marrow
J
spleen
K
liver
% OVA tetramer+ of CD3+
microchimeric T cells

Figure 9. Transfer of OVA-specific MMc from mother to fetus.

(A) Infection, mating and identification strategy for maternal microchimeric cells (MMc) in offspring of CD45.2^{+}H-2D^{b+} C57BL/6 females mated with CD45.1^{+}H-2D^{d+} Balb/c males. **(B-D)** Numbers of MMc in 10^{6} fetal cells on gd 18.5; **(B)** bone marrow (*n*=14, *n*=13), **(C)** spleen (*n*=14, *n*=12), **(D)** liver (*n*=13, *n*=12). **(E-G)** Percentages of MMc subtypes characterized by expression of CD3, B220, CD11b and CD11c of CD3^{+} T cells of total MMc; **(E)** fetal bone marrow (*n*=13-14), **(F)** fetal spleen (*n*=12-13), **(G)** fetal liver (*n*=13-14). **(H)** Representative dot plots for OVA-tetramer staining of CD3^{+} MMc from spleens of fetuses of previously infected or non-infected mothers. **(I-K)** percentage of OVA-specific MMc stained with OVA tetramers among CD3^{+} T cell MMc; **(I)** bone marrow (*n*=13 each), **(J)** spleen (*n*=12 each), **(K)** liver (n=11, *n*=12). **(B-G, I-K)** Scatter-plots represent mean ±SEM. Asterisks indicate significance level of unpaired Student's t-test or Mann-Whitney-U test after testing for normal distribution.

3.1.3 Neonates born to preconceptually infected mothers show a higher robustness against infection.

In order to investigate the consequence of OVA-specific MMc for the immune response of the neonates, neonates born to preconceptually infected mothers and control mice were infected with *L. monocytogenes* and analysed indicators of neonatal fitness as well as MMc numbers.

Neonates were infected with an LmOVA strain deficient for the *act*A gene (LmOVA Δ*act*A) at day 7 after birth (Fig. 10A). LmOVA Δ*act*A induces a profound immune response without killing the neonate due to deficiency of the actin polymerizing ActA protein required for transcellular dissemination of the pathogen within the host.[122] Starting with the day of infection, neonatal weight as a surrogate for overall fitness was monitored at 4 different time points (Fig. 10B). Neonates born to previously infected mothers show a higher body weight at postnatal day 14 – 7 days after infection with LmOVA Δ*act*A – when compared to infected offspring born to control mothers indicating a higher robustness of neonates to homologous infection (Fig. 10C-F).

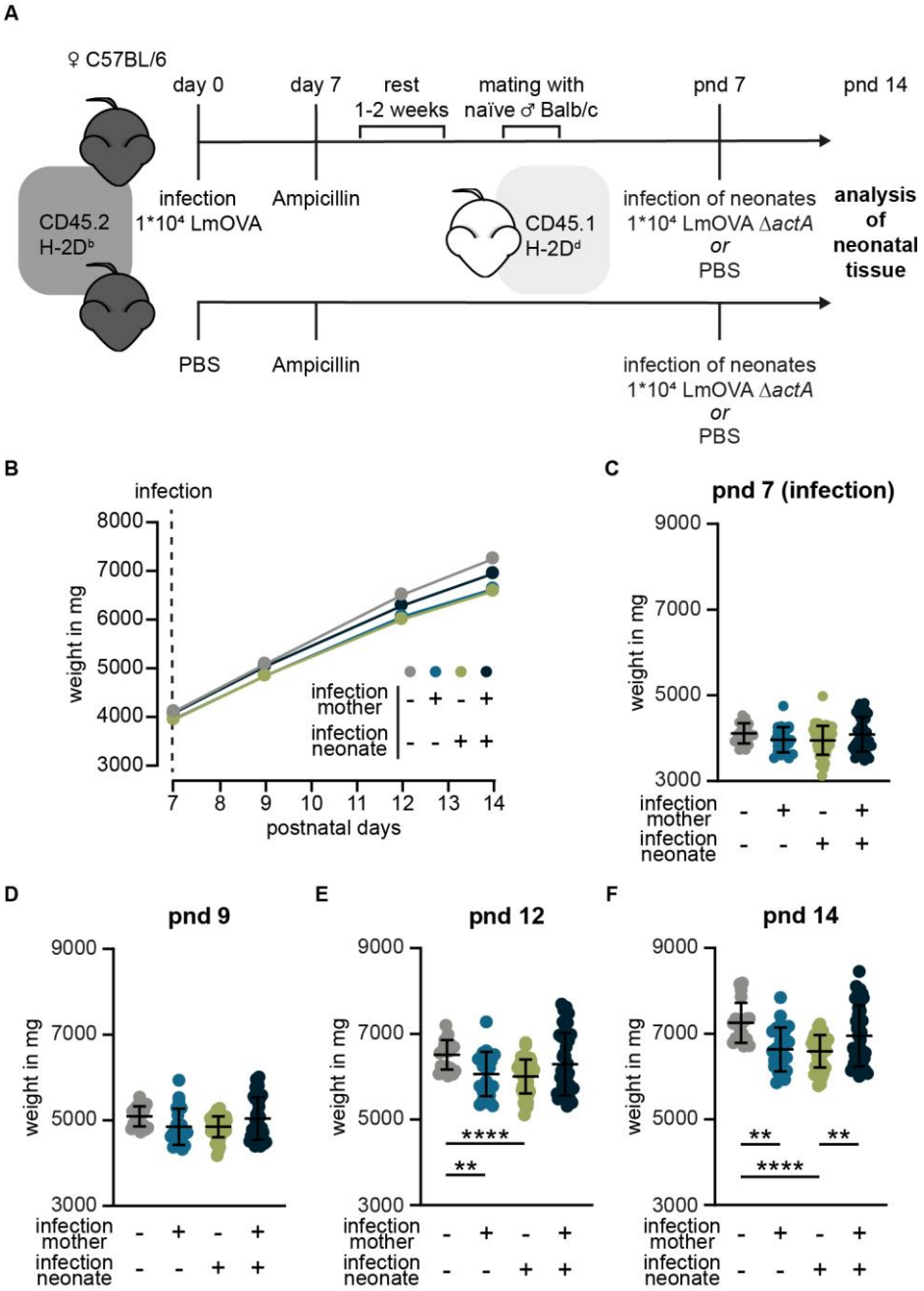

Figure 10. Higher robustness to infection of offspring born to preconceptually infected mothers. **(A)** Mating strategy and infection of neonates. **(B)** Neonatal body weight development in mg after infection of neonates at postnatal day 7. **(C-F)** Body weight gain in mg starting at day of infection with LmOVA Δ*act*A (*n*=20-55); **(C)** pnd 7 (day of infection), **(D)** pnd 9, **(E)** pnd 12, **(F)** pnd 14. **(C-F)** Scatter-plots represent mean ±SEM. Asterisks indicate significance level of Ordinary one-way ANOVA or Kruskal-Wallis test after testing for normal distribution. pnd: postnatal day.

3.1.4 OVA-specific MMc are associated with an activated phenotype of CD3$^+$ T cells following neonatal infection.

Since a higher robustness of neonates born to preconceptually infected mothers was observed, in a next step the expansion of OVA-specific MMc and the neonatal immune response against infection were investigated.

At day 14 after birth and 7 days after infection with LmOVA Δ*act*A, MMc could be still detected in the neonatal spleen and liver (Fig. 11A, B) and CD3$^+$ T cell frequencies within the MMc subset were comparable between neonates born to preconceptually infected mothers and control mothers (Fig 11C, D). Within the CD3$^+$ T cell compartment, only background levels of OVA-specific T cells in the spleen and liver of neonates born to preconceptually infected mothers were detected (Fig. 11E-F). Thus, infection of the neonates with LmOVA Δ*act*A did not result in the expansion of OVA-specific T cell MMc. However, infection with LmOVA Δ*act*A induced an immune response in the neonates as indicated by elevated offspring CD3$^+$ T cells number and the formation of OVA-specific offspring CD3$^+$ T cells in the spleens of infected neonates (Fig. 11G, H). Further, infection with LmOVA Δ*act*A led to activation of neonatal CD3$^+$ T cells indicated by expression of CD11b$^+$ and CD11c$^+$ which was more pronounced in neonates born to previously infected mothers (Fig. 11I, J).

OVA-specific MMc were not expanding upon homologous infection of neonates. Instead a more pronounced activated phenotype of T cells in neonates born to preconceptually infected mothers compared to controls was identified indicating a function of OVA-specific MMc other than pathogen-clearance.

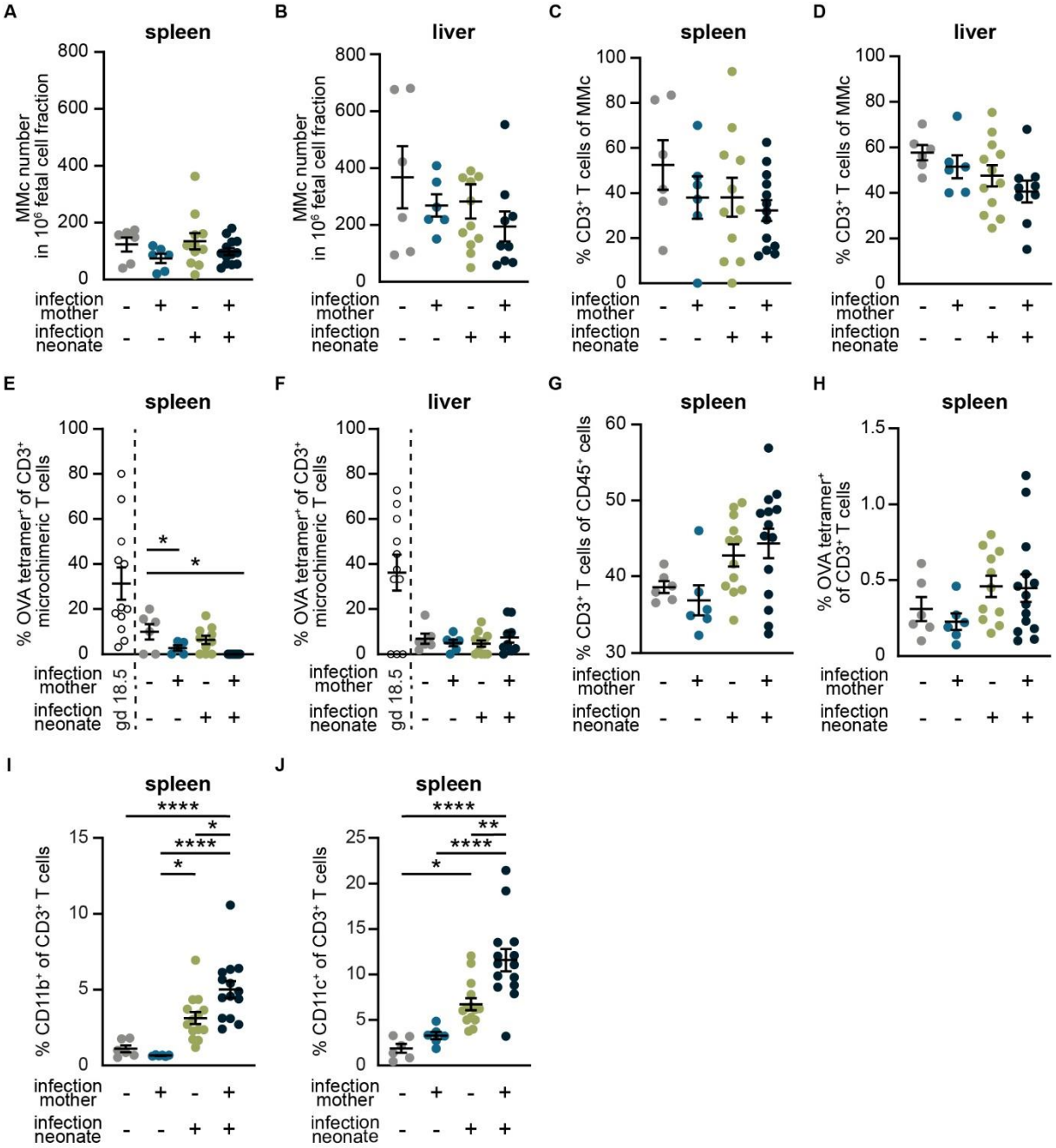

Figure 11. Transfer of OVA-specific MMc is associated with increased activation of neonatal T cells.

(A, B) Number of MMc in 10^6 fetal cells on day 7 after infection; **(A)** spleen (*n*=6-14), **(B)** liver (*n*=6-11). **(C, D)** Percentage of $CD3^+$ T cells among MMc; **(C)** spleen (*n*=6-13), **(D)** liver (*n*=6-12). **(E, F)** Percentages of OVA tetramer$^+$ cells among $CD3^+$ MMc (percentages of OVA tetramer$^+$ among $CD3^+$ MMc at gd 18.5 [Fig. 9J, K] are included for direct comparison); **(E)** spleen (*n*=5-10), **(F)** liver (*n*=5-10). **(G-J)** Neonatal T cell response. **(G)** Percentage of $CD3^+$ T cells of $CD45^+$ spleen cells (*n*=6-14). **(H)** Percentage of OVA-specific cells of $CD3^+$ T cells from spleens (*n*=6-14). **(I)** Percentage of $CD11b^+$ of $CD3^+$ T cells (*n*=6-14). **(J)** Percentage of $CD11c^+$ of $CD3^+$ T cells (*n*=6-14). **(A-J)** Scatter-plots represent mean ±SEM. Asterisks indicate significance level of Ordinary one-way ANOVA or Kruskal-Wallis test after testing for normal distribution.

3.2 Modulation of brain tissue by MMc

For this section, I conducted a follow up project to the findings reported in Schepanski *et al*., which highlights the role of MMc in the developing murine brain by maintaining microglia homeostasis.[73] MMc were shown to cluster in the prefrontal cortex, where they impede excessive microglia phagocytosis of neuronal branches. Accordingly, the absence of MMc in murine brains leads to increased presynaptic elimination, which manifest in neurocognitive impairments of neonates. For my project, I aimed to use an *ex vivo* method that provides information on the effects of MMc depletion on the surrounding brain tissue. For this, I established a cooperation with the ALBA synchrotron in Catalonia, Spain, to perform synchrotron-based µFTIR on brain section of MMc_{low} mice. Spectroscopy techniques such as FTIR spectroscopy are widely established for optical analysis of biomaterials. They provide spectral phenotyping of single (living) cells or tissues based on their biochemical properties. FTIR has the advantage of being labelling free, nondestructive to the tissue, and that it requires a minimum of sample preparation. However, it provides information on a molecular level by giving insights on functional groups and molecular conformations of biomolecules.[117,123] In short, based on the vibrational frequency of molecules present within a substance, infrared radiation is absorbed resulting in a characteristic spectral profile of the sample. A coupling of FTIR spectroscopy and microscopy allows the focus of the infrared laser on a distinct point on the sample instead of providing an averaged signal from the whole sample.[124] Sections of the prefrontal cortex of neonatal mice were analyzed to gain insights on the biochemical profile in the presence or absence of MMc.

3.2.1 Mapping of the prelimbic cortex and whole brain sections of MMc_{low} and control mice

To analyse the effects of MMc on their surrounding tissue a mouse model was used in which MMc were experimentally reduced. For this $Rag2^{-/-}$IL-2r$\gamma c^{-/-}$ female mice were mated with wildtype males. $Rag2^{-/-}$IL-2r$\gamma c^{-/-}$ lack T and B cells and have reduced numbers of innate lymphoid cells leaving them immunodeficient. The offspring of this mating combination are immocompetent but are deprived of the respective microchimeric immune cell populations and are therefore referred to as MMc_{low} (Fig. 12A).

In order to visualize the infrared profile of the prefrontal cortex in MMc_{low} and control mice, five brain sections of each group were prepared (Fig. 12B). Since clustering of MMc was demonstrated in the prelimbic cortex, responsible for decision making processes and working memory, this area was closely mapped by µFTIR resulting in 1 raw infrared spectrum per measurement point and 650 spectra for the whole target area (Fig. 12C). After normalization, all spectra of each MMc_{low} or control group sample (650 spectra each) were averaged. The averaged spectra provide insights on the functional groups of the tissue section based on their characteristic spectral profiles (Fig. 12D).

In addition to the high-resolution mapping of the prelimbic cortex, I further performed mapping of whole brain sections, to generate overviews on the dominant functional groups across the tissue. The whole section of the brain was scanned overnight in high resolution resulting in over 11.500 spectra. By calculating the ratio of specific functional groups for each measurement point, a detailed map can be generated that shows the local differences within the brain areas. As an example the ratio of lipids and amids for the control group is shown (Fig. 12E).

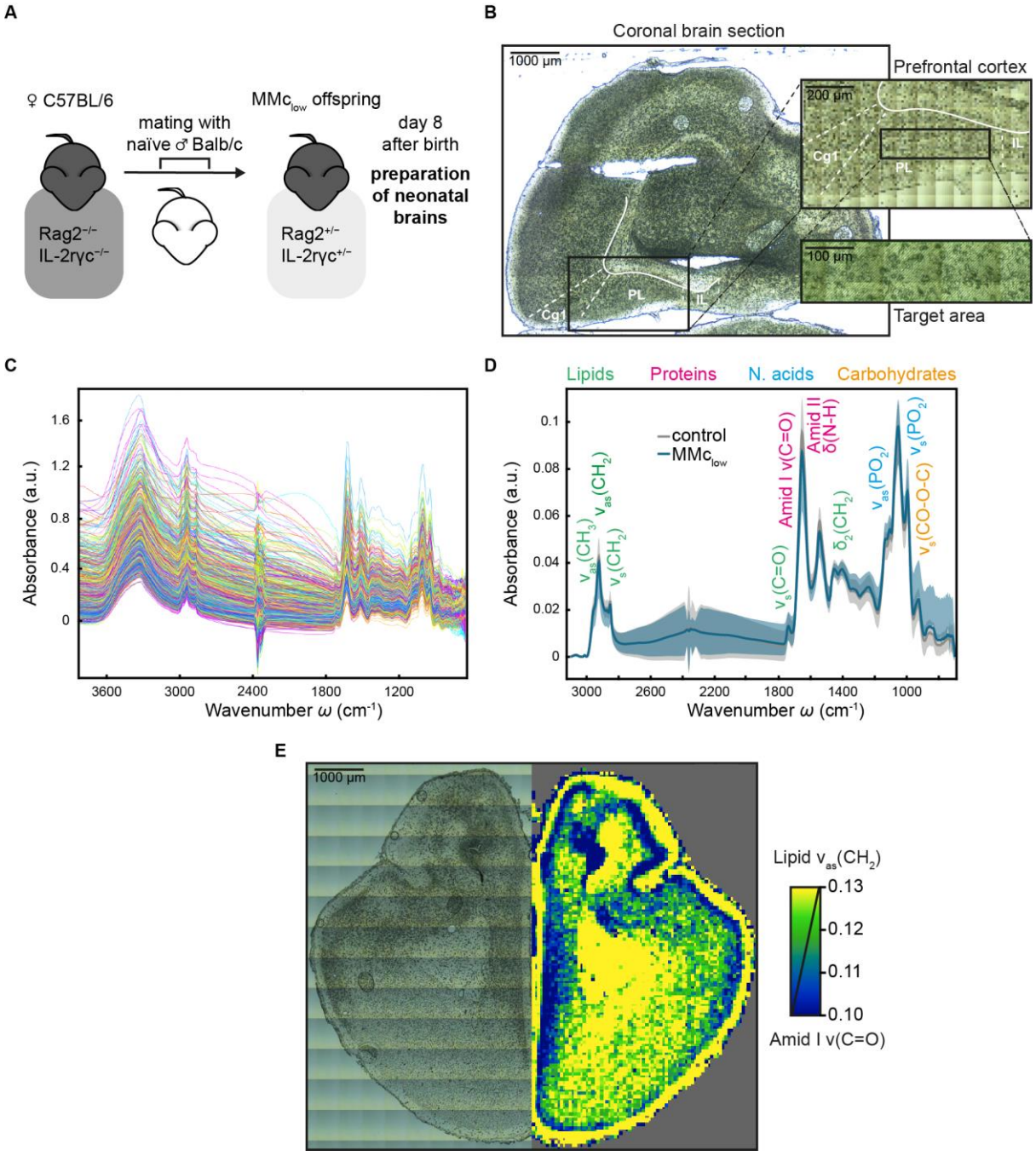

Figure 12. Processing of biochemical spectra derived neonatal murine brain prelimbic cortex and whole brain sections.

(A) Mating strategy of Rag2$^{-/-}$ IL-2rγc$^{-/-}$ and wiltype Balb/c males to generate male offspring with reduced levels of MMc (MMc_{low}) **(B)** Coronal brain section of neonatal murine brain. Detailed depiction of the prefrontal cortex with the cingulate area (Cg1), prelimbic cortex (PL) and infralimibic cortex (IL). Zoomed in illustration of the target are within the prelimbic cortex mapped via µFTIR. **(C)** Exemplary depiction of 100 raw spectra obtained from mapping the prelimbic cortex; each spectra represents the biochemical profile of an 10 µm x 10 µm. **(D)** Normalized and averaged biological spectra of the prelimbic cortex of control and MMc_{low} mice depicted for the wavenumber of 3100-800 cm^{-1}. Spectra shadowing indicates standard deviation (*n*=5 for each group; average spectra calculated based on 650 spectra of each sample). Exemplary peak assignments for their respective functional group are depicted, where v=stretching vibrations, δ=bending vibrations, s=symmetric vibrations, as=asymmetric vibrations. **(E)** Exemplary depiction of the lipid/amid ratio of a control neonatal murine brain.

3.2.2 Carbohydrate properties prelimbic cortex differ between control and MMc_{low} mice

To enable statistical analysis of peaks as representative of various functional groups and their biochemical properties, the second derivation of the normalized, averaged spectra was calculated (Fig. 13A). Infrared spectra were analysed for differences in the lipid, protein, carbohydrate and nucleic acid region as listed in Table 9. Significant differences between groups of mice were found within the region of carbohydrates highlighted in grey (Fig. 13A) and depicted in detail based on variation of the average spectra between groups (Fig. 13B). To quantify the difference of carbohydrates in the prelimbic cortex of neonatal murine brains, ratios of the respective infrared wavenumber absorptions after the second derivative were performed. For carbohydrates, stretching vibrations of hydroxyl (C-OH), ester (CO-O-C), unsaturated olefinic (C=C), and carbonyl (C-O) groups normalized to the Amid I band were quantified. Our results show that the prelimbic cortex of MMc_{low} neonates contain more hydroxyl (Fig. 13C), ester (Fig. 13D), and unsaturated olefinic/carbonyl (Fig. 13E) groups compared to control group. This indicates that MMc shape their local microenvironment and depletion of MMc results in alteration of the biochemical properties of their respective tissue. These alterations are especially affecting functional groups related to carbohydrates.

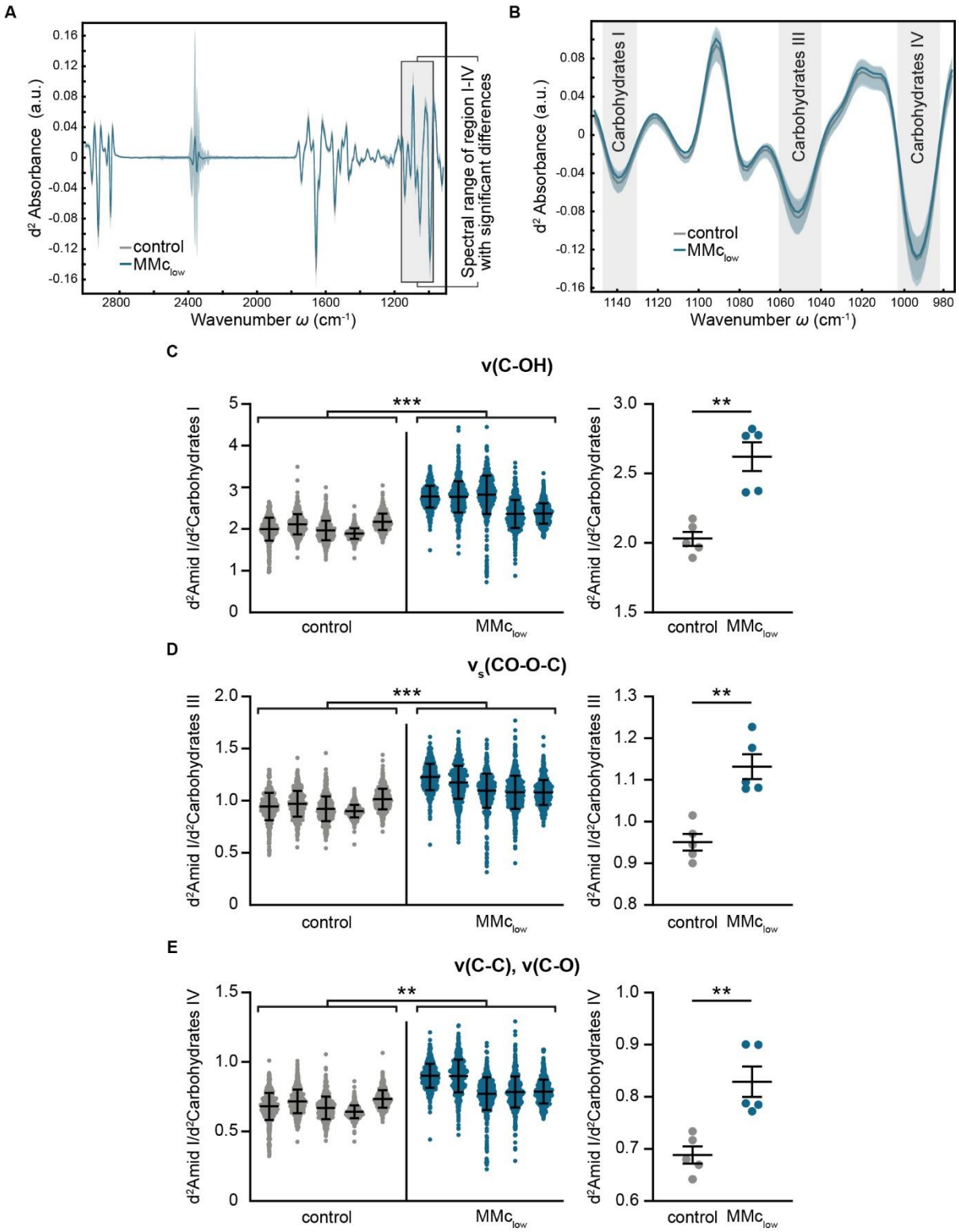

Figure 13. Differences in carbohydrates in the prelimbic cortex of control and MMc_{low} mice.

(A) Averaged biological spectra after the second derivatives were calculated and unit vector normalization was performed. Grey area depicts spectral regions with significant differences between control and MMc_{low} mice; a.u.=arbitrary units **(B)** Zoomed in grey region highlighted in A. Peaks for defined chemical profiles characteristic for carbohydrates (see Table 9) are highlighted in grey and are statistically analysed for differences. **(C-E)** Graphs represent absorbance second derivate (d^2) ratios of carbohydrate functional normalized to the Amid I band (1649-1664 cm^{-1}). Left: Measurements of 5 independent brain sections for each group – control and MMc_{low} mice – are depicted, where each dot represents one of 650 obtained spectra. Scatter-plots represent mean ±SEM. Asterisks indicate significance level of nested T-test. Right: Each dot indicates the mean of 650 infrared measurements

from one murine brain section (*n*=5). Scatter-plots represent mean ±SEM. Asterisks indicate significance level of unpaired Student's t-test.

3.3 Placenta-derived EV as indicator for cellular placental transfer

MMc need to trespass the placental barrier to reach the fetal tissue. Although, it can be assumed that the placenta plays a pivotal role in the regulation of MMc transfer, little is known regarding the properties of the placental tissue that promote or impair MMc transfer. This is partly due to the limited options for the evaluation of placenta function during an ongoing pregnancy, which is currently restricted to ultrasound assessments. In the clinics, ultrasound assessments are well established but they provide no information on the placental transfer rate. I sought to analyse placenta-derived EV isolated from maternal blood samples as a proxy for the placental tissue, since their proteomic profile mirrors that of the placenta. Placenta-derived EV were assessed in healthy pregnant women that participated in the PRINCE study and pregnant women that suffered from SARS-CoV-2 infection during pregnancy that participated in the PRINCE-COVID study.

3.3.1 COVID-19 infection during pregnancy alters placental cellular transfer and the formation of placenta-derived EV

Screening for maternal microchimerism in the cord blood was performed as described in Stelzer *at al*.[72] Assessment of MMc in the cord blood of healthy mothers of the PRINCE study revealed a high variation in the number of MMc (Fig. 14A). Pregnancy-associated SARS-CoV-2 infection impaired the transfer capacity of the placenta by strongly reducing the transfer of MMc from the mother to the fetus as demonstrated for the PRINCE-COVID cohort (Fig. 14A). EV were isolated from serum samples of pregnant women by using cushion-ultracentrifugation (Fig. 14B). Analysis of EV by imaging flow cytometry showed no differences in the total number of tetraspanin$^+$ EV between non-pregnant controls, the women of the PRINCE cohort and women of the PRINCE-COVID cohort (Fig. 14C). However, evaluation of placental-derived EV by using the placenta-specific antibody PLAP demonstrate a higher percentage of placenta-derived EV in women of the PRINCE-COVID cohort (Fig. 14D).

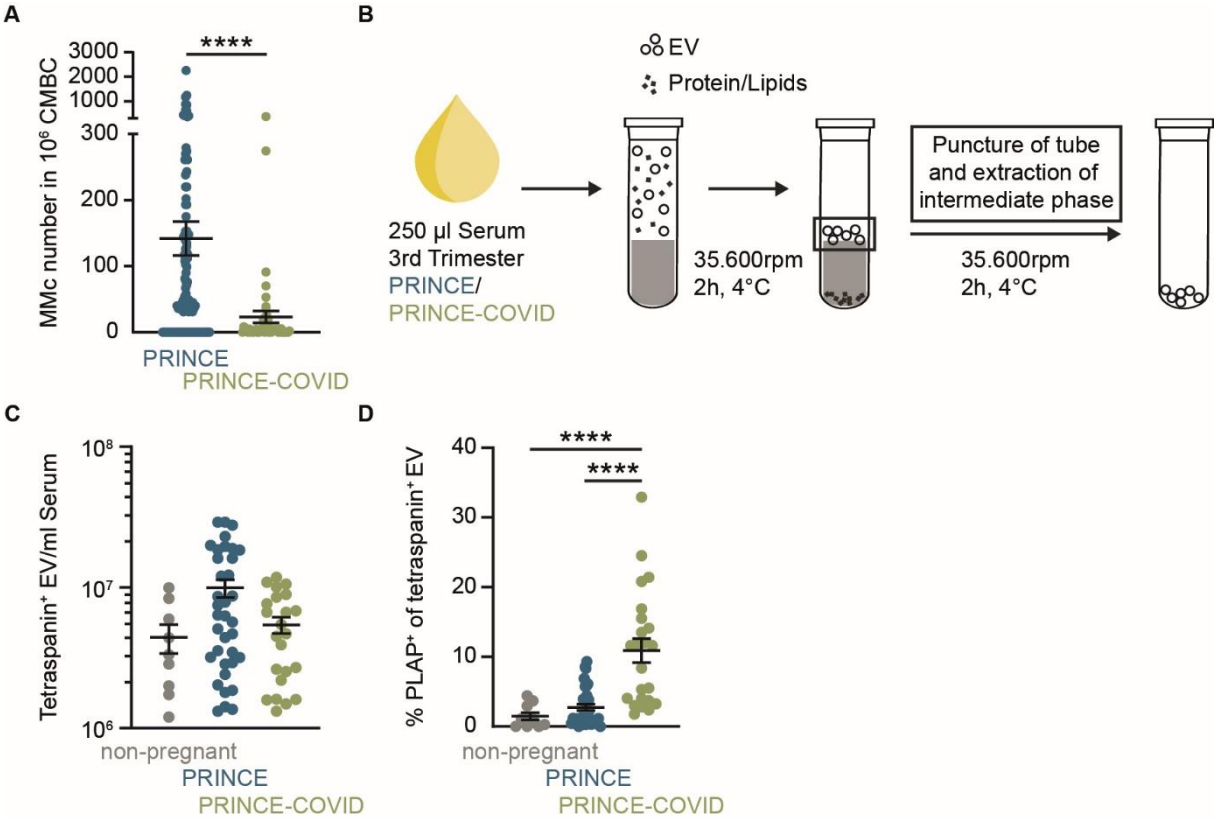

Figure 14. SARS-CoV-2 infection during pregnancy increases the percentage of placenta-derived EV.

(A) Number of MMc in 10^6 cord blood mononuclear blood cells (CMBC) (PRINCE: *n*=123, PRINCE-COVID: *n*=51). **(B)** Isolation of EV via cushion ultracentrifugation from maternal 3rd trimester serum samples. **(C)** Number of tetraspanin⁺ EV per ml serum measured via Imaging Flow Cytometry (*n*=9-36). **(D)** Percentage of PLAP⁺ EV among tetraspanin⁺ EV (*n*=10-34). **(A, C, D)** Scatter-plots represent mean ±SEM. Asterisks indicate significance level of **(A)** Mann-Whitney-U test, **(C, D)** Ordinary one-way ANOVA or Kruskal-Wallis test after testing for normal distribution.

3.3.2 Sex-specific differences in the dysregulation of MMc transfer and EV formation

In order to directly link the transfer of MMc to the formation of EV, they were either correlated with the total number of tetraspanin⁺ EV or placenta-derived EV. Comparison between participants of the PRINCE and the PRINCE-COVID study revealed sex-specific differences between groups. Within the PRINCE study, the number of tetraspanin⁺ EV was positively correlated with the number of MMc found in the cord blood of female neonates (Fig. 15A). This correlation was reversed for female neonates born to SARS-CoV-2 infected mothers of the PRINCE-COVID study (Fig. 15B). In male neonates, no correlation was observed (Fig. 18A, B, Supplement) Similarly, the number of PLAP⁺ EV was positively correlated with the number of MMc found in the cord blood of female neonates (Fig. 15C). This correlation was absent in female neonates born to participants of PRINCE-COVID study (Fig. 15D). In male neonates of the PRINCE study, no positive correlation of PLAP⁺ EV with MMc numbers was observed (Fig. 18C, D, Supplement).

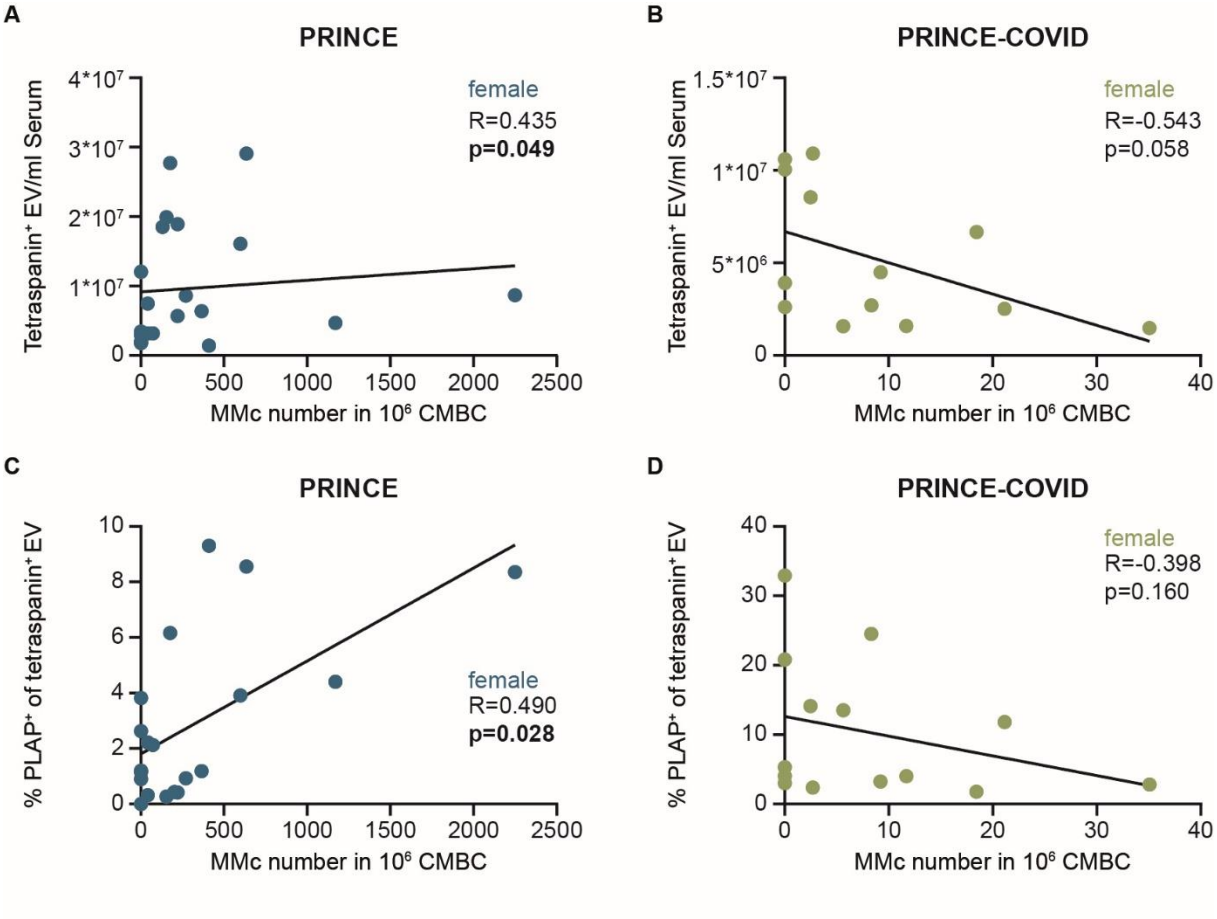

Figure 15. Maternal immune activation by SARS-CoV-2 infection abrogates the correlation of EV and MMc.

Correlation of tetraspanin$^+$ EV with the number of MMc in 10^6 cord blood mononuclear blood cells (CMBC) from female neonates born to mothers that participated in the **(A)** PRINCE study or **(B)** PRINCE-COVID study. Correlation of PLAP$^+$ EV with the number of MMc in 10^6 CMBC from female neonates born to mothers that participated in the **(C)** PRINCE study or **(D)** PRINCE-COVID study.

3.3.3 Placenta-derived EV share a common proteomic profile according to the placental transfer of MMc

In order to investigate whether placenta-derived EV provide information on the placental cellular transfer, proteomic profiling of PLAP$^+$ EV derived from the PRINCE cohort was conducted.

In order to increase the purity of PLAP$^+$ EV for proteomic analysis of healthy PRINCE, they were specifically coupled to magnetic beads that bind to the PLAP-conjugated fluorophore and subsequent enriched by applying a magnetic field. As shown by the fold increase, PLAP$^+$ EV (before enrichment ≈10%) were significantly enriched in the tube bound fraction compared to the supernatant (Fig. 16A). In order to identify possible differences in the protein profile of enriched PLAP$^+$ EV according to the cellular transfer capacity of the respective placenta, nine PLAP$^+$ EV samples were selected that originate from women with no transferred MMc up to women with very high transfer numbers of MMc as detected in their cord blood. Using proteomic analysis 1955 proteins could be quantified. Principal component analysis of the proteomic data revealed clustering of samples based on the number of MMc in found in the

cord blood. In order to form groups for statistical analysis, they were manually assigned to MMc_{low}, MMc_{mid} and MMc_{high} groups (Fig. 16B). Comparison of differentially expressed proteins (DEPs) (n=103) between MMc_{low} and MMc_{high} samples based on their p-value and the log2-fold change of individual proteins revealed clear differences between groups as depicted as the normalized log2 intensity in a heat map (Fig. 16C). The MMc_{mid} sample was integrated as a control for the transition of MMc_{low} to MMc_{high}. DEPs were separated in proteins that were up-regulated in samples belonging to the MMc_{low} and MMc_{high} group of PRINCE study participants. This revealed that placenta-derived EV from pregnant women who transfer low numbers of MMc are characterized by a unique protein fingerprint (84 proteins with higher expression), whereas substantially less proteins were up-regulated in the samples of mother that transfer high numbers of MMc (19 proteins with higher expression) (Fig 16D). Full names of DEPs depicted in Fig. 16C and D together with their respective p-value and log2 fold change are listed in Table 10 within the supplement section. As shown based on their log2-fold change, some proteins are particularly differently expressed between groups, e.g., FLOT1, HMGA2, HMGN1 in MMc_{low}.

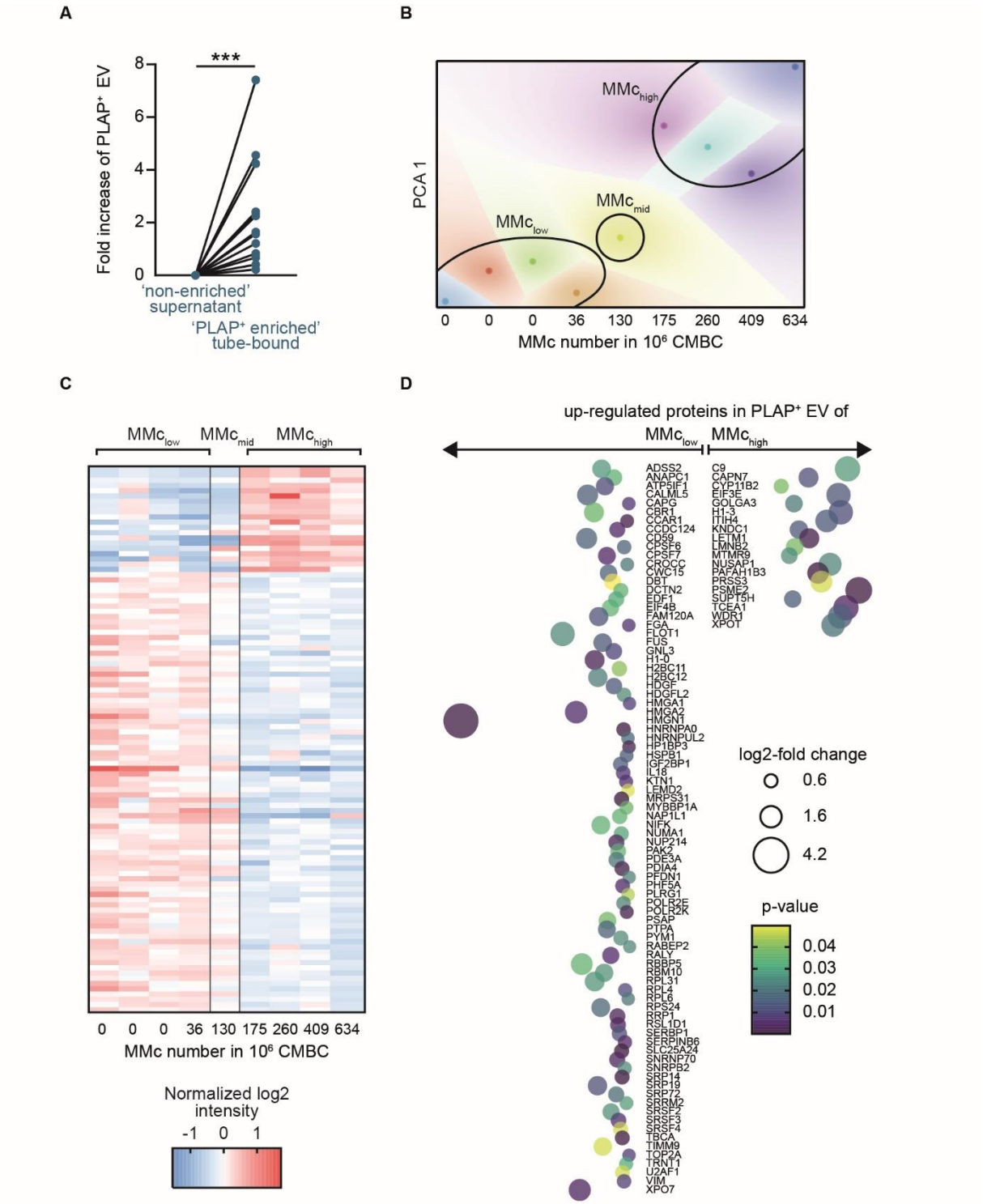

Figure 16. EV samples from MMc$_{low}$ and MMc$_{high}$ study participants cluster and show a distinct proteomic profile.

(A) Fold increase of PLAP$^+$ EV among tetraspanin$^+$ EV in the enriched and non-enriched fraction after magnetic activated sorting (*n*=14). **(B)** PCA of the proteomic data derived from enriched PLAP$^+$ EV samples of mothers that participated in the PRINCE study selected based on their MMc transfer. Each dot represents one biological replicate. Clustering allows manual categorization into groups of MMc$_{low}$, MMc$_{mid}$ and MMc$_{high}$. **(C)** Heat map of DEPs between MMc$_{low}$ and MMc$_{high}$ samples (n=103) depicted as normalized log2 intensity. **(D)** Individual up-regulated DEPs (MMc$_{high}$ n=84 and MMc$_{low}$ n=19) in enriched PLAP$^+$ EV from samples of PRINCE study participants. The circle size depicts the log2-fold change and the circle color the p-value. **(A)** Asterisks indicate significance level of Mann-Whitney-U test.

3.3.4 Placentas that transfer low numbers of MMc share a unique EV fingerprint strongly related to RNA binding

Functional gene ontology analysis of DEPs using the DAVID Bioinformational Database revealed that they are mostly comprised of proteins located in the nucleoplasm and the cellular nucleus but also encompass proteins from the cytosol (Fig 17A). The vast majority of proteins are functionally involved in binding of RNA and protein. Accordingly, DAVID functional GO analysis further indicate that the identified proteins are biological processes associated with mRNA splicing and transcription (Fig 17A). This is further substantiated by the Pathway analysis using the Reactome Database. DEPs were mainly associated with mRNA splicing and processing (Fig. 17B). Further, they are linked to the formation of senescence-associated heterochromatin foci, indicating a senescent status of the placenta tissue which is reflected by the protein profile of their EV.

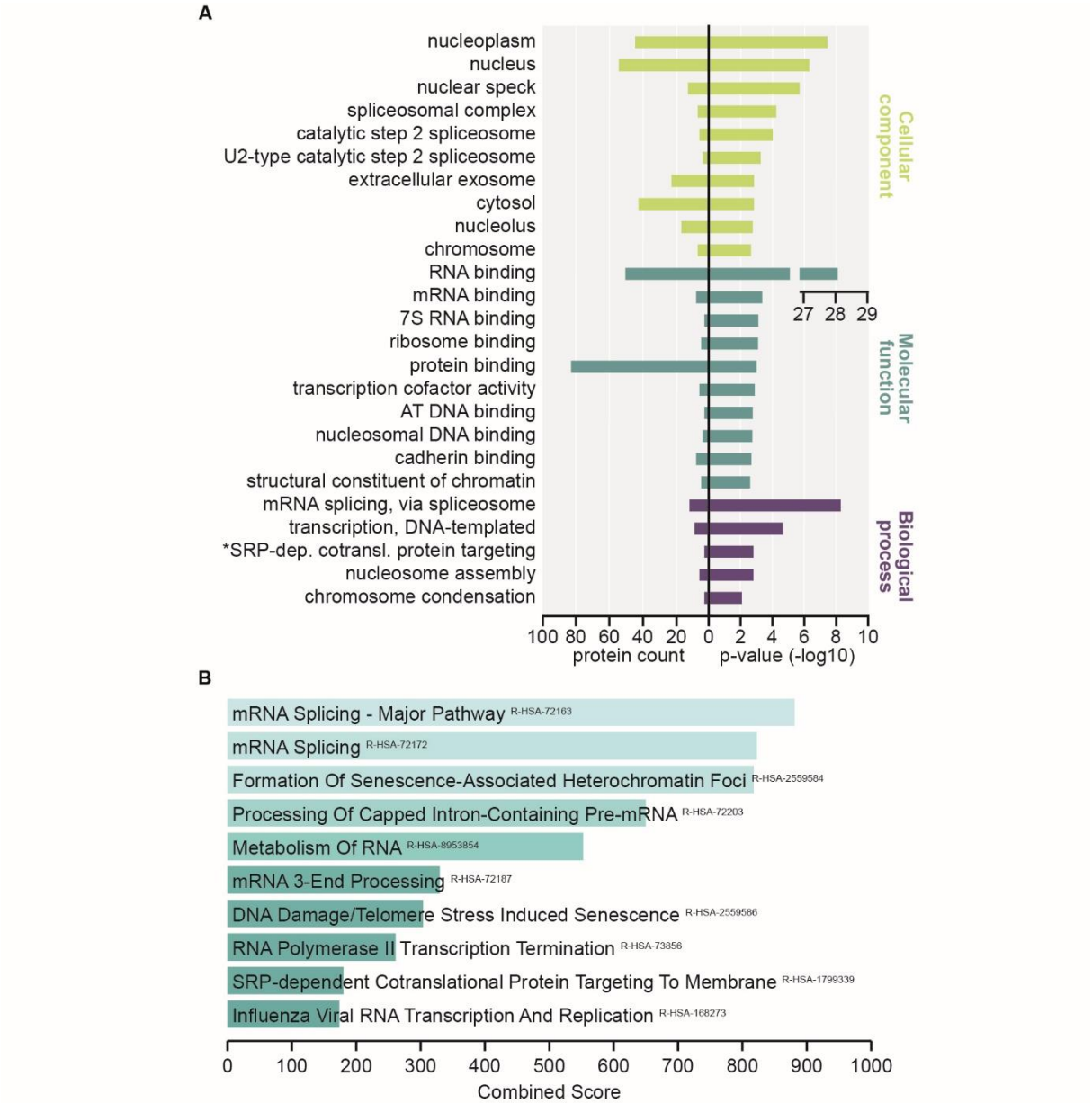

Figure 17. Placenta-derived EV samples have a unique proteomic profile associated with RNA binding and processing.

(A) DAVID functional GO analysis of DEPs between MMc_{low} and MMc_{high} samples depicting the protein count identified in DAVID-assigned terms (left) and their corresponding p-value (right). **(B)** Reactome pathway analysis based on DEPs between MMc_{low} and MMc_{high} samples depicting the Combined Score (created by the Reactome software based on the protein count, p-value and odds ratio). Superscript text indicate the exact pathway as listed in the Reactome data base. *SRP-dependent cotranslational protein targeting to membrane.

4 Discussion

This thesis aims to elucidate the function of MMc in the offspring and to contribute to the understanding of maternofetal transfer of cells. To comprehensively address these objectives, this work is structured in three different sections that cover the memory transfer by MMc, their relevance for the fetal brain tissue and the underlying regulation of MMc transfer. Each aspect contributes to the understanding of the overall relevance of MMc for the mother-child pair.

4.1 Maternofetal transfer of antigen-specific T cell

The first part of my dissertation provides first evidence for the intrauterine transfer of immune memory cells in the mouse model. Infection of female mice with LmOVA leads to the accumulation of $CD4^+$ and $CD8^+$ T cells in the uterus that include long-lasting OVA-specific $CD8^+$ EM T cells. During pregnancy OVA-specific cells were transferred to the fetus in which they colonize distant fetal organs. Offspring equipped with OVA-specific T cells exhibit a higher robustness to neonatal infection and show an increased activation of neonatal T cells.

Murine infection with listeria results in the preferential colonization of the liver and the spleen. Infection leads to a profound immune response that includes $CD4^+$ and $CD8^+$ T cells. After activation, $CD4^+$ and $CD8^+$ T cells accumulate in nonlymphoid tissues.[36,37,125] This includes the different compartments of the female reproductive tract, e.g., the ovary, vagina, cervix and the uterus.[39,126]

The properties of activated T cells in peripheral organs are altered by the usage of laboratory mice, which are reared in strictly controlled animal facilities. Through the lack of contact with pathogens and commensal they possess naïve peripheral organs lacking cell heterogeneity and a diverse microbiome, which affects the interaction with activated T cells.[127,128] Although immunologically naïve laboratory animals are highly advantageous for studying infection responses, there is valid doubt whether immunological findings provide sufficient external validity outside the laboratory context. Thus, it has been postulated to amend studies conducted in traditional laboratory animals with wild-derived mouse models, to reflect the reality of an experienced immune system.[128-130]

The enrichment of $CD8^+$ in the murine uterus following LmOVA infection is mainly comprised of EM T cells that have been shown to be partly OVA-specific. Accumulation of T cells in the uterus is not limited to listeria infection as it has been equally demonstrated in mice and humans after viral infection with HIV-1, HSV-2, CMV and EBV[131-133] or bacterial infection with chlamydia.[126,12]

Given the fact that the overall number of $CD4^+$ and $CD8^+$ T cells and the percentage of EM $CD8^+$ T cells remain elevated even after weeks following initial infection, they may have formed a tissue-resident T cell subset.[134,135] Although for my study this needs to be verified by using CD69 as marker for tissue-residency or CD103 as a marker for resident T cells within mucosal

tissues, parabiosis experiments conducted in mice infected with LCMV demonstrated the resident phenotype of memory T cells in the female reproductive tract.[39]

By focusing on gd 18.5, I analyzed the transfer of MMc after the end of the third trimester. It has been shown that MMc transfer starts with the successful placentation at the beginning of the second trimester in humans and around gd 10.5 in mice.[53,54,136,137] It is intriguing to speculate on the initial distribution of MMc, as they might colonize a specific organ at earlier time points in pregnancy and further spread or being relocated among other tissues. To answer this question a comprehensive study on MMc transfer and distribution is urgently needed.

On the maternal side, it is interesting to hypothesize on the origin of MMc that are transferred to the fetus. To date it is not entirely clear how MMc transfer is mediated and whether MMc are a result of placental leakage or whether specific cells are actively recruited to the feto-maternal interface. In this context, authors of a similar study postulate that the feto-maternal barrier favours the enrichment antigen-experienced T cells. They provide evidence for higher frequencies of OVA-specific $CD8^+$ T cells in the decidua after re-infection of pregnant mice with LmOVA following preconceptual infection.[138] This local enrichment might benefit the intrauterine transfer of antigen-specific MMc.

Similarly, one might speculate on how exactly MMc are selected since they are composed of various maternal cell types.[139] For now, it remains to be shown how the cellular composition of MMc is regulated or whether MMc are selected regarding their prevalence in the maternal blood circulation. Although my analysis solely focused on leucocytes, it already highlighted the cellular heterogeneity of MMc as they consist of T cells, B cells, myeloid cells, and dendritic cells. Despite the aforementioned MMc subtypes, I further identified $CD3^+B220^+$ MMc which were significantly higher in the bone marrow and liver after preconceptual infection of the mother compared to the control. Although there are several publications describing cells with these phenotype[140-142], their function and origin remain highly controversial and a matter of ongoing speculation.

With my study, I provide first evidence for the intrauterine transfer of maternal OVA-specific T cells to the fetus. These antigen-specific MMc could be detected in the fetal bone marrow, liver and spleen at gd 18.5. The observation of distribution of antigen-specifc MMc across different fetal organs matches the results for maternal OVA-specific $CD8^+$ EM T cells that were identified in the peripheral blood, lymph nodes, uterus, and spleen. Since MMc have been demonstrated to colonize a broad array of fetal tissues including the lung, skin and heart, it can be hypothesized that antigen-specific MMc might also be found in other fetal organs in addition to those analyzed. Still, in the case of OVA-specific MMc, they might prefere colonizing the fetal liver and spleen since they are known as the primary infection side of listeria.

My data shows high variablity cocerning the percentage of OVA-specifc T cells among total MMc. This observation reflects the MMc counts identified in human cord blood samples, which

vary drastically between mother-child pairs.[72,79] To date, there is no explanation for the variation between individuals. By performing histological evaluation of murine placentas, I can exclude morphological alterations affecting the size labyrinth zone, which in turn would affect contact of trophoblast cells and maternal blood. Further, it has been speculated that the activation status of the placental tissue plays an important role in mediating cellular transfer, since MMc need to bind to the tissue in order to overcome the placental barrier in a second step. It would be interesting to analyse murine placentas for cellular adhesion markers and link the results to the number of transferred MMc.

In a next step, I investigated the relevance of these OVA-specific MMc during infection of the offspring. To make sure that neonates are not influenced by the preconceptual infection of the mother, non-specific immune activation of the fetal immune system was excluded. Even after exposing the pregnant mice to a 'second-hit' of listeria infection, no activation of the neonatal myleoid immune populations could be detected. Still infection of the neonate indicated a higher robustness of offspring equipped with OVA-specific MMc, although no expansion of OVA-specific MMc could be detected as they were absent 7 days after infection. Still, infection led to an activation of neonatal T cells which verifies both the immunogenic properties of the used pathogen and the responsiveness of the neonatal immune system. Activaton of neonatal $CD3^+$ T cells in response to listeria was associated with an upregulation of the surface proteins CD11b and CD11c[143,144], which belong to the β2-integrin family and function as adhesion molecules for various ligands involved in cellular adhesion and phagocytosis.[145,146] Since the expression of CD11b and CD11c was significantly higher in neonates born to preconceptually infected mothers, antigen-specific MMc are associated with an enhancement of the neonatal T cell response during pathogen encounter.

This observation goes in line with data provided within a recent study, which shows that MMc are associated with an improved polyfunctional $CD4^+$ T cell response to Bacillus Calmette-Guérin vaccination. The authors further propose that MMc are involved in neonatal T cell regulation.[147,148] Thus, this observation contributes to the proposed concept that antigen-specific MMc seem to shape/educate the neonatal T cell response, rather than eliminating the pathogen directly.

This interpretation is challenged by a recent study on immunity against listeria. Typically, protection against intracellular pathogens is mediated through cellular immunity rather humoral protection.[149-151] However, this study conducted in mice now provides evidence that pregnancy creats an environment in which antibodies against listeria are differently glycosylated.[152] Their vertical transfer to the fetus and subsequent binding to regulatory B cells results in decreased IL-10 production and, as a consequence, a boosted immune response against neonatal infection with listeria. Although the finding of pregnancy as a unique state of antibody modification is exciting, it remains to be seen whether this mechanism is transferable to

different experimental settings. I used a low infection dosage of a virulent listeria strain in my experimental approach which contrasts to the high dosage of an attenuated listeria strain in the published study. Additionally, female mice underwent a strict antibiotic treatment, which might as well affect the formation of antibodies. Thus, I only detected marginal anti-listeria antibody titers in either the mother or the fetus. Consequently, I would argue that the increased neonatal T cell activation is associated with the antigen-specific MMc rather than an antibody transfer. However, as both mechanisms lead to a boosted T cell activity, it might be possible that they equally contribute to shaping the neonatal immune response.

Further, our experimental approach does not address the transfer of MMc via breast milk.[56] However, the absence of OVA-specific MMc at day 14 after birth suggest that their transfer mainly occurs intrauterine. Still, this needs to be validated by cross-fostering experiments.

Our findings raise question for the consequences of preconceptual or prenatal infection in women and the possible transfer of antigen-specific MMc in the womb. Since I used a well-established but artificial infection model, by utilizing an ovalbumin recombinant listeria strain to generate OVA-specific T cells, it will be interesting if the transfer of antigen-specific MMc can demonstrated for other pathogens as well. Also, it remains to be seen, if such transfer occurs during human pregnancy. If confirmed, e.g., in human cord blood samples, this might as well add another aspect to our understanding of vaccination strategies for pregnant women.

The transfer of antigen-specific MMc broadens our understanding on the transfer of immunological memory. Lining up with the well-known transport of antibodies through the placenta, MMc add a cellular component to the concept of maternal passive immunity.

4.2 Modulation of brain tissue by MMc

The second part of my dissertation covers a follow up project to the work published by Schepanski *et al.*[73] I investigated how MMc in the brain shape their surrounding tissue.

By applying µFTIR spectroscopy on brain tissue samples derived from murine neonates, alterations in the carbohydrate profile of the brain tissue in neonates deprived from MMc were detected. This observation contributes to our understanding of the direct effects of MMc on their surrounding tissue.

I was able to detect alterations in the biochemical profile of the brain parenchyma in MMc_{low} neonates. Spectral analysis provided evidence for changes in functional groups of carbohydrates (980-1200 cm^{-1}). The increase in hydroxyl, ester and carbonyl groups in MMc_{low} samples compared to the control group might reflect aberrations in carbohydrate macromolecules such as glycogen or within the glycocalyx on the cell surface. Since deoxyribose and ribose form the backbone of the DNA or respectively the RNA, they might as well be attributed to alterations on the genomic structure.

In tissue samples of patients suffering of Parkinson's disease, alterations in a similar spectral region (1000-1380 cm^{-1}) were demonstrated between pathological and control neurons. The authors conclude that diseased nerve cells show alterations in their biochemical profile that occurs before they exhibit morphological differences.[153] In accordance with this notion, MMc_{low} neonates appear visually healthy but show cognitive impairments such as altered learning behaviour. This might be attributed to changes in the biochemical composition of the prefrontal cortex. Interestingly, a study conducted in homogenates of rat brain tissue could demonstrate that altered learning behaviour is reflected by changes in their FTIR spectra.[154] As proposed, the biochemical differences observed in the brain of MMc_{low} neonates might be attributed to alterations in nucleic acids. Nucleic acid damage detection in DNA and RNA using FTIR has been demonstrated in various studies with comparable alterations in the spectral profile of samples.[155-157] The activation of microglia cells and the subsequent elimination of synaptic connections in MMc_{low} neonates might lead to nucleic acid damage and release during high rates of phagocytosis. This goes in line with the downregulation of anti-inflammatory markers of fetal microglia cells as reported by Schepanski *et al.*, which might result in a latent inflammatory environment within the prefrontal cortex. Nucleic acid damage might be an additional damage signal in the neonatal brain.

Despite the increase in carbohydrate-associated functional groups, I could not identify differences in spectral regions representative for lipids or amids. A main finding by Schepanksi *et al.* is the excessive synaptic pruning and since neuronal branches are mainly composed of myelin, it could have been expected to find differences in lipids between MMc_{low} and MMc_{high} samples. One possible explanation why I could not detect differences in myelin between groups might be the focus prefrontal cortex which is located in the grey matter of the brain.

Alterations of lipids might be more like to be identified in the white matter of the brain, in which myelin-coated neural axons are primarily located.[116] The loss of myelination has been measured using µFTIR in demyelinating diseases such as multiple sclerosis.[158,159] Instead, grey matter of the brain is characterized by a high density of neural cell bodies, which aligns with my observation of nucleic acid damage in MMc_{low} neonates.

The interpretation of our findings is limited by the difficulty to attribute the various peaks of the derived infrared spectra to their functional group. Beside the masking of peaks derived from low abundant functional groups by other more frequent biomolecules, the reference literature on FTIR spectroscopy is based on various biomaterials measured under different conditions and treatments. For instance, most publications that investigate the usage of FTIR in the identification of nucleic acid damage are based on either cancer cell lines and *ex vivo* cancer samples or even after the application of DNA damaging factors such as mutagenic chemicals, UV-light or ionizing radiation.[155] The transferability of the findings to healthy tissue is to be used with caution.

The analysis of the spectra derived from our samples is further impaired by the usage of sucrose for conservation of the murine brains during the sample preparation. The distinct infrared profile of sucrose overlays the spectral region in which differences between MMc_{low} and control animals have been identified. Although sample preparation of both groups has been consistent, the alterations in carbohydrates and nucleic acids need to be confirmed. For this, Raman spectroscopy, another technique that relies on the acquisition of visual spectra of biological samples, could be used.[160] Raman spectroscopy requires even less sample preparation and can, in contrast to FTIR, also be used with aqueous samples which would make the conservation of tissues with sucrose redundant. Hence, a recent publication used Raman spectroscopy to confirm the grading of brain tumours slides based on their glycosylation signature.[161]

Despite the depicted limitations of this work, our analysis serves as a proof-of-concept study to the functional readout by Schepanski *et al.* Our *ex vivo* approach in working with whole tissue samples provides a deeper understanding of the functional relevance of MMc in the brain tissue and contributes to our knowledge on the consequences of MMc transfer.

4.3 Placenta-derived extracellular vesicles as indicator for placental MMc transfer

As outlined above, our knowledge regarding the regulation of MMc transfer and the contribution of the placenta is fragmentary at best. The third part of my dissertation addresses this issue by investigating how the status of the placental tissue influence the transfer rate of MMc. Since the accessibility of the human placenta during pregnancy is limited, this study relies on placenta-derived EV isolated from maternal serum samples as fingerprints of the placental tissue. Proteomic analysis revealed that placenta-derived EV possess a distinct protein composition that is indicative for the efficiency of MMc transfer. Interestingly, especially placenta-derived EV that originate from mothers who transfer very low numbers of MMc to their offspring carry a unique proteomic profile.

Analyses of human cord blood samples show high variety of transferred MMc among healthy individuals, which is in accordance with similar studies. Although it is hypothesized that the placenta plays an important role in regulating this transfer, there is currently no study that addresses this theory conclusively. Interestingly, the transfer of MMc is strongly reduced in women that were infected with SARS-CoV-2 during pregnancy. Despite individual cases, there is now consensus that SARS-CoV-2 does not infect the placenta.[19] Nevertheless, even though the pregnant women included in our study only report light to moderate COVID-19 infection symptoms and no SARS-CoV-2 associated pregnancy adversities, infection with SARS-CoV-2 leads to an immune activation of the mother accompanied by a cytokine storm that equally affects the placental tissue.[20,162] The quantification of placenta-derived EV reflects this dysregulation as their number is significantly increased compared to healthy pregnant individuals. Similarly, upregulation of placenta-derived EV is known to be associated with pregnancy adversities such as preeclampsia.[100,163] Here, impaired spiral artery remodelling and utero-placental malperfusion leads to increased placental EV production, which might contribute to the systemic manifestation of the disease.[163-165] I did not expect the relatively low frequency of $PLAP^+$ EV in healthy mothers. However, comparable studies on their number in the maternal blood remain inconclusive. Whereas some studies postulate the increase of placenta-derived EV during pregnancy progression, other studies highlight their decrease in the third trimester.[93,94,166] This discrepancy might be as well attributable to differences in the techniques used for EV isolation. Although general guidelines are permanently updated, so far there is no gold standard in EV isolation.[83,89,167] Given the high amount of variability in EV size, concentration and purity based on the particular isolation method, comparability between studies is at least partly limited.[89,168,169] Another factor that is relevant for the relatively low frequency of $PLAP^+$ EV within the PRINCE cohort might be, as outlined above, their increase in pregnancy adversities. Since the PRINCE cohort is only comprised of healthy mothers, it would be interesting to obtain the frequency of $PLAP^+$ EV from other pregnancy cohorts that encompass cardiovascular diseases or cases of obesity.

In healthy mothers placenta-derived EV have been demonstrated to be vastly distributed in the maternal circulation reaching a broad array of distant organs and tissues.[170] Further, they critically contribute to feto-maternal communication by binding to various cell types, e.g., endothelial and immune cells.[171] With my results, I provide first evidence, that percentages of total and placenta-derived EV correlate with MMc numbers from cord blood of female fetuses. Interestingly, no such positive correlation can be observed for women prenatally infected with SARS-CoV-2, which aligns with the interpretation regarding immune dysregulation following infection that affects the placental tissue.

To further answer the question if placenta-derived EV provide direct information on the placental function regarding their capacity to transfer MMc to the offspring, I aimed to analyse their proteomic profile in healthy pregnant women using LC–MS/MS. To do so $PLAP^+$ EV were specifically enriched using magnetic beads with resulted in a 2-to 3-fold increase in the concentration of $PLAP^+$ EV within the enriched sample. I conducted proteomic analysis of 9 maternal serum samples that correspond to different MMc numbers found in the neonatal cord blood. Using LC–MS/MS I was able to quantify 1955 proteins. The total number of proteins identified aligns with numbers reported in similar studies that use proteomic analysis of placenta-derived EV.[98,172] Interestingly, principal component analysis revealed a clear clustering of samples that belong to mothers who transferred low or no MMc (MMc_{low}) and clustering of samples with high numbers of MMc found in the neonatal cord blood (MMc_{high}) with one sample (MMc_{mid}) located in between. To generate in-depth information on the difference between $PLAP^+$ EV from MMc_{low} and MMc_{high} samples, statistical analysis revealed 103 DEPs between groups. Depiction of DEPs as heat map shows a clear distinction between groups and further demonstrate that MMc_{low} samples are characterized by a higher number of up-regulated proteins compared to MMc_{high}. Since the MMc_{mid} sample was not considered for the calculation of DEPs, it's integration in the heat map verifies the connection of DEPs and the MMc number as it marks the transition between the groups. Visualization of the single DEPs further underlines that placenta-derived EV of MMc_{low} samples are characterized by a multitude of up-regulated proteins, whereas in placenta-derived EV of MMc_{high} sample show a comparably low number of up-regulated proteins. Additionally, there is a high variation on the expression level of the proteins and their corresponding p-value.

Some proteins seem to be highly differently expressed between groups compared to others. HMGN1 (High mobility group nucleosome binding domain 1) stands out particularly as it is highly expressed in MMc_{low} samples in contrast to those of the MMc_{high} group. HMGN1 belongs to the "high mobility group" (HMG) protein family, which are highly evolutionarily conserved and are generally located in the nucleus. Beside the role of HMGN1 in regulating chromatin structure and histone modifications, it has been described as alarmin that recruits dendritic

cells promotes a pro-inflammatory milieu.[173] During a cellular stress response, e.g., to infection or tissue damage, HMG proteins can shuttle to the cytoplasm and even be secreted on EV.[174] Thus, EV artificially modified with the N-terminal domain of HMGN1 have been used to activate DCs which is tested as novel cancer treatment as it could increase antitumor immunity or could improve vaccine efficiency.[175,176] Despite HMGN1, HMGA1 and HMGA2 were also identified to be up-regulated in $PLAP^+$ EV of MMc_{low} samples. The presence of several members of the HMG family emphasizes their presence on placenta-derived EV as an indicator for a stress response of the placental tissue. Interestingly, a recent publication postulates that HMGB1, another member of the HMG protein family, on fetal EV contributes to induce preterm birth which underlines its role as alarmin in pregnancy.[177] Such a stress response at the feto-maternal interface might impair the transfer of MMc. This hypothesis is further supported by the upregulation of Interleukin-18 (IL-18) in placenta-derived EV of MMc_{low} participants. IL-18 is a pro-inflammatory cytokine that targets Th1 $CD4^+$ helper T cells and natural killer cells and induces the production of interferon-γ. Taken together, IL-18 and proteins of the HMG family might be associated with placental tissue activation during an acute stress response which affects the transfer of MMc.[178,179]

Pathway analysis of DEPs associates the presence of HMGA1 and HMGA2 together with specific histone proteins (H1-0, H2BC12, H2BC11) with DNA damage/telomere stress induced senescence. This culminates in the formation of senescence-associated heterochromatin foci typically formed in senescent cells.[180] Senescence describes a state of terminal cell cycle arrest and is closely interrelated with cellular aging. During pregnancy progression the placenta naturally ages until birth when the placenta ultimately fulfilled its function. On a cellular stage, fusion of cells to form the syncytiotrophoblasts is closely related to their senescence in order to halt excessive proliferation of cells.[181,182] This study relies on samples from the third trimester. It might be conceivable that placentas of MMc_{low} study participants enter the natural state of placental aging and senescence more rapidly than those belonging to the MMc_{high} group. This might result in an impairment of MMc transfer, which normally increases with pregnancy progression. Senescence is accompanied by shifting to a pro-inflammatory phenotype of cells, which results in a characteristic senescence-associated secretory phenotype of cells.[183] Recently it became evident that EV execute a crucial role the secretome of senescent cells, which might include the sorting of HMG and histone proteins of aging trophoblast cells in placenta-derived EV.[184,185]

Another aspect that results from the proteomic analysis of placenta-derived EV is the high abundance of proteins relevant for RNA binding and processing as indicated by DAVID functional GO analysis. Among the family of RNA binding proteins (RBPs) several proteins were up-regulated in MMc_{low} samples, e.g., FUS, SRP14, SRP19, IGF2BP1 and various hnRNPs, which aligns with comparable proteomic analysis of EV.[186,187] EV are known to

transport various subtypes of RNA as cargo material. The RNA found in EV differs greatly from RNA detected in the host cell, which indicates a specific sorting mechanism during EV synthesis. RBPs are responsible for the packing and sorting of different types of RNA in EV, which are comprised of both coding (mRNA) and noncoding (miRNA, circRNA, lncRNA, tRNA, snRNA) RNAs. Although the presence of specific RBPs does not necessarily require the enrichment of their associated RNAs, it is likely that placenta-derived EV of MMc_{low} samples possess a unique RNA profile that have been sorted by their respective RBPs.[187] Thus, in order to gain insight into their cargo, in a next step RNA isolation and sequencing should be applied.

As already discussed for the frequency and purity of EV, the isolation approach is equally critical for the results of proteomic analysis. Especially nuclear proteins – e.g., HMG protein family, SERBP1, EIF3E – vary strongly depending on the isolation method used.[188]

This study confirms the suitability of placenta-derived EV obtained from serum samples as direct indicators of placental functionality in healthy. Their proteomic profile can be directly linked to the transplacental transfer of MMc by providing information on the status of the placental tissue.

4.4 Scientific significance and outlook

Over the last decades, substantial efforts have been made to unearth the function of MMc for the fetal and neonatal development. Still, many open questions in the field of MMc research remain to be answered. My thesis tries to address this knowledge gap by providing novel insights on MMc antigen-specificity, their effect on local tissue microenvironment and how MMc transfer is regulated by the placenta in the first place.

The evidence of antigen-specificity among microchimeric T cells following bacterial infection adds another aspect to our concept of maternal passive immunity. My study provides a first proof-of-concept in the mouse model for the transfer antigen-specific MMc and their association of with a higher neonatal robustness to infection. In a next step, it needs to be addressed whether the detection of antigen-specific MMc is only possible in a highly artificial setting using a genetically modified listeria strain or whether the presence of these cells can be also identified in human pregnancy. If confirmed, e.g., in cord blood samples of neonates after maternal SARS-CoV-2 infection, this would result in major follow-up questions for the mother-child pair. Firstly, it needs to be addressed how they interact with the fetal and neonatal immune system and whether they provide protection against infection. Secondly, their relevance for maternal infection and especially vaccination schemes before or during pregnancy needs to be clarified. Together with our established understanding of pregnancy-associated antibody transfer, antigen-specific MMc add another aspect to the intergenerational transfer of immunological memory.

My follow-up study to the work published by Schepanski *et al.* supports the relevance of MMc transfer for the tissue homeostasis of the neonatal brain. The observed increase in carbohydrates following MMc depletion and their interpretation as nucleic acid damage emphasizes the vast consequences of MMc depletion for their microenvironment. Given the limitations of my study, these results need to be validated by additional experiments and corresponding methods. Since the DESY synchrotron is located in Hamburg, a cooperation to conduct additional measurements with a different sample preparation technique using µFTIR or RAMAN spectroscopy would be well-suited. It should also be mentioned that the approach to use µFTIR spectroscopy on murine brain samples at the infrared beamline MIRAS of the ALBA synchrotron was established by Sanchez-Molina *et al.* In accordance with their study, my experiments were mainly focuses on a specific region within the brain to obtain quantifiable data. However, by analysing brain tissue sections over night, I was able to establish the mapping of whole-brain samples, which was a first at the MIRAS beamline. This approach allows the visualization of different functional groups associated with their respective macromolecules for the whole brain. As demonstrated for the lipid/amid ratio, one can generate complete maps of the brain tissue and gain insights on regional differences with exciting possibilities for further measurements.

Finally, analyses of placenta-derived EV have been shown to be an eligible tool to gain insights on the status of the placental tissue at the time of the blood draw. Furthermore, placenta-derived EV provide information on the placental proteins associated with the MMc transfer to the fetus. It can be speculated that placental aging and early senescence might have an impact on the cellular transfer function. Given the high abundancy of RNA binding proteins identified on placenta-derived EV, RNA isolation and sequencing might provide additional information on their function and target tissue. By refining and harmonizing EV isolation protocols and techniques for functional analysis, comparability between studies will be increases further. This might establish placenta-derived EV as a novel indicator for placental health that can be accessed during an ongoing pregnancy. With the rapid progress in understanding EV synthesis, trafficking and function, I am firmly convinced that future EV research will contribute to improve our understanding of feto-maternal communication.

5 Abstract

During pregnancy maternal cells are transferred across the placenta to the fetus and seed into fetal organs. These cells are referred to as maternal microchimeric cells (MMc) and have the potential to persist in the offspring for decades.

MMc reflect the cellular heterogeneity of the mother and thus encompass a large fraction of leukocytes, among which T cells are highly abundant. In the first part of this thesis, I addressed the hypothesis, that the mother transfers antigen-specific T cells to the fetus, which might protect the offspring from infection. To test this, I preconceptually infected female mice with ovalbumin (OVA) recombinant *L. monocytogenens* leading to the formation of OVA-specific effector memory T cells. During pregnancy, OVA-specific T cells are transferred *in-utero* and colonize the fetal bone marrow, spleen and liver. The transfer of OVA-specific T cells is associated with a higher robustness of neonates born to preconceptually infected mothers against infection and an activated phenotype of neonatal T cells compared to controls. Using a mouse model, this work provides first evidence that MMc have the potential to transfer memory between generations.

Besides their antigen-specificity, MMc exert a variety of functions within the developing fetus. As recently shown, MMc contribute to brain development by limiting microglia activity and thereby the excessive pruning of neurons in the murine prefrontal cortex.

By preparing *ex vivo* brain section of neonatal mice deprived of MMc, I investigated the effects of MMc depletion on the tissue-homeostasis using Fourier Transform Infrared Microspectroscopy. A lack of MMc altered the local tissue microenvironment of the prefrontal cortex leading to a higher abundance of functional groups attributed to carbohydrates typically found in nucleic acids. Increased phagocytosis by microglia cells might damage neurons, resulting in the release of nucleic acids and subsequent inflammation of the tissue. My experiment serves as a proof-of-concept study highlighting the relevance of MMc for tissue homeostasis.

Despite the recent progress in understanding the relevance of MMc for the development of the fetus and the neonate, little is known regarding the transfer of MMc and the specific role of the placenta as central barrier at the maternofetal interface. The third part of my dissertation addresses this knowledge gap by investigating placenta-derived extracellular vesicles (EV) as fingerprints of the placental tissue.

Placenta-derived EV were isolated from third trimester serum samples derived from healthy pregnant women and women that were infected with SARS-CoV-2 during pregnancy. Using imaging flow cytometry, overall numbers of EV as well as the percentage of placenta-derived EV were quantified. Their excessive production in SARS-CoV-2 infected women indicated an activation of the placental tissue as a consequence of infection. Percentages of placenta-

derived EV derived from healthy pregnant were shown to positively correlate with the number of MMc found in the cord blood of the respective women. This correlation was reversed in SARS-CoV-2 infected women. After enrichment of placenta-derived EV from healthy pregnant participants, proteomic analysis revealed a unique fingerprint of samples derived from mothers that transfer no or very low numbers of MMc, which was absent in mothers transferring high numbers of MMc to their offspring. In-depth analyses indicate a senescence-like phenotype of the placental tissue that might impair MMc transfer. This thesis provides first evidence that placenta-derived EV can be used as indicators of the placental transfer capacity during an ongoing pregnancy.

6 Zusammenfassung

Während einer Schwangerschaft treten mütterliche Zellen über die Plazenta in den Fetus über und reichern sich in den fetalen Organen an. Diese Zellen werden als mütterliche mikrochimärische Zellen (MMc) bezeichnet und haben das Potenzial, für Jahre in den Nachkommen zu verbleiben.

MMc spiegeln die zelluläre Heterogenität der Mutter wieder und umfassen somit auch Leukozyten, die sich wiederum zu großen Teilen aus T-Zellen zusammensetzen. Der erste Teil meiner Doktorarbeit widmet sich daher der Hypothese, dass die Mutter Antigen-spezifische T-Zellen auf den Fetus überträgt, die wiederum das Potenzial besitzen, Nachkommen vor Infektionen zu schützen. Weibliche Mäuse wurden vor Beginn der Schwangerschaft mit Ovalbumin (OVA)-rekombinanten *L. monocytogenes* infiziert, was zur Bildung von OVA-spezifischen Effektor-Gedächtnis-T-Zellen führt. Während der Schwangerschaft treten diese Zellen *in-utero* auf den Fetus über, wo sie im Knochenmark, der Milz und der Leber nachgewiesen werden konnten. Der Transfer dieser Zellen war mit einer erhöhten Fitness der Neonaten gegenüber Infektionen und einem aktivierten Phänotyp der neonatalen T Zellen assoziiert. Der Transfer von MMc im Mausmodel umfasst somit auch den Transfer eines immunologischen Gedächtnisses von der Mutter auf die Nachkommen.

Neben ihrer Antigen-Spezifizität übernehmen MMc weitere Funktionen innerhalb des sich entwickelnden Fetus. Wie kürzlich gezeigt wurde, tragen MMc zur Entwicklung des Gehirns bei, indem sie die Aktivität von Mikrogliazellen und damit den übermäßigen Untergang von Neuronen im Präfrontalen Cortex begrenzen.

Unter Nutzung von *ex-vivo*-Gehirnschnitten neonataler Mäuse, die eine stark verminderte Population an MMc aufweisen, wurde die Auswirkung des Fehlens von MMc auf die Gewebehomöostase mittels Fourier-Transformations-Infrarot-Mikrospektroskopie untersucht. Das Fehlen von MMc im präfrontalen Cortex beeinflusste das lokale Gewebe, was zu einer höheren Abundanz von funktionellen Gruppen führte, die Zuckerstrukturen zugeordnet werden, wie sie typischerweise in Nukleinsäuren vorkommen. Die Freisetzung von Nukleinsäuren könnte eine Folge der verstärkten Phagozytose durch Mikrogliazellen und ein Indikator für eine lokale Entzündung des Gewebes darstellen. Mein Experiment dient somit als Proof-of-Concept-Studie, die die Bedeutung von MMc für ihr umliegendes Gewebe unterstreicht.

Trotz der Fortschritte im Verständnis der funktionalen Bedeutung von MMc für die Entwicklung des Fetus und des Neugeborenen ist wenig über die eigentliche Übertragung von MMc bekannt und welche Rolle dabei der Plazenta als zentrale Schnittstelle zwischen Mutter und Fetus zukommt. Der dritte Teil meiner Dissertation adressiert diese Wissenslücke durch die

Untersuchung von Plazenta-spezifischen Extrazellulären Vesikeln (EV), die von der Plazenta in die mütterliche Blutbahn freigesetzt werden.

Plazenta-spezifische EV wurden aus Serumproben des dritten Trimesters isoliert, die sowohl von gesunden schwangeren Frauen, als auch von Frauen stammen, die während der Schwangerschaft mit SARS-CoV-2 infiziert waren. Mit Hilfe der bildgebenden Durchflusszytometrie wurde die Zahl der EV sowie der Prozentsatz der Plazenta-spezifischen EV quantifiziert. Ihre übermäßige Produktion bei SARS-CoV-2-infizierten Frauen deutete dabei auf eine Aktivierung des Plazentagewebes als Folge der Infektion hin. Es zeigte sich, dass der prozentuale Anteil der aus der Plazenta stammenden EV von gesunden Schwangeren positiv mit der Anzahl der im Nabelschnurblut der jeweiligen Frauen gefundenen MMc korrelierte. Keine solche positive Korrelation konnte bei SARS-CoV-2-infizierten Frauen beobachtet werden. Nach Anreicherung der Plazenta-spezifischen EV von gesunden schwangeren Frauen, ergab die Analyse des Proteoms einen einzigartigen Fingerabdruck solcher Proben, die von Müttern stammten, die keine oder nur eine sehr geringe Anzahl von MMc übertragen. Ein solch charakteristischer Fingerabdruck konnte jedoch nicht bei Müttern festgestellt werden, die eine hohe Anzahl von MMc auf ihre Nachkommen übertragen. Eine tiefergehende Analyse des Proteoms deutete auf einen Seneszenz-ähnlichen Phänotyp des Plazentagewebes hin, der die MMc-Übertragung beeinträchtigen könnte. Diese Arbeit zeigt, dass Plazenta-spezifische EV als Indikatoren für die Transferkapazität der Plazenta im Zuge einer laufenden Schwangerschaft genutzt werden können.

7 Abbreviations

µFTIR	Fourier Transform Infrared Microspectroscopy
BaF_2	Barium fluoride
BSA	Bovine serum albumin
CFU	Colony forming units
Cg1	Cingulate area
circRNA	Circular RNA
CMBC	Cord blood mononuclear blood cells
CMV	Cytomegalovirus
COVID-19	Coronavirus disease 2019
DAVID	Database for Annotation, Visualization, Integrated Discovery
DEPs	Differentially expressed proteins
DNA	Deoxyribonucleic acid
EBV	Epstein-Barr virus
EDTA	Ethylenediaminetetraacetic acid
EV	Extracellular vesicles
FCS	Fetal calf serum
FMO	Fluorescence minus one
gd	Gestation day
HBSS	Hanks' balanced salt solution
HIV	Human immunodeficiency viruses
HMG	High mobility group
HMGN1	High mobility group nucleosome binding domain 1
HSV-2	Herpes simplex virus
IAUC	Area underneath the curve
Ig	Immunoglobulin
IL	Infralimibic cortex
JZ	Junctional zone
L	Interleukin, Placental labyrinth
LC–MS/MS	Liquid chromatography–tandem mass spectrometer
LCMV	Lymphocytic choriomeningitis
lEV	Large extracellular vesicles
LmOVA	Ovalbumin recombinant *Listeria monocytogenes*
LmOVA Δ*act*A	Attenuated LmOVA strain deleted for actA
lncRNA	*Long non-conding RNA*

MACS	Magnetic activated cell sorting
miRNA	Micro RNA
MMc	Maternal microchimeric cells
mRNA	Messenger RNA
NaCl	Sodium chloride
NRS	Normal rat serum
PBS	Dulbecco’s Phosphate Buffered Saline
PCA	Principal component analysis
PFA	Paraformaldehyde
PL	Prelimbic cortex
PLAP	Placental alkaline phosphatase
pnd	Postnatal day
PRINCE	Prenatal Identification of Children's Health
Rag2	Recombination activating gene 2 protein
RBPs	RNA binding proteins
RNA	Ribonucleic acid
RPMI	Roswell park memorial institute
SARS-CoV-2	Severe acute respiratory syndrome coronavirus type 2
SDC	Sodium deoxycholate
SEM	Standard error of the mean
sEV	Small extracellular vesicles
snRNA	Small nuclear RNA
T_{CM}	Central memory T cells
TEAB T	riethylammonium bicarbonate buffer
T_{EM}	Effector memory T cells
T_{RM}	Resident memory T cells
tRNA	Transfer RNA
TSB	Tryptic Soy Broth
UPLC	Ultra Performance Liquid Chromatography

8 References

1 Medawar, P. B. Some immunological and endocrinological problems raised by the evolution of viviparity in vertebrates. *Symp Soc Exp Biol.* **7**, 320–338 (1953).

2 Male, V. Medawar and the immunological paradox of pregnancy: in context. *Oxford Open Immunology* **2**, :iqaa006, doi:10.1093/oxfimm/iqaa006 (2021).

3 Mor, G. & Cardenas, I. The Immune System in Pregnancy: A Unique Complexity. *Am. J. Reprod. Immunol.* **63**, 425-433, doi:10.1111/j.1600-0897.2010.00836.x (2010).

4 Mor, G., Aldo, P. & Alvero, A. B. The unique immunological and microbial aspects of pregnancy. *Nat Rev Immunol* **17**, 469-482, doi:10.1038/nri.2017.64 (2017).

5 Yüzen, D., Arck, P. C. & Thiele, K. Tissue-resident immunity in the female and male reproductive tract. *Semin Immunopathol* **44**, 785-799, doi:10.1007/s00281-022-00934-8 (2022).

6 Heit, J. A. *et al.* Trends in the Incidence of Venous Thromboembolism during Pregnancy or Postpartum: A 30-Year Population-Based Study. *Annals of Internal Medicine* **143**, 697-706, doi: 10.7326/0003-4819-143-10-200511150-00006 (2005).

7 Abu-Raya, B., Michalski, C., Sadarangani, M. & Lavoie, P. M. Maternal Immunological Adaptation During Normal Pregnancy. *Front Immunol* **11**, 575197, doi:10.3389/fimmu.2020.575197 (2020).

8 Cvoro, A. *et al.* Selective estrogen receptor-beta agonists repress transcription of proinflammatory genes. *J Immunol* **180**, 630-636, doi:10.4049/jimmunol.180.1.630 (2008).

9 Erlebacher, A., Vencato, D., Price, K. A., Zhang, D. & Glimcher, L. H. Constraints in antigen presentation severely restrict T cell recognition of the allogeneic fetus. *J Clin Invest* **117**, 1399-1411, doi:10.1172/JCI28214 (2007).

10 Kumar, M., Saadaoui, M. & Al Khodor, S. Infections and Pregnancy: Effects on Maternal and Child Health. *Front Cell Infect Microbiol* **12**, 873253, doi:10.3389/fcimb.2022.873253 (2022).

11 He, J. *et al.* A Systematic Review and Meta-Analysis of Influenza A Virus Infection During Pregnancy Associated with an Increased Risk for Stillbirth and Low Birth Weight. *Kidney Blood Press Res* **42**, 232-243, doi:10.1159/000477221 (2017).

12 Engels, G. *et al.* Pregnancy-Related Immune Adaptation Promotes the Emergence of Highly Virulent H1N1 Influenza Virus Strains in Allogenically Pregnant Mice. *Cell Host Microbe* **21**, 321-333, doi:10.1016/j.chom.2017.02.020 (2017).

13 Kourtis, A. P., Read, J. S. & Jamieson, D. J. Pregnancy and infection. *N Engl J Med* **370**, 2211-2218, doi:10.1056/NEJMra1213566 (2014).

14 Weckman, A. M., Ngai, M., Wright, J., McDonald, C. R. & Kain, K. C. The Impact of Infection in Pregnancy on Placental Vascular Development and Adverse Birth Outcomes. *Frontiers in microbiology* **10**, 1924, doi:10.3389/fmicb.2019.01924 (2019).

15 Mostrom, M. J. *et al.* Immune Profile of the Normal Maternal-Fetal Interface in Rhesus Macaques and Its Alteration Following Zika Virus Infection. *Front Immunol* **12**, 719810, doi:10.3389/fimmu.2021.719810 (2021).

16 Vazquez-Boland, J. A., Krypotou, E. & Scortti, M. Listeria Placental Infection. *mBio* **8**, e00949-00917, doi:10.1128/mBio.00949-17 (2017).

17 Le Monnier, A., Join-Lambert, O. F., Jaubert, F., Berche, P. & Kayal, S. Invasion of the placenta during murine listeriosis. *Infect Immun* **74**, 663-672, doi:10.1128/IAI.74.1.663-672.2006 (2006).

18 Lamond, N. M. & Freitag, N. E. Vertical Transmission of Listeria monocytogenes: Probing the Balance between Protection from Pathogens and Fetal Tolerance. *Pathogens* **7**, 52, doi:10.3390/pathogens7020052 (2018).

19 Kreis, N. N., Ritter, A., Louwen, F. & Yuan, J. A Message from the Human Placenta: Structural and Immunomodulatory Defense against SARS-CoV-2. *Cells* **9**, 1777, doi:10.3390/cells9081777 (2020).

20 Vazquez-Alejo, E. *et al.* SARS-CoV2 Infection During Pregnancy Causes Persistent Immune Abnormalities in Women Without Affecting the Newborns. *Front Immunol* **13**, 947549, doi:10.3389/fimmu.2022.947549 (2022).

21 Shook, L. L., Fourman, L. T. & Edlow, A. G. Immune Responses to SARS-CoV-2 in Pregnancy: Implications for the Health of the Next Generation. *J Immunol* **209**, 1465-1473, doi:10.4049/jimmunol.2200414 (2022).

22 Jamieson, D. J. & Rasmussen, S. A. An update on COVID-19 and pregnancy. *Am. J. Obstet. Gynecol.* **226**, 177-186, doi:10.1016/j.ajog.2021.08.054 (2022).

23 Vivier, E. & Malissen, B. Innate and adaptive immunity: specificities and signaling hierarchies revisited. *Nature Immunology* **6**, 17-21, doi:10.1038/ni1153 (2005).

24 Alanio, C., Lemaitre, F., Law, H. K., Hasan, M. & Albert, M. L. Enumeration of human antigen-specific naive CD8+ T cells reveals conserved precursor frequencies. *Blood* **115**, 3718-3725, doi:10.1182/blood-2009-10-251124 (2010).

25 Davis, M. M. & Bjorkman, P. J. T-cell antigen receptor genes and T-cell recognition. *Nature* **334**, 395-402 (1988).

26 Arstila, T. P. A Direct Estimate of the Human ab T Cell Receptor Diversity. *Science* **286**, 958-961 (1999).

27 Blattman, J. N. *et al.* Estimating the precursor frequency of naive antigen-specific CD8 T cells. *J Exp Med* **195**, 657–664, doi:10.1084/jem.20001021 (2002).

28 Pogorelyy, M. V. *et al.* Exploring the pre-immune landscape of antigen-specific T cells. *Genome Med.* **10**, 68, doi:10.1186/s13073-018-0577-7 (2018).

29 Chaplin, D. D. Overview of the immune response. *J Allergy Clin Immunol* **125**, S3-23, doi:10.1016/j.jaci.2009.12.980 (2010).

30 Harty, J. T. & Badovinac, V. P. Shaping and reshaping CD8+ T-cell memory. *Nat Rev Immunol* **8**, 107-119, doi:10.1038/nri2251 (2008).

31 Weisel, F. J., Zuccarino-Catania, G. V., Chikina, M. & Shlomchik, M. J. A Temporal Switch in the Germinal Center Determines Differential Output of Memory B and Plasma Cells. *Immunity* **44**, 116-130, doi:10.1016/j.immuni.2015.12.004 (2016).

32 Cancro, M. P. & Tomayko, M. M. Memory B cells and plasma cells: The differentiative continuum of humoral immunity. *Immunol Rev* **303**, 72-82, doi:10.1111/imr.13016 (2021).

33 Akkaya, M., Kwak, K. & Pierce, S. K. B cell memory: building two walls of protection against pathogens. *Nat Rev Immunol* **20**, 229-238, doi:10.1038/s41577-019-0244-2 (2020).

34 Youngblood, B. *et al.* Effector CD8 T cells dedifferentiate into long-lived memory cells. *Nature* **552**, 404-409, doi:10.1038/nature25144 (2017).

35 Akondy, R. S. *et al.* Origin and differentiation of human memory CD8 T cells after vaccination. *Nature* **552**, 362-367, doi:10.1038/nature24633 (2017).

36 Masopust, D., Vezys, V., Marzo, A. L. & Lefrançois, L. Preferential localization of effector memory cells in nonlymphoid tissue *Science* **291**, 2413-2417, doi:10.1126/science.1058867 (2001).

37 Masopust, D. *et al.* Activated primary and memory CD8 T cells migrate to nonlymphoid tissues regardless of site of activation or tissue of origin. *J Immunol* **172**, 4875-4882, doi:10.4049/jimmunol.172.8.4875 (2004).

38 Parga-Vidal, L. & van Gisbergen, K. Area under Immunosurveillance: Dedicated Roles of Memory CD8 T-Cell Subsets. *Cold Spring Harb. Perspect. Biol.* **12**, a037796, doi:10.1101/cshperspect.a037796 (2020).

39 Steinert, E. M. *et al.* Quantifying Memory CD8 T Cells Reveals Regionalization of Immunosurveillance. *Cell* **161**, 737-749, doi:10.1016/j.cell.2015.03.031 (2015).

40 Fonseca, R. *et al.* Developmental plasticity allows outside-in immune responses by resident memory T cells. *Nat Immunol* **21**, 412-421, doi:10.1038/s41590-020-0607-7 (2020).

41 Wijeyesinghe, S. *et al.* Expansible residence decentralizes immune homeostasis. *Nature* **592**, 457-462, doi:10.1038/s41586-021-03351-3 (2021).
42 Albrecht, M. & Arck, P. C. Vertically Transferred Immunity in Neonates: Mothers, Mechanisms and Mediators. *Front Immunol* **11**, 555, doi:10.3389/fimmu.2020.00555 (2020).
43 Albrecht, M. *et al.* Infant immunity against viral infections is advanced by the placenta-dependent vertical transfer of maternal antibodies. *Vaccine* **40**, 1563-1571, doi:10.1016/j.vaccine.2020.12.049 (2022).
44 Atyeo, C. & Alter, G. The multifaceted roles of breast milk antibodies. *Cell* **184**, 1486-1499, doi:10.1016/j.cell.2021.02.031 (2021).
45 Hall, J. M. *et al.* Detection of maternal cells in human umbilical cord blood using fluorescence in situ hybridization. *Blood* **86**, 2829-2832 (1995).
46 Kinder, J. M. *et al.* Cross-Generational Reproductive Fitness Enforced by Microchimeric Maternal Cells. *Cell* **162**, 505-515, doi:10.1016/j.cell.2015.07.006 (2015).
47 Maloney, S. *et al.* Microchimerism of maternal origin persists into adult life. *J. Clin. Invest.* **104**, 41–47, doi:10.1172/JCI6611 (1999).
48 Kinder, J. M., Stelzer, I. A., Arck, P. C. & Way, S. S. Immunological implications of pregnancy-induced microchimerism. *Nat Rev Immunol* **17**, 483-494, doi:10.1038/nri.2017.38 (2017).
49 Nelson, J. L. The otherness of self: microchimerism in health and disease. *Trends Immunol* **33**, 421-427, doi:10.1016/j.it.2012.03.002 (2012).
50 Karlmark, K. R. *et al.* Grandmaternal cells in cord blood. *EBioMedicine* **74**, 103721, doi:10.1016/j.ebiom.2021.103721 (2021).
51 Lo, Y. M., Hjelm, N. M. & Thilaganathan, B. Transfer of nucleated maternal cells into fetal circulation during the second trimester of pregnancy. *Br. J. Haematol.* **100**, 605-606, doi:10.1046/j.1365-2141.1998.0636a.x. (1998).
52 Mold, J. E. *et al.* Maternal alloantigens promote the development of tolerogenic fetal regulatory T cells in utero. *Science* **322**, 1562-1565, doi:10.1126/science.1164511 (2008).
53 Rossant, J. & Cross, J. C. Placental development: Lessons from mouse mutants. *Nature reviews - Genetics* **2**, 538-548 (2001).
54 Vernochet, C., Caucheteux, S. M., Gendron, M.-C., Wantyghem, J. & Kanellopoulos-Langevin, C. Affinity-dependent alterations of mouse B cell development by noninherited maternal antigen. *Biol. Reprod.* **72**, 460-469, doi:10.1095/biolreprod.104.035048 (2005).
55 Pan, T. D. *et al.* Predictors of maternal-origin microchimerism in young women in the Philippines. *Am. J. Phys. Anthropol.* **174**, 213-223, doi:10.1002/ajpa.24191 (2021).
56 Moles, J. P. *et al.* Breastmilk cell trafficking induces microchimerism-mediated immune system maturation in the infant. *Pediatr Allergy Immunol* **29**, 133-143, doi:10.1111/pai.12841 (2018).
57 Piotrowski, P. & Croy, B. A. Maternal Cells are Widely Distributed in Murine Fetuses in Utero. *Biol. Reprod.* **54**, 1103-1110, doi:10.1095/biolreprod54.5.1103 (1996).
58 Stelzer, I. A., Thiele, K. & Solano, M. E. Maternal microchimerism: lessons learned from murine models. *J Reprod Immunol* **108**, 12-25, doi:10.1016/j.jri.2014.12.007 (2015).
59 Nijagal, A. *et al.* Maternal T cells limit engraftment after in utero hematopoietic cell transplantation in mice. *J. Clin. Invest.* **121**, 582-592, doi:10.1172/JCI44907 (2011).
60 Vernochet, C., Caucheteux, S. M. & Kanellopoulos-Langevin, C. Bi-directional cell trafficking between mother and fetus in mouse placenta. *Placenta* **28**, 639-649, doi:10.1016/j.placenta.2006.10.006 (2007).

61 Srivastava, R. *et al.* CXCL17 Chemokine-Dependent Mobilization of CXCR8(+)CD8(+) Effector Memory and Tissue-Resident Memory T Cells in the Vaginal Mucosa Is Associated with Protection against Genital Herpes. *J Immunol* **200**, 2915-2926, doi:10.4049/jimmunol.1701474 (2018).

62 Stevens, A. M., Hermes, H. M., Rutledge, J. C., Buyon, J. P. & Nelson, J. L. Myocardial-tissue-specific phenotype of maternal microchimerism in neonatal lupus congenital heart block. *Lancet* **362**, 1617-1623, doi:10.1016/S0140-6736(03)14795-2 (2003).

63 Khosrotehrani, K. *et al.* Presence of chimeric maternally derived keratinocytes in cutaneous inflammatory diseases of children: the example of pityriasis lichenoides. *J. Invest. Dermatol.* **126**, 345-348, doi:10.1038/sj.jid.5700060 (2006).

64 Leveque, L. *et al.* Selective organ specific inflammation in offspring harbouring microchimerism from strongly alloreactive mothers. *J Autoimmun* **50**, 51-58, doi:10.1016/j.jaut.2013.10.005 (2014).

65 Neelson, J. L. *et al.* Maternal microchimerism in peripheral blood in type 1 diabetes and pancreatic islet beta cell microchimerism. *PNAS* **104**, 1637–1642 (2007).

66 Roy, E. *et al.* Specific maternal microchimeric T cells targeting fetal antigens in beta cells predispose to auto-immune diabetes in the child. *J Autoimmun* **36**, 253-262, doi:10.1016/j.jaut.2011.02.003 (2011).

67 Ye, Y. *et al.* Maternal microchimerism in muscle biopsies from children with juvenile dermatomyositis. *Rheumatology (Oxford)* **51**, 987-991, doi:10.1093/rheumatology/ker430 (2012).

68 Zaborowski, M. P., Balaj, L., Breakefield, X. O. & Lai, C. P. Extracellular Vesicles: Composition, Biological Relevance, and Methods of Study. *Bioscience* **65**, 783-797, doi:10.1093/biosci/biv084 (2015).

69 Tapia, G. *et al.* Maternal microchimerism in cord blood and risk of childhood-onset type 1 diabetes. *Pediatr. Diabetes* **20**, 728-735, doi:10.1111/pedi.12875 (2019).

70 Iwai, S. *et al.* Controlled induction of immune tolerance by mesenchymal stem cells transferred by maternal microchimerism. *Biochemical and biophysical research communications* **539**, 83-88, doi:10.1016/j.bbrc.2020.12.032 (2021).

71 Dutta, P. *et al.* Microchimerism is strongly correlated with tolerance to noninherited maternal antigens in mice. *Blood* **114**, 3578-3587, doi:10.1182/blood-2009-03-213561 (2009).

72 Stelzer, I. A. *et al.* Vertically transferred maternal immune cells promote neonatal immunity against early life infections. *Nat Commun* **12**, 4706, doi:10.1038/s41467-021-24719-z (2021).

73 Schepanski, S. *et al.* Pregnancy-induced maternal microchimerism shapes neurodevelopment and behavior in mice. *Nat Commun* **13**, 4571, doi:10.1038/s41467-022-32230-2 (2022).

74 Kanold, A. M. J., Westgren, M. & Gotherstrom, C. Cellular Subsets of Maternal Microchimerism in Umbilical Cord Blood. *Cell Transplant.* **28**, 522-528, doi:10.1177/0963689718779783 (2019).

75 Kanaan, S. B. *et al.* Maternal microchimerism is prevalent in cord blood in memory T cells and other cell subsets, and persists post-transplant. *Oncoimmunology* **6**, e1311436, doi:10.1080/2162402X.2017.1311436 (2017).

76 Koh, J.-Y. *et al.* Impact of maternal engrafted cytomegalovirus-specific CD8+ T cells in a patient with severe combined immunodeficiency. *Clinical & Translational Immunology* **10**, e1272, doi:10.1002/cti2.1272 (2021).

77 Touzot, F. *et al.* Massive expansion of maternal T cells in response to EBV infection in a patient with SCID-Xl *Blood* **120**, 1957-1959, doi:10.1182/blood-2012-04-426833 (2012).

78 Bianchi, D. W. *et al.* Forever Connected: The Lifelong Biological Consequences of Fetomaternal and Maternofetal Microchimerism. *Clinical Chemistry* **67**, 351-362, doi:10.1093/clinchem/hvaa304 (2021).

79 Harrington, W. E. *et al.* Maternal Microchimerism Predicts Increased Infection but Decreased Disease due to Plasmodium falciparum During Early Childhood. *J Infect Dis* **215**, 1445-1451, doi:10.1093/infdis/jix129 (2017).

80 Leite, A. R. *et al.* Novel Biomarkers for Evaluation of Endothelial Dysfunction. *Angiology* **71**, 397-410, doi:10.1177/0003319720903586 (2020).

81 Simon, N. *et al.* Peripheral Plasmodium falciparum Infection in Early Pregnancy Is Associated With Increased Maternal Microchimerism in the Offspring. *J Infect Dis* **224**, 2105-2112, doi:10.1093/infdis/jiab275 (2021).

82 Greening, D. W. & Simpson, R. J. Understanding extracellular vesicle diversity - current status. *Expert Rev Proteomics* **15**, 887-910, doi:10.1080/14789450.2018.1537788 (2018).

83 Thery, C. *et al.* Minimal information for studies of extracellular vesicles 2018 (MISEV2018): a position statement of the International Society for Extracellular Vesicles and update of the MISEV2014 guidelines. *J Extracell Vesicles* **7**, 1535750, doi:10.1080/20013078.2018.1535750 (2018).

84 Kowal, J. *et al.* Proteomic comparison defines novel markers to characterize heterogeneous populations of extracellular vesicle subtypes. *Proceedings of the National Academy of Sciences* **113**, E968-E977, doi:10.1073/pnas.1521230113 (2016).

85 Wiklander, O. P. B. *et al.* Systematic Methodological Evaluation of a Multiplex Bead-Based Flow Cytometry Assay for Detection of Extracellular Vesicle Surface Signatures. *Front Immunol* **9**, 1326, doi:10.3389/fimmu.2018.01326 (2018).

86 Malkin, E. Z. & Bratman, S. V. Bioactive DNA from extracellular vesicles and particles. *Cell Death Dis.* **11**, 584, doi:10.1038/s41419-020-02803-4 (2020).

87 Doyle, L. & Wang, M. Overview of Extracellular Vesicles, Their Origin, Composition, Purpose, and Methods for Exosome Isolation and Analysis. *Cells* **8**, 727, doi:10.3390/cells8070727 (2019).

88 Morgan, C. P., Chan, J. C. & Bale, T. L. Driving the Next Generation: Paternal Lifetime Experiences Transmitted via Extracellular Vesicles and Their Small RNA Cargo. *Biol. Psychiatry* **85**, 164-171, doi:10.1016/j.biopsych.2018.09.007 (2019).

89 Brennan, K. *et al.* A comparison of methods for the isolation and separation of extracellular vesicles from protein and lipid particles in human serum. *Sci Rep* **10**, 1039, doi:10.1038/s41598-020-57497-7 (2020).

90 Antounians, L. *et al.* Fetal lung underdevelopment is rescued by administration of amniotic fluid stem cell extracellular vesicles in rodents. *Sci. Transl. Med.* **13**, eaax5941 (2021).

91 Dlugolecka, M. *et al.* Characterization of Extracellular Vesicles from Bronchoalveolar Lavage Fluid and Plasma of Patients with Lung Lesions Using Fluorescence Nanoparticle Tracking Analysis *Cells* **10**, 3473, doi:10.3390/cells10123473 (2021).

92 Ortega, M. A. *et al.* Unfolding the role of placental-derived Extracellular Vesicles in Pregnancy: From homeostasis to pathophysiology. *Front Cell Dev Biol* **10**, 1060850, doi:10.3389/fcell.2022.1060850 (2022).

93 Salomon, C. *et al.* Gestational Diabetes Mellitus Is Associated With Changes in the Concentration and Bioactivity of Placenta-Derived Exosomes in Maternal Circulation Across Gestation. *Diabetes* **65**, 598-609, doi:10.2337/db15-0966 (2016).

94 Sarker, S. *et al.* Placenta-derived exosomes continuously increase in maternal circulation over the first trimester of pregnancy. *J. Transl. Med.* **12**, 204, doi:10.1186/1479-5876-12-204 (2014).

95 Zabel, R. R. *et al.* Enrichment and characterization of extracellular vesicles from ex vivo one-sided human placenta perfusion. *Am J Reprod Immunol* **86**, e13377, doi:10.1111/aji.13377 (2021).

96 Sharma, U., Pal, D. & Prasad, R. Alkaline phosphatase: an overview. *Indian J. Clin. Biochem.* **29**, 269-278, doi:10.1007/s12291-013-0408-y (2014).

97 Alegre, E. *et al.* In vivo identification of an HLA-G complex as ubiquitinated protein circulating in exosomes. *Eur J Immunol* **43**, 1933-1939, doi:10.1002/eji.201343318 (2013).

98 Tong, M. *et al.* Proteomic characterization of macro-, micro- and nano-extracellular vesicles derived from the same first trimester placenta: relevance for feto-maternal communication. *Hum. Reprod.* **31**, 687-699, doi:10.1093/humrep/dew004 (2016).

99 Han, C. *et al.* Placenta-derived extracellular vesicles induce preeclampsia in mouse models. *Haematologica* **105**, 1686-1694, doi:10.3324/haematol.2019.226209 (2020).

100 Levine, L. *et al.* Syncytiotrophoblast extracellular microvesicle profiles in maternal circulation for noninvasive diagnosis of preeclampsia. *Sci Rep* **10**, 6398, doi:10.1038/s41598-020-62193-7 (2020).

101 James-Allan, L. B. *et al.* Regulation of glucose homeostasis by small extracellular vesicles in normal pregnancy and in gestational diabetes. *FASEB J.* **34**, 5724-5739, doi:10.1096/fj.201902522RR (2020).

102 Fitzgerald, W. *et al.* A System of Cytokines Encapsulated in ExtraCellular Vesicles. *Sci. Rep.* **8**, 8973, doi:10.1038/s41598-018-27190-x (2018).

103 Fitzgerald, W., Gomez-Lopez, N., Erez, O., Romero, R. & Margolis, L. Extracellular vesicles generated by placental tissues ex vivo: A transport system for immune mediators and growth factors. *Am J Reprod Immunol* **80**, e12860, doi:10.1111/aji.12860 (2018).

104 Donker, R. B. *et al.* The expression profile of C19MC microRNAs in primary human trophoblast cells and exosomes. *Molecular Human Reproduction* **18**, 417-424, doi:10.1093/molehr/gas013 (2012).

105 Liu, H. *et al.* Estimation of the burden of human placental micro- and nano-vesicles extruded into the maternal blood from 8 to 12 weeks of gestation. *Placenta* **72-73**, 41-47, doi:10.1016/j.placenta.2018.10.009 (2018).

106 Chang, G. *et al.* Expression and trafficking of placental microRNAs at the feto-maternal interface. *FASEB J.* **31**, 2760-2770, doi:10.1096/fj.201601146R (2017).

107 Burnett, L. A. & Nowak, R. A. Exosomes mediate embryo and maternal interactions at implantation and during pregnancy. *Front. Biosci.* **8**, 79-96, doi:10.2741/s448 (2016).

108 Wallace, A. E., Fraser, R. & Cartwright, J. E. Extravillous trophoblast and decidual natural killer cells: a remodelling partnership. *Hum Reprod Update* **18**, 458-471, doi:10.1093/humupd/dms015 (2012).

109 Jin, J. & Menon, R. Placental exosomes: A proxy to understand pregnancy complications. *Am J Reprod Immunol* **79**, e12788, doi:10.1111/aji.12788 (2018).

110 Cronqvist, T. *et al.* Syncytiotrophoblast derived extracellular vesicles transfer functional placental miRNAs to primary human endothelial cells. *Sci Rep* **7**, 4558, doi:10.1038/s41598-017-04468-0 (2017).

111 Villalobos-Labra, R. *et al.* Placenta-derived extracellular vesicles from preeclamptic and healthy pregnancies impair ex vivo vascular endothelial function. *Biosci. Rep.* **42**, doi:10.1042/BSR20222185 (2022).

112 Sabapatha, A., Gercel-Taylor, C. & Taylor, D. D. Specific isolation of placenta-derived exosomes from the circulation of pregnant women and their immunoregulatory consequences. *Am J Reprod Immunol* **56**, 345-355, doi:10.1111/j.1600-0897.2006.00435.x (2006).

113 Stenqvist, A. C., Nagaeva, O., Baranov, V. & Mincheva-Nilsson, L. Exosomes secreted by human placenta carry functional Fas ligand and TRAIL molecules and convey apoptosis in activated immune cells, suggesting exosome-mediated immune

privilege of the fetus. *J Immunol* **191**, 5515-5523, doi:10.4049/jimmunol.1301885 (2013).

114 Morelli, A. E. & Sadovsky, Y. Extracellular vesicles and immune response during pregnancy: A balancing act. *Immunol Rev*, doi:10.1111/imr.13074 (2022).

115 Moon, J. J. *et al.* Naïve CD4+ T cell frequency varies for different epitopes and predicts repertoire diversity and response magnitude. *Immunity* **27**, 203–213, doi:10.1016/j.immuni.2007.07.007 (2007).

116 Sanchez-Molina, P. *et al.* From Mouse to Human: Comparative Analysis between Grey and White Matter by Synchrotron-Fourier Transformed Infrared Microspectroscopy. *Biomolecules* **10**, doi:10.3390/biom10081099 (2020).

117 Talari, A. C. S., Martinez, M. A. G., Movasaghi, Z., Rehman, S. & Rehman, I. Advances in Fourier transform infrared (FTIR) spectroscopy of biological tissues. *Applied Spectroscopy Reviews* **52**, 456-506, doi:10.1080/05704928.2016.1230863 (2016).

118 Diemert, A. *et al.* Maternal progesterone levels are modulated by maternal BMI and predict birth weight sex-specifically in human pregnancies. *J Reprod Immunol* **121**, 49-55, doi:10.1016/j.jri.2017.05.005 (2017).

119 Zhao, F. *et al.* A unique maternal and placental galectin signature upon SARS-CoV-2 infection suggests galectin-1 as a key alarmin at the maternal-fetal interface. *Front Immunol* **14**, 1196395, doi:10.3389/fimmu.2023.1196395 (2023).

120 Hughes, C. S. *et al.* Single-pot, solid-phase-enhanced sample preparation for proteomics experiments. *Nat. Protoc.* **14**, 68-85, doi:10.1038/s41596-018-0082-x (2019).

121 Kement, D. *et al.* Neuroserpin Is Strongly Expressed in the Developing and Adult Mouse Neocortex but Its Absence Does Not Perturb Cortical Lamination and Synaptic Proteome. *Front Neuroanat.* **15**, 627896, doi:doi: 10.3389/fnana.2021.627896 (2021).

122 Kollmann, T. R. *et al.* Induction of protective immunity to Listeria monocytogenes in neonates. *J Immunol.* **178**, 3695–3701., doi:10.4049/jimmunol.178.6.3695 (2007).

123 Movasaghi, Z., Rehman, S. & Rehman, I. Fourier Transform Infrared (FTIR) Spectroscopy of Biological Tissues. *Applied Spectroscopy Reviews* **43**, 134-179, doi:10.1080/05704920701829043 (2008).

124 Fadlelmoula, A., Pinho, D., Carvalho, V. H., Catarino, S. O. & Minas, G. Fourier Transform Infrared (FTIR) Spectroscopy to Analyse Human Blood over the Last 20 Years: A Review towards Lab-on-a-Chip Devices. *Micromachines (Basel)* **13**, doi:10.3390/mi13020187 (2022).

125 Beura, L. K. *et al.* CD4(+) resident memory T cells dominate immunosurveillance and orchestrate local recall responses. *J Exp Med* **216**, 1214-1229, doi:10.1084/jem.20181365 (2019).

126 Nakanishi, Y., Lu, B., Gerard, C. & Iwasaki, A. CD8(+) T lymphocyte mobilization to virus-infected tissue requires CD4(+) T-cell help. *Nature* **462**, 510-513, doi:10.1038/nature08511 (2009).

127 Abolins, S. *et al.* The comparative immunology of wild and laboratory mice, Mus musculus domesticus. *Nat Commun* **8**, 14811, doi:10.1038/ncomms14811 (2017).

128 Beura, L. K. *et al.* Normalizing the environment recapitulates adult human immune traits in laboratory mice. *Nature* **532**, 512-516, doi:10.1038/nature17655 (2016).

129 Huggins, M. A., Jameson, S. C. & Hamilton, S. E. Embracing microbial exposure in mouse research. *J. Leukoc. Biol.* **105**, 73-79, doi:10.1002/JLB.4RI0718-273R (2019).

130 Rosshart, S. P. *et al.* Laboratory mice born to wild mice have natural microbiota and model human immune responses. *Science* **365**, eaaw4361, doi:10.1126/science.aaw4361 (2019).

131 Tang, V. A. & Rosenthal, K. L. Intravaginal infection with herpes simplex virus type-2 (HSV-2) generates a functional effector memory T cell population that persists in the

murine genital tract. *J Reprod Immunol* **87**, 39-44, doi:10.1016/j.jri.2010.06.155 (2010).

132 van der Zwan, A. *et al.* Mixed signature of activation and dysfunction allows human decidual CD8(+) T cells to provide both tolerance and immunity. *Proc Natl Acad Sci U S A* **115**, 385-390, doi:10.1073/pnas.1713957115 (2018).

133 Zhu, J. *et al.* Persistence of HIV-1 receptor-positive cells after HSV-2 reactivation is a potential mechanism for increased HIV-1 acquisition. *Nat Med* **15**, 886-892, doi:10.1038/nm.2006 (2009).

134 Davé, V. A. *et al.* Cervicovaginal Tissue Residence Confers a Distinct Differentiation Program upon Memory CD8 T Cells. *J Immunol* **206**, 2937-2948, doi:10.4049/jimmunol.2100166 %J The Journal of Immunology (2021).

135 Peng, T. *et al.* Distinct populations of antigen-specific tissue-resident CD8+ T cells in human cervix mucosa. *JCI Insight* **6**, e149950, doi:10.1172/jci.insight.149950 (2021).

136 Marleau, A. M., Greenwood, J. D., Wei, Q., Singh, B. & Croy, B. A. Chimerism of murine fetal bone marrow by maternal cells occurs in late gestation and persists into adulthood. *Lab. Invest.* **83**, 673-681, doi:10.1097/01.lab.0000067500.85003.32 (2003).

137 Hemberger, M., Hanna, C. W. & Dean, W. Mechanisms of early placental development in mouse and humans. *Nat Rev Genet* **21**, 27-43, doi:10.1038/s41576-019-0169-4 (2020).

138 Clark, D. R. *et al.* Perinatal Listeria monocytogenes susceptibility despite preconceptual priming and maintenance of pathogen-specific CD8(+) T cells during pregnancy. *Cell Mol Immunol* **11**, 595-605, doi:10.1038/cmi.2014.84 (2014).

139 Loubiere, L. S. *et al.* Maternal microchimerism in healthy adults in lymphocytes, monocyte/macrophages and NK cells. *Lab. Invest.* **86**, 1185-1192, doi:10.1038/labinvest.3700471 (2006).

140 Vacani-Martins, N. *et al.* After Experimental Trypanosoma cruzi Infection, Dying Hepatic CD3(+)TCRalphabeta(+)B220(+) T Lymphocytes Are Rescued from Death by Peripheral T Cells and Become Activated. *Pathogens* **9**, 717, doi:10.3390/pathogens9090717 (2020).

141 Rharbaoui, F. *et al.* Characterization of a B220+ lymphoid cell subpopulation with immune modulatory functions in nasal-associated lymphoid tissues. *J Immunol* **174**, 1317-1324, doi:10.4049/jimmunol.174.3.1317 (2005).

142 Douagi, I., Colucci, F., Di Santo, J. P. & Cumano, A. Identification ofthe earliest prethymic bipotent T/NK progenitor in murine fetal liver. *Blood* **99**, 463-471, doi:10.1182/blood.v99.2.463 (2002).

143 Chen, Z. *et al.* CD11c(high) CD8+ regulatory T cell feedback inhibits CD4 T cell immune response via Fas ligand-Fas pathway. *J Immunol* **190**, 6145-6154, doi:10.4049/jimmunol.1300060 (2013).

144 Lin, Y., Roberts, T. J., Sriram, V., Cho, S. & Brutkiewicz, R. R. Myeloid marker expression on antiviral CD8+ T cells following an acute virus infection. *Eur J Immunol* **33**, 2736-2743, doi:10.1002/eji.200324087 (2003).

145 McFarland, H. I., Nahill, S. R., Maciaszek, J. W. & Welsh, R. M. CD11b (Mac-1): a marker for CD8+ cytotoxic T cell activation and memory in virus infection. *The Journal of Immunology* **149**, 1326-1333, doi:10.4049/jimmunol.149.4.1326 (1992).

146 Huleatt, J. W. & Lefrançois, L. Antigen-driven induction of CD11c on intestinal intraepithelial lymphocytes and CD8+ T cells in vivo. *The Journal of Immunology* **154**, 5684-5693, doi:10.4049/jimmunol.154.11.5684 (1995).

147 Balle, C. *et al.* Factors influencing maternal microchimerism throughout infancy and its impact on infant T cell immunity. *J Clin Invest* **132**, doi:10.1172/JCI148826 (2022).

148 Castellan, F. S. & Irie, N. Postnatal depletion of maternal cells biases T lymphocytes and natural killer cells' profiles toward early activation in the spleen. *Biol Open* **11**, doi:10.1242/bio.059334 (2022).

149 Mackaness, G. B. Cellular Resistance to Infection. *J. Exp. Med.* **116**, 381-406, doi:10.1084/jem.116.3.381 (1962).

150 Portnoy, D. A., Auerbuch, V. & Glomski, I. J. The cell biology of Listeria monocytogenes infection: the intersection of bacterial pathogenesis and cell-mediated immunity. *J. Cell Biol.* **158**, 409-414, doi:10.1083/jcb.200205009 (2002).

151 Asano, K. *et al.* Passive immunization with anti-ActA and anti-listeriolysin O antibodies protects against Listeria monocytogenes infection in mice. *Sci Rep* **6**, 39628, doi:10.1038/srep39628 (2016).

152 Erickson, J. J. *et al.* Pregnancy enables antibody protection against intracellular infection. *Nature* **606**, 769-775, doi:10.1038/s41586-022-04816-9 (2022).

153 Szczerbowska-Boruchowska, M. *et al.* Biomolecular investigation of human substantia nigra in Parkinson's disease by synchrotron radiation Fourier transform infrared microspectroscopy. *Arch. Biochem. Biophys.* **459**, 241-248, doi:10.1016/j.abb.2006.12.027 (2007).

154 Yoshida, S. *et al.* Fourier transform infrared spectroscopic analysis of rat brain microsomal membranes modified by dietary fatty acids: Possible correlation with altered learning behavior. *Biospectroscopy* **3**, 281-290, doi:10.1002/(sici)1520-6343(1997)3:4<281::Aid-bspy3>3.0.Co;2-7 (1997).

155 Sofinska, K., Wilkosz, N., Szymonski, M. & Lipiec, E. Molecular Spectroscopic Markers of DNA Damage. *Molecules* **25**, 561, doi:10.3390/molecules25030561 (2020).

156 Mello, M. L. & Vidal, B. C. Changes in the infrared microspectroscopic characteristics of DNA caused by cationic elements, different base richness and single-stranded form. *PLoS One* **7**, e43169, doi:10.1371/journal.pone.0043169 (2012).

157 Dovbeshko, G. I., Gridina, N. Y., Pashchuk, O. P. & Kruglova, E. B. FTIR spectroscopy studies of nucleic acid damage. *Talanta* **53**, 233–246 (2000).

158 LeVine, S. M. & Wetzel, D. L. Chemical analysis of multiple sclerosis lesions by FT-IR microspectroscopy. *Free Radic Biol Med.* **25**, 33-41, doi:10.1016/s0891-5849(98)00019-7 (1998).

159 Heraud, P. *et al.* Early detection of the chemical changes occurring during the induction and prevention of autoimmune-mediated demyelination detected by FT-IR imaging. *Neuroimage* **42**, 1180-1189, doi:10.1016/j.neuroimage.2009.09.053 (2010).

160 Movasaghi, Z., Rehman, S. & Rehman, I. U. Raman Spectroscopy of Biological Tissues. *Applied Spectroscopy Reviews* **42**, 493-541, doi:10.1080/05704920701551530 (2007).

161 Quesnel, A. *et al.* Glycosylation spectral signatures for glioma grade discrimination using Raman spectroscopy. *BMC Cancer* **23**, 174, doi:10.1186/s12885-023-10588-w (2023).

162 Garcia-Flores, V. *et al.* Maternal-Fetal Immune Responses in Pregnant Women Infected with SARS-CoV-2. *Nature Communications* **13**, 320, doi:10.1038/s41467-021-27745-z (2021).

163 Han, C. *et al.* Syncytiotrophoblast-Derived Extracellular Vesicles in Pathophysiology of Preeclampsia. *Front. Physiol.* **10**, 1236, doi:10.3389/fphys.2019.01236 (2019).

164 Vatish, M., Redman, C. W. G. & Davidge, S. T. in *Chesley's Hypertensive Disorders in Pregnancy* (eds R. N. Taylor *et al.*) 155-163 (2022).

165 Cooke, W. R., Jones, G. D., Redman, C. W. G. & Vatish, M. Syncytiotrophoblast Derived Extracellular Vesicles in Relation to Preeclampsia. *Maternal-Fetal Medicine* **3**, 151-160, doi:10.1097/FM9.0000000000000009 (2021).

166 Mitchell, M. D. *et al.* Placental exosomes in normal and complicated pregnancy. *Am. J. Obstet. Gynecol.* **213**, 173-181, doi:10.1016/j.ajog.2015.07.001 (2015).

167 Crescitelli, R., Lasser, C. & Lotvall, J. Isolation and characterization of extracellular vesicle subpopulations from tissues. *Nat. Protoc.* **16**, 1548-1580, doi:10.1038/s41596-020-00466-1 (2021).

168 Antounians, L. *et al.* The Regenerative Potential of Amniotic Fluid Stem Cell Extracellular Vesicles: Lessons Learned by Comparing Different Isolation Techniques. *Sci Rep* **9**, 1837, doi:10.1038/s41598-018-38320-w (2019).

169 Azkargorta, M. *et al.* Human Serum Extracellular Vesicle Proteomic Profile Depends on the Enrichment Method Employed. *Int J Mol Sci* **22**, 11144, doi:10.3390/ijms222011144 (2021).

170 Kang, M., Blenkiron, C. & Chamley, Lawrence W. The biodistribution of placental and fetal extracellular vesicles during pregnancy following placentation. *Clin. Sci.* **137**, 385-399, doi:10.1042/cs20220301 (2023).

171 Salomon, C. *et al.* A gestational profile of placental exosomes in maternal plasma and their effects on endothelial cell migration. *PLoS One* **9**, e98667, doi:10.1371/journal.pone.0098667 (2014).

172 Ouyang, Y. *et al.* Isolation of human trophoblastic extracellular vesicles and characterization of their cargo and antiviral activity. *Placenta* **47**, 86-95, doi:10.1016/j.placenta.2016.09.008 (2016).

173 Yang, D., Han, Z., Alam, M. M. & Oppenheim, J. J. High-mobility group nucleosome binding domain 1 (HMGN1) functions as a Th1-polarizing alarmin. *Semin. Immunol.* **38**, 49-53, doi:10.1016/j.smim.2018.02.012 (2018).

174 Chen, R., Kang, R. & Tang, D. The mechanism of HMGB1 secretion and release. *Exp. Mol. Med.* **54**, 91-102, doi:10.1038/s12276-022-00736-w (2022).

175 Yang, D. *et al.* High-mobility group nucleosome-binding protein 1 acts as an alarmin and is critical for lipopolysaccharide-induced immune responses. *J Exp Med* **209**, 157-171, doi:10.1084/jem.20101354 (2012).

176 Zuo, B. *et al.* Alarmin-painted exosomes elicit persistent antitumor immunity in large established tumors in mice. *Nat Commun* **11**, 1790, doi:10.1038/s41467-020-15569-2 (2020).

177 Radnaa, E. *et al.* Extracellular vesicle mediated feto-maternal HMGB1 signaling induces preterm birth. *Lab Chip* **21**, 1956-1973, doi:10.1039/d0lc01323d (2021).

178 Kretschmer, T. *et al.* Effect of Maternal Obesity in Mice on IL-6 Levels and Placental Endothelial Cell Homeostasis. *Nutrients* **12**, 296, doi:10.3390/nu12020296 (2020).

179 Umapathy, A., Chamley, L. W. & James, J. L. Reconciling the distinct roles of angiogenic/anti-angiogenic factors in the placenta and maternal circulation of normal and pathological pregnancies. *Angiogenesis* **23**, 105-117, doi:10.1007/s10456-019-09694-w (2020).

180 Narita, M. *et al.* Rb-mediated heterochromatin formation and silencing of E2F target genes during cellular senescence. *Cell* **113**, 703-716, doi:10.1016/s0092-8674(03)00401-x (2003).

181 Cox, L. S. & Redman, C. The role of cellular senescence in ageing of the placenta. *Placenta* **52**, 139-145, doi:10.1016/j.placenta.2017.01.116 (2017).

182 Chuprin, A. *et al.* Cell fusion induced by ERVWE1 or measles virus causes cellular senescence. *Genes Dev.* **27**, 2356-2366, doi:10.1101/gad.227512.113 (2013).

183 Wallis, R., Mizen, H. & Bishop, C. L. The bright and dark side of extracellular vesicles in the senescence-associated secretory phenotype. *Mech Ageing Dev.* **189**, doi:10.1016/j.mad.2020.111263 (2020).

184 Takasugi, M. Emerging roles of extracellular vesicles in cellular senescence and aging. *Aging Cell* **17**, doi:10.1111/acel.12734 (2018).

185 Lehmann, B. D. *et al.* Senescence-associated exosome release from human prostate cancer cells. *Cancer Res.* **68**, 7864-7871, doi:10.1158/0008-5472.CAN-07-6538 (2008).

186 Statello, L. *et al.* Identification of RNA-binding proteins in exosomes capable of interacting with different types of RNA: RBP-facilitated transport of RNAs into exosomes. *PLoS One* **13**, e0195969, doi:10.1371/journal.pone.0195969 (2018).

187 Fabbiano, F. *et al.* RNA packaging into extracellular vesicles: An orchestra of RNA-binding proteins? *J Extracell Vesicles* **10**, e12043, doi:10.1002/jev2.12043 (2020).

188 Kugeratski, F. G. *et al.* Quantitative proteomics identifies the core proteome of exosomes with syntenin-1 as the highest abundant protein and a putative universal biomarker. *Nat. Cell Biol.* **23**, 631-641, doi:10.1038/s41556-021-00693-y (2021).

9 Supplement

Table 10. DEPs of placenta-derived EV after proteomic analysis

Upregulated in MMc_{high}				
Gene Symbol	**UniProt Accession**	**Name**	**p-value**	**Log2 fold change**
PAFAH1B3	Q15102	Platelet-activating factor acetylhydrolase IB subunit alpha1	0.0007	-1.5542
PSME2	Q9UL46	Proteasome activator complex subunit 2	0.0011	-2.4238
LETM1	O95202	Mitochondrial proton/calcium exchanger protein	0.0021	-1.3673
TCEA1	P23193	Transcription elongation factor A protein 1	0.0046	-2.1513
H1-3	P16402	Histone H1.3	0.0128	-2.0399
CAPN7	Q9Y6W3	Calpain-7	0.0133	-1.3508
EIF3E	P60228	Eukaryotic translation initiation factor 3 subunit E	0.0150	-1.9918
WDR1	O75083	WD repeat-containing protein 1	0.0152	-2.0252
KNDC1	Q76NI1	Kinase non-catalytic C-lobe domain-containing protein 1	0.0153	-1.1456
ITIH4	Q14624	Inter-alpha-trypsin inhibitor heavy chain H4	0.0154	-1.7389
SUPT5H	O00267	Transcription elongation factor SPT5	0.0162	-1.0145
XPOT	O43592	Exportin-T	0.0207	-1.8769
GOLGA3	Q08378	Golgin subfamily A member 3	0.0226	-1.0409
NUSAP1	Q9BXS6	Nucleolar and spindle-associated protein 1	0.0245	-1.8114
MTMR9	Q96QG7	Myotubularin-related protein 9	0.0259	-0.9409
C9	P02748	Complement component C9	0.0281	-2.1851
LMNB2	Q03252	Lamin-B2	0.0379	-1.0563
CYP11B2	P19099	Cytochrome P450 11B2, mitochondrial	0.0386	-0.7688
PRSS3	P35030	Trypsin-3	0.0474	-1.6265
Upregulated in MMc_{low}				
Gene Symbol	**UniProt Accession**	**Name**	**p-value**	**Log2 fold change**
ADSS2	P30520	Adenylosuccinate synthetase isozyme 2	0.0272	1.1822
ANAPC1	Q9H1A4	Anaphase-promoting complex subunit 1	0.0328	0.9186
ATP5IF1	Q9UII2	ATPase inhibitor, mitochondrial	0.0121	1.1117
CALML5	Q9NZT1	Calmodulin-like protein 5	0.0170	1.4816
CAPG	P40121	Macrophage-capping protein	0.0075	0.6011
CBR1	P16152	Carbonyl reductase [NADPH] 1	0.0355	1.3456
CCAR1	Q8IX12	Cell division cycle and apoptosis regulator protein 1	0.0019	0.6371
CCDC124	Q96CT7	Coiled-coil domain-containing protein 124	0.0051	0.8484

CD59	P13987	CD59 glycoprotein	0.0176	1.5024
CPSF6	Q16630	Cleavage and polyadenylation specificity factor subunit 6	0.0176	0.7006
CPSF7	Q8N684	Cleavage and polyadenylation specificity factor subunit 7	0.0051	1.0702
CROCC	Q5TZA2	Rootletin	0.0223	0.6356
CWC15	Q9P013	Spliceosome-associated protein CWC15 homolog	0.0176	1.0349
DBT	P11182	Lipoamide acyltransferase component of branched-chain alpha-keto acid dehydrogenase complex, mitochondrial	0.0498	0.9465
DCTN2	Q13561	Dynactin subunit 2	0.0331	0.7705
EDF1	O60869	Endothelial differentiation-related factor 1	0.0301	0.8705
EIF4B	P23588	Eukaryotic translation initiation factor 4B	0.0338	0.9932
FAM120A	Q9NZB2	Constitutive coactivator of PPAR-gamma-like protein 1	0.0140	1.2441
FGA	P02671	Fibrinogen alpha chain	0.0072	0.6008
FLOT1	O75955	Flotillin-1	0.0252	2.0152
FUS	P35637	RNA-binding protein FUS	0.0155	1.1608
GNL3	Q9BVP2	Guanine nucleotide-binding protein-like 3	0.0109	0.9216
H1-0	P07305	Histone H1.0	0.0033	1.3316
H2BC11	P06899	Histone H2B type 1-J	0.0406	0.8034
H2BC12	O60814	Histone H2B type 1-K	0.0231	1.2630
HDGF	P51858	Hepatoma-derived growth factor	0.0146	0.9196
HDGFL2	Q7Z4V5	Hepatoma-derived growth factor-related protein 2	0.0259	0.7038
HMGA1	P17096	High mobility group protein HMG-I/HMG-Y	0.0091	0.5866
HMGA2	P52926	High mobility group protein HMGI-C	0.0061	1.7244
HMGN1	P05114	Non-histone chromosomal protein HMG-14	0.0014	4.1850
HNRNPA0	Q13151	Heterogeneous nuclear ribonucleoprotein A0	0.0009	0.7124
HNRNPUL2	Q1KMD3	Heterogeneous nuclear ribonucleoprotein U-like protein 2	0.0191	0.6196
HP1BP3	Q5SSJ5	Heterochromatin protein 1-binding protein 3	0.0023	0.5966
HSPB1	P04792	Heat shock protein beta-1	0.0156	0.6502
IGF2BP1	Q9NZI8	Insulin-like growth factor 2 mRNA-binding protein 1	0.0158	0.7770
IL18	Q14116	Interleukin-18	0.0078	0.7216
KTN1	Q86UP2	Kinectin	0.0065	0.6605
LEMD2	Q8NC56	LEM domain-containing protein 2	0.0481	0.6176
MRPS31	Q92665	28S ribosomal protein S31, mitochondrial	0.0001	0.7562
MYBBP1A	Q9BQG0	Myb-binding protein 1A	0.0360	0.6526

NAP1L1	P55209	Nucleosome assembly protein 1-like 1	0.0331	0.7964
NIFK	Q9BYG3	MKI67 FHA domain-interacting nucleolar phosphoprotein	0.0325	1.1978
NUMA1	Q14980	Nuclear mitotic apparatus protein 1	0.0294	0.7621
NUP214	P35658	Nuclear pore complex protein Nup214	0.0032	0.8667
PAK2	Q13177	Serine/threonine-protein kinase PAK 2	0.0340	0.8281
PDE3A	Q14432	cGMP-inhibited 3',5'-cyclic phosphodiesterase 3A	0.0212	0.8640
PDIA4	P13667	Protein disulfide-isomerase A4	0.0019	0.7473
PFDN1	O60925	Prefoldin subunit 1	0.0241	0.5936
PHF5A	Q7RTV0	PHD finger-like domain-containing protein 5A	0.0057	0.7348
PLRG1	O43660	Pleiotropic regulator 1	0.0449	0.6164
POLR2E	P19388	DNA-directed RNA polymerases I, II, and III subunit RPABC1	0.0240	0.7142
POLR2K	P53803	DNA-directed RNA polymerases I, II, and III subunit RPABC4	0.0021	0.6466
PSAP	P07602	Prosaposin	0.0368	1.0582
PTPA	Q15257	Serine/threonine-protein phosphatase 2A activator	0.0172	1.0713
PYM1	Q9BRP8	Partner of Y14 and mago	0.0259	0.7718
RABEP2	Q9H5N1	Rab GTPase-binding effector protein 2	0.0248	0.5837
RALY	Q9UKM9	RNA-binding protein Raly	0.0057	0.9864
RBBP5	Q15291	Retinoblastoma-binding protein 5	0.0336	1.6050
RBM10	P98175	RNA-binding protein 10	0.0269	1.1278
RPL31	P62899	60S ribosomal protein L31	0.0271	1.3304
RPL4	P36578	60S ribosomal protein L4	0.0124	0.6792
RPL6	Q02878	60S ribosomal protein L6	0.0218	0.6144
RPS24	P62847	40S ribosomal protein S24	0.0184	1.2006
RRP1	P56182	Ribosomal RNA processing protein 1 homolog A	0.0036	0.8449
RSL1D1	O76021	Ribosomal L1 domain-containing protein 1	0.0041	0.8318
SERBP1	Q8NC51	Plasminogen activator inhibitor 1 RNA-binding protein	0.0131	0.8024
SERPINB6	P35237	Serpin B6	0.0054	0.6841
SLC25A24	Q6NUK1	Calcium-binding mitochondrial carrier protein SCaMC-1	0.0007	0.7554
SNRNP70	P08621	U1 small nuclear ribonucleoprotein 70 kDa	0.0040	0.8498
SNRPB2	P08579	U2 small nuclear ribonucleoprotein B''	0.0253	0.6918
SRP14	P37108	Signal recognition particle 14 kDa protein	0.0003	0.7456
SRP19	P09132	Signal recognition particle 19 kDa protein	0.0136	1.2708
SRP72	O76094	Signal recognition particle subunit SRP72	0.0199	0.8718

SRRM2	Q9UQ35	Serine/arginine repetitive matrix protein 2	0.0284	0.6525
SRSF2	Q01130	Serine/arginine-rich splicing factor 2	0.0265	0.9813
SRSF3	P84103	Serine/arginine-rich splicing factor 3	0.0067	0.8216
SRSF4	Q08170	Serine/arginine-rich splicing factor 4	0.0476	0.7761
TBCA	O75347	Tubulin-specific chaperone A	0.0015	0.7408
TIMM9	Q9Y5J7	Mitochondrial import inner membrane translocase subunit Tim9	0.0475	1.1584
TOP2A	P11388	DNA topoisomerase 2-alpha	0.0092	0.5967
TRNT1	Q96Q11	CCA tRNA nucleotidyltransferase 1, mitochondrial	0.0307	0.6585
U2AF1	Q01081	Splicing factor U2AF 35 kDa subunit	0.0474	0.7371
VIM	P08670	Vimentin	0.0095	0.7035
XPO7	Q9UIA9	Exportin-7	0.0045	1.6497

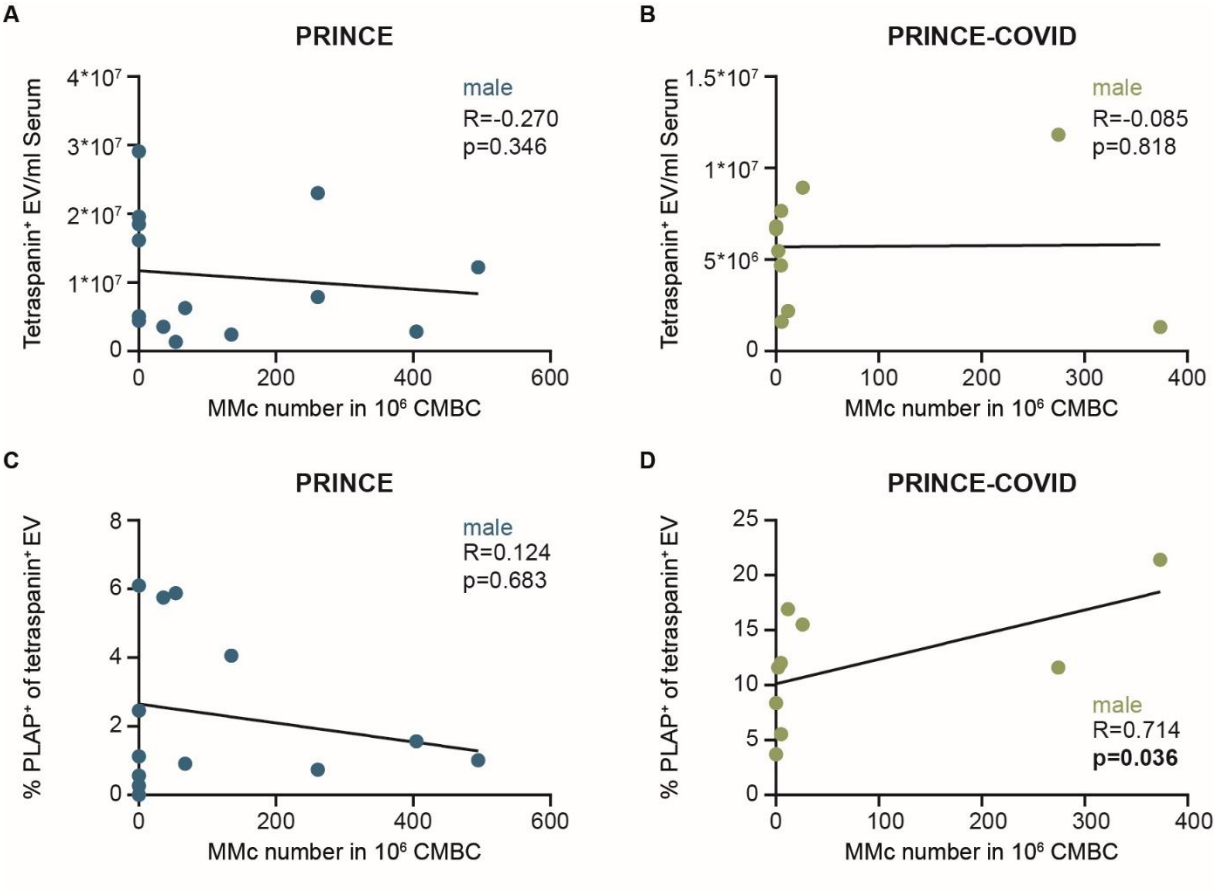

Figure 18. No correlation of EV and MMc for mothers pregnant giving birth to male neonates.
Correlation of tetraspanin⁺ EV with the number of MMc in 10^6 cord blood mononuclear blood cells (CMBC) from male neonates born to mothers that participated in the **(A)** PRINCE study or **(B)** PRINCE-COVID study. Correlation of PLAP⁺ EV with the number of MMc in 10^6 CMBC from male neonates born to mothers that participated in the **(C)** PRINCE study or **(D)** PRINCE-COVID study.

10 Acknowledgements

entfällt aus datenschutzrechtlichen Gründen

11 Curriculum vitae

entfällt aus datenschutzrechtlichen Gründen

entfällt aus datenschutzrechtlichen Gründen

entfällt aus datenschutzrechtlichen Gründen

12 Publications

Research articles

Yüzen DI et al. (accepted, 2023) Pregnancy-induced transfer of pathogen-specific T cells from mother to fetus in mice. *EMBO Reports*.

Yüzen DI & Graf I (2023) Increased late preterm birth risk and altered uterine blood flow upon exposure to heat stress. *eBioMedicine*. doi: 10.1016/j.ebiom.2023.104651.

Review articles

Yüzen DI & Graf I et al. (2023) Climate change and pregnancy complication: from hormones to the immune response. *Front. Endocrinol*. 14. doi: 10.3389/fendo.2023.1149284.

Yüzen DI et al. (2022) Tissue-resident immunity in the female and male reproductive tract. Semin. Immunopathol. 44, 785-799. doi: 10.1007/s00281-022-00934-8.

13 Affidavit

Ich versichere ausdrücklich, dass ich die Arbeit selbständig und ohne fremde Hilfe verfasst, andere als die von mir angegebenen Quellen und Hilfsmittel nicht benutzt und die aus den benutzten Werken wörtlich oder inhaltlich entnommenen Stellen einzeln nach Ausgabe (Auflage und Jahr des Erscheinens), Band und Seite des benutzten Werkes kenntlich gemacht habe. Teilergebnisse der vorliegenden Arbeit – die in 3.1 beschriebenen Ergebnisse und der entsprechende Methodenabschnitt – wurden zur Veröffentlichung in *EMBO Reports* angenommen (Juli 2023). Teile der in 3.3 beschriebenen Ergebnisse und des entsprechenden Methodenabschnitts sind Teil der medizinischen Dissertation von Isabel Graf. Etablierung der Tests sowie Analysen wurden gemeinsam durchgeführt.

Ferner versichere ich, dass ich die Dissertation bisher nicht einem Fachvertreter an einer anderen Hochschule zur Überprüfung vorgelegt oder mich anderweitig um Zulassung zur Promotion beworben habe.

Ich erkläre mich einverstanden, dass meine Dissertation vom Dekanat der Medizinischen Fakultät mit einer gängigen Software zur Erkennung von Plagiaten überprüft werden kann.

Unterschrift: .....

Dennis Yüzen, Hamburg im August 2023